

# **Antimicrobial peptides as new potential antibiotics**

## **Inaugural-Dissertation**

zur  
Erlangung des Doktorgrades  
der Mathematisch-Naturwissenschaftlichen Fakultät  
der Universität zu Köln

vorgelegt von

**André Reinhardt**  
aus Reutlingen

Köln

2017

Berichtersteller:  
(Gutachter)

Prof. Dr. Ines Neundorf

Prof. Dr. Karin Schnetz

Tag der mündlichen Prüfung: 02.06.2017

Die im Rahmen der vorliegenden Arbeit durchgeführten Experimente und Untersuchungen wurden im Zeitraum von Oktober 2013 bis April 2017 am Institut für Biochemie der Universität zu Köln unter der Anleitung von Frau Prof. Dr. Ines Neundorf durchgeführt.

## Abstract

In recent years, the rapid increase of antibiotic resistances and the expansion of multi-resistant bacterial strains have provoked the need to develop novel antibiotics. So-called antimicrobial peptides (AMPs) are short, amphiphilic, cationic peptides and part of the innate immune system. Their unique membrane disrupting mechanism and the low propensity for developing resistances attracted their attention in pharmaceutical medicine. AMPs are active against a wide spectrum of microorganisms, such as gram-positive and gram-negative bacteria, fungi, viruses and parasites.

The present thesis focuses on improving the antimicrobial activity of AMPs by using different strategies like synthesis of AMP-conjugates, membrane immobilization of AMPs, and amino acid exchanges within the AMP sequence. For this, multiple imidazolium-salts, already described as antibacterial agents, were conjugated to AMPs via solid phase peptide synthesis, developing a branched conjugate. Combination of both compounds resulted in a higher antimicrobial activity against multi-resistant bacterial strains. Selectivity of the novel compounds was demonstrated against human-red blood cells, which was further investigated by lipid interaction studies with cholesterol. The most selective compound IL-KKA (**3a**) could be used as a future lead structure for the development of new antimicrobial agents.

Since 80% of human infections are caused by biofilms, the newly designed compound IL-KKA (**3a**) was coupled covalently via a peptide bond or with electron beam radiation on polyether sulfone membranes (PES). Both immobilization techniques were successfully performed, still showing a high antimicrobial activity of the immobilized compound.

The cell-penetrating peptide sC18 was converted to an AMP by amino acid exchanges with isoleucine and phenylalanine. Isoleucine and phenylalanine mono mutants already exhibited an increased activity against a wide spectrum of bacteria. A higher amount of phenylalanine in the sequence leads to a further increased antimicrobial activity. The insertion of hydrophobic amino acids at position 10 led to the formation of a characteristic  $\alpha$ -helix, while the positions 15 and 16 seemed to be necessary for hydrophobic membrane interactions.

All in all, this thesis highlights the successful modification of AMPs to more active antimicrobial agents, which make them extremely interesting for the design of future antibiotics and the application of potential anti-biofilm agents.

## Zusammenfassung

Die Vermehrung von Antibiotikaresistenzen und somit multi-resistenten Bakterien macht die Entwicklung von alternativen Antibiotika, in Form von antimikrobiellen Peptiden (AMPs), nötig. AMPs sind kurze, amphipathische, kationische Peptide und Teil des angeborenen Immunsystems. Ihr einzigartiger Wirkmechanismus und das seltene Aufkommen von Resistenzen, machen AMPs interessant für die Pharmazie. AMPs sind aktiv gegen unterschiedlichste Mikroorganismen u.a. gram-positive und gram-negative Bakterien sowie Pilze, Viren und Parasiten.

In dieser Arbeit soll die antimikrobielle Aktivität von AMPs durch Herstellung von AMP-Konjugaten, Membranimmobilisierung von AMPs und den Austausch von Aminosäuren innerhalb der AMP Sequenz weiter erhöht werden. Unterschiedlich modifizierte Imidazoliumsalze, die bereits für ihre antimikrobielle Aktivität bekannt sind, wurden mit Hilfe der Festphasenpeptidsynthese an AMPs gekuppelt. Die Kombination der beiden Komponenten zeigte eine höhere Aktivität gegen multiresistente Bakterien. Eine der neuen Verbindungen, IL-KKA (**3a**), zeigte die höchste Selektivität und kann als Leitstruktur für die Entwicklung von neuen Antibiotika verwendet werden.

80% der heutigen Infektionen werden durch Biofilme verursacht. Deshalb wurde das neu designte IL-KKA (**3a**) mit unterschiedlichen Linkern an Polyethersulfon-Membranen immobilisiert. Dies wurde entweder durch eine kovalente Peptidbindung oder mit Hilfe von Elektronenbestrahlung bewerkstelligt. Beide Techniken waren erfolgreich und die so aktivierten Membranen zeigten weiterhin eine antimikrobielle Aktivität.

Das zellpenetrierende Peptid sC18 wurde durch den Austausch der Aminosäuren an Position 10, 15 und 16 durch Isoleucin oder Phenylalanin in ein AMP umgewandelt. Die Einzelmutanten zeigten bereits eine erhöhte Aktivität gegenüber unterschiedlichsten Bakterienstämmen. Durch das Einfügen von bis zu 3 Phenylalaninen konnte die antimikrobielle Aktivität weiter erhöht werden. Hierbei sorgte der Austausch an Position 10 für eine besser ausgebildete  $\alpha$ -Helix, während der Austausch an den Positionen 15 und 16 die hydrophoben Membraninteraktionen verstärkten.

Zusammenfassend zeigt diese Arbeit, dass die Modifikation von antimikrobiellen Peptiden zu einer erhöhten Aktivität führen kann. Die in dieser Arbeit neu

entwickelten AMPs haben das Potential, als neue Antibiotika oder als Anti-Biofilm Wirkstoffe eingesetzt zu werden.

## Table of contents

<b>1. Introduction.....</b>	<b>1</b>
1.1. Antibiotics and the connected problem to antimicrobial resistances.....	1
1.2. Antimicrobial peptides – a new class of antibiotics?.....	2
1.3. Antibacterial AMPs – mechanism of action .....	7
1.4. Structural properties of antimicrobial peptides.....	9
1.5. Bacterial resistance mechanisms against antimicrobial peptides .....	10
1.6. Biofilms – a problem of bacterial infections .....	11
1.7. General structure of bacterial membranes .....	12
1.8. Ionic liquids.....	14
1.9. Preliminary work.....	15
1.10. Aim of the thesis.....	17
<b>2. Materials and methods .....</b>	<b>19</b>
2.1. Materials.....	19
2.1.1. Equipment.....	20
2.1.2. Buffers.....	21
2.1.3. Bacterial strains .....	22
2.1.4. Peptide sequences .....	22
2.2. Solid phase peptide synthesis (SPPS) .....	24
2.2.1. Loading of Wang-resin with the first amino acid.....	24
2.2.2. Determination of the first residue attachment.....	25
2.2.3. Automated peptide synthesis .....	25
2.2.4. Manual coupling of ionic liquids and 5(6)-carboxyfluorescein .....	26
2.2.5. Endcapping .....	26
2.2.6. Fmoc cleavage.....	26
2.2.7. Cleavage of the Dde-protection group .....	27
2.2.8. Kaiser test.....	27
2.2.9. Sample cleavage .....	27
2.2.10. Full cleavage.....	28
2.2.11. LC-mass spectrometry with 0.1% FA for qualitative analysis.....	28
2.2.12. RP-HPLC with 0.1% TFA for purity analysis .....	29
2.2.13. Preparative RP-HPLC with 0.1% TFA.....	29
2.2.14. Synthesis of ionic liquids .....	29

2.3.	Characterization methods.....	29
2.3.1.	Circular dichroism spectroscopy .....	29
2.3.2.	Preparation of large unilamellar vesicle (LUVs) .....	30
2.3.3.	Circular dichroism with LUVs .....	30
2.3.4.	Preparation of giant unilamellar vesicle (GUVs).....	30
2.3.5.	CLSM observation of GUVs treated with peptide conjugates.....	31
2.4.	Biological methods .....	31
2.4.1.	Antimicrobial activity .....	31
2.4.2.	Killing assay using resistant bacterial strains.....	32
2.4.3.	Hemolytic activity .....	32
2.4.4.	Immobilization and characterization of polyether sulfone.....	33
	membranes (PES) .....	33
2.4.5.	Antimicrobial activity with immobilized PES membranes .....	33
<b>3.</b>	<b>Results and discussion.....</b>	<b>35</b>
3.1.	Improvement of imidazolium salt-peptide conjugates and their mechanism of action.....	35
3.1.1.	Synthesis of imidazolium salt-peptide conjugates.....	35
3.1.2.	pH influence on the secondary structure of compound <b>3c</b> .....	39
3.1.3.	Antimicrobial activity against resistant bacterial strains .....	40
3.1.4.	Hemolytic activity studies .....	42
3.2.	Electron beam immobilization of novel antimicrobial, short peptide motifs leads to membrane surfaces with promising anti-biofilm properties .....	48
3.2.1.	Synthesis of <b>3a</b> and its derivatives <b>3d</b> , <b>3e</b> and <b>3f</b> .....	49
3.2.2.	Membrane immobilization and characterization .....	51
3.2.3.	Antimicrobial activity of the functionalized PES membranes.....	53
3.3.	Optimizing the antimicrobial activity of the CPP sC18.....	57
3.3.1.	Synthesis of sC18 variants.....	58
3.3.2.	Antimicrobial activity of sC18 isoleucine variants.....	63
3.3.3.	Antimicrobial activity of phenylalanine variants .....	70
3.3.4.	Characterization of peptides via CD-spectrometry.....	76
3.3.5.	Peptide interaction with artificial membrane vesicles .....	79
<b>4.</b>	<b>Conclusion and Outlook .....</b>	<b>83</b>
<b>5.</b>	<b>Literature .....</b>	<b>85</b>
<b>6.</b>	<b>Attachment.....</b>	<b>96</b>

6.1.	List of abbreviations .....	96
6.2.	List of Figures.....	99
6.3.	List of tables .....	101
6.4.	Acknowledgment.....	102

# 1. Introduction

## 1.1. Antibiotics and the connected problem to antimicrobial resistances

In 1928, Alexander Fleming discovered penicillin, the first antibiotic substance. This discovery opened one of the most important research fields in medical history. Nearly 90 years later, antibiotics are still the major tools against infectious diseases. However, due to their excessive and overdosed application, in the last decades, bacteria became more and more resistant against common antibiotics (1). The resulting antimicrobial resistances have become a major health problem (1-4). Antibiotic resistances are listed as one of the greatest threats to human health (5), as a lot of resistant bacteria can be found in hospitals, where they cause serious infections. So-called superbugs refer to bacteria, which have adapted to resist multiple classes of antibiotics (multidrug-resistant). They demonstrate an enhanced morbidity and the therapeutic options to kill them are only limited (6). The most famous superbug is the gram-positive and methicillin-resistant bacterium *Staphylococcus aureus* (MRSA) (7). One additional problem is the use of antibiotics in non-human niches like agriculture, aquaculture and waste disposal that has steadily increased during the last years (8). For example, the resistance of *Escherichia coli* against ciprofloxacin has been associated with the use of fluoroquinolones, a broad-spectrum antibiotic, in aviculture (9). When bacteria acquired resistances, they are able to preserve them through genetic and biochemical mechanisms (Table 1). These mechanisms include e.g. genetic mutations or transfer of genetic gene material between bacteria via conjugation, transformation or transduction (10, 11). Biochemical resistance mechanisms on the other side can be divided into different resistance types, like an decreased uptake of the antibiotic, enzymatic modification and degradation, or an altered targeting within the cell, or via efflux pumps that remove the antibiotic out of the cell directly after the uptake (12, 13). However, the most popular mechanism is the enzymatic inactivation of antibiotics. The three main enzyme classes are  $\beta$ -lactamases, aminoglycoside-modifying enzymes and chloramphenicol acetyltransferases.  $\beta$ -lactamases hydrolyze ester and amide bonds from  $\beta$ -lactam antibiotics like penicillin (14). Aminoglycoside-modifying enzymes reduce the affinity of aminoglycosides and fluoroquinolones, resulting in a weaker binding to the 30S ribosomal subunit (15,

16). So-called acetyltransferases inactivate chloramphenicol and aminoglycosides by binding adenylyl-, phosphoryl- or acetyl-groups to the antibiotics (17).

**Table 1: Common antibiotics and their bacterial resistance mechanisms.**

Antibiotic class	Antibiotics	Target	Resistance mechanism
$\beta$ -lactams (18)	Penicillin	Peptidoglycan biosynthesis	Hydrolysis
	Ampicillin		
	Methicillin		
Aminoglycosides (19)	Gentamicin	Translation	Phosphorylation
	Streptomycin		Acetylation
Glycopeptides (20)	Vancomycin	Peptidoglycan biosynthesis	Reprogramming of peptidoglycan biosynthesis
Tetracyclines (21)	Minocycline	Translation	Monooxygenation
Phenicol (22)	Chloramphenicol	Translation	Enzymatic degradation

During the last years, an alternative antibiotic class, namely antimicrobial peptides (AMPs), attracted the attention in pharmaceutical medicine owing to their different activity mechanisms, and their antimicrobial activity against a broad spectrum of microorganisms, such as gram-positive and gram-negative bacteria as well as fungi, parasites and viruses (23-25).

## 1.2. Antimicrobial peptides – a new class of antibiotics?

Antimicrobial peptides are part of the innate immune system and play an important role in the defense against pathogenic microorganisms (26, 27). Thus, AMPs are of

great interest in averting infections before they cause symptoms, and additionally, they participate in inflammation and wound healing processes (28). Based on their structural properties, AMPs can be further divided into four subgroups, namely  $\alpha$ -helical,  $\beta$ -sheet, extended and loop peptides (Figure 1 and Table 2) (27, 29, 30). Most AMPs are short-length peptides, sharing an amphipathic character with a positive net charge and a high content of hydrophobic residues, belonging to the subgroup of  $\alpha$ -helical AMPs (31). Well-known examples, which belong to this group, are magainin, LL-37 and cecropin (32, 33). The subgroup of  $\beta$ -sheet proteins, including protegrin and the defensin family is characterized by two or more disulfide bridges, which stabilize their conformation (27). Thirdly, the extended AMPs contain a high content of arginine, tryptophan and proline residues in their amino acid sequence. Indolicidin and bactenecins are well-known representatives of this subgroup (34, 35). The smallest subgroup is represented by hairpin-like loop structures consisting of highly stable peptides interconnected by at least one disulfide bridge. For example, gramicidin and dodecapeptide belong to this class of AMPs (36-38). Some AMPs, like indolicidin, form their secondary structure only when interacting with target membranes (39).

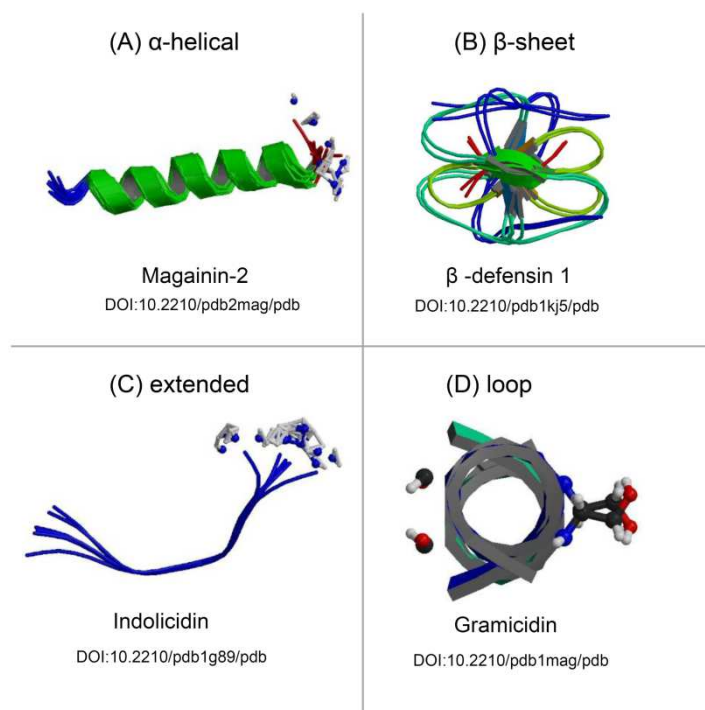


**Figure 1: The four classes of antimicrobial peptides represented by protein models.** Subgroups of antimicrobial peptides: (A)  $\alpha$ -helical peptides, (B)  $\beta$ -sheet peptides, (C) extended peptides and (D) loop-peptides. All structures were obtained from the RCSB Protein Data Bank (PDB) (40).

In the last years, researchers optimized natural AMPs and developed related synthetic ones (41, 42). Especially the reduction of size leads to an optimization of metabolic stability and bioavailability. Furthermore, shorter peptide sequences would advantageously reduce the production costs dramatically (43). Modifications of peptide bonds by introduction of hydrogen bonds in the AMP sequence as well as insertion of unnatural amino acids and replacement, might also increase the antimicrobial activity (44). The conjugation of AMPs to drugs, photosensitizer, nanoparticles or organometallic complexes could convert AMPs into useful delivery vectors (45). Moreover, there are different strategies to apply AMPs therapeutically. On the one hand, they can be used as single anti-infective reagents, or in combination with common antibiotics to obtain a synergetic effect. On the other hand, AMPs can be used as immunostimulatory agents resulting in an enhanced innate immune system. Lastly, the application of AMPs as endotoxin-neutralizing agents is possible to prevent septic shocks induced by bacterial virulence factors (46).

**Table 2: Some examples of antimicrobial peptides, their sequences, structures and mechanisms of action.**

Peptide and Sequence	Structure	Mechanism
Apidaecin 1b (47) <b>GNNRPVYIPQPRPPHPRL</b>	Polyproline helix type II	Inhibition of ATPase
Cecropin A (48) <b>KWKLFFKKIEKVGQNIRDGII</b> <b>KAGPAVAVVGQATQIAK</b>	$\alpha$ -helix	Disruption of cell membrane
Histatin-5 (49) <b>DSHAKRHHGYKRKFHEKHSHRGY</b>	$\alpha$ -helix	Intracellular targeting
Indolicidin (50) <b>ILPWKWPWWPWR</b>	Extended	Inhibition of DNA/RNA synthesis
KLA (51) <b>(KLAKLAK)<sub>2</sub></b>	$\alpha$ -helix	Pore-forming

<p>LL-37 (52)</p> <p><b>LLGDLFRKSKEKIGKEFKRI</b></p> <p><b>VQRIKDFLRNLVPRTES</b></p>	<p><math>\alpha</math>-helix</p>	<p>Pore-forming (Carpet-like)</p>
<p>Magainin 2 (53)</p> <p><b>GIGKFLHSAKKFGKAFVGEIMNS</b></p>	<p><math>\alpha</math>-helix</p>	<p>Pore-forming (Toroidal)</p>
<p>Melittin (54)</p> <p><b>GIGAVLKVLTTGLPALIS</b></p>	<p><math>\alpha</math>-helix</p>	<p>Pore-forming (Toroidal)</p>
<p>sC18 (55)</p> <p><b>GLRKRLRKFRNKIKEK</b></p>	<p><math>\alpha</math>-helix</p>	<p>-</p>
<p>Sushi (56)</p> <p><b>GFKLKGMARISCLPNGQWS</b></p> <p><b>NFPPKCIRECAMVS</b></p>	<p><math>\alpha</math>-helix</p>	<p>Pore-forming (Carpet-like)</p>

Through their activity against a broad spectrum of microorganisms (23, 24, 30), AMPs can be classified not only by their secondary structure, but also by their target organism as antiviral, antifungal, antiparasitic and antibacterial peptides. Antiviral peptides neutralize the viral absorption, lyse viruses or affect the viral envelope (57, 58). Integration of AMPs into viral envelopes causes membrane instability leaving the virus unable to infect host cells (59). However, the antiviral activity of AMPs is always related to their secondary structure, signifying that  $\beta$ -sheet peptides show higher effects than  $\alpha$ -helical AMPs. Defensins are  $\beta$ -sheet AMPs that are able to bind to viral glycoproteins, which results in the inability of the herpes simplex virus (HSV) to bind to host cells (60). In contrast, AMPs like NP-1 prevent the host-cell virus interaction by changing the gene expression profile of host cells (61).

Another class of AMPs comprises antifungal peptides, which are able to kill fungi by cell wall targeting, or interaction with intracellular components (62, 63). Most antifungal peptides are isolated from plants and display a high content of polar and neutral amino acids in their primary sequence (64). In contrast to bacteria, fungi cell walls contain chitin, a derivate of glucose. Some antifungal peptides have the ability to bind to chitin, resulting in a selective fungi targeting (65). Antifungal AMPs are

mostly membrane active and kill the fungi by disrupting the membrane integrity, forming pores or increasing the membrane permeabilization (66, 67).

The smallest class of AMPs are the antiparasitic peptides. Magainin was the first peptide which demonstrated a killing activity against *Paramecium caudatum*, a ciliophoran (68). Some years later, cathelicidin was discovered to kill *Caenorhabditis elegans* by forming membrane pores. The main mechanism of antiparasitic AMPs is the interaction with cell membranes, too (69).

The most-studied class is represented by antibacterial peptides. Antibacterial peptides interact with bacteria's cell membrane. They either cause membrane permeation or pass the cell membrane and bind intercellular targets (70). The amphipathic structure of antibacterial peptides provides the possibility to bind lipid components with their hydrophobic region, and face the lumen of the pore with their hydrophilic region (71). Intracellular active AMPs tend to inhibit important cell pathways like DNA replication or protein synthesis. These AMPs contain an active site in their sequence for binding to their target (72). In some cases, AMPs like nisin can also kill antibiotic-resistant bacteria (73).

Most of the AMPs are active against one class of microorganisms, however, indolicidin is one of the exceptions, because it effectively targets bacteria, fungi and viruses (74).

For some so called cell-penetrating peptides, also antimicrobial activity has been observed. The same holds true for sC18, which showed only a moderate antimicrobial activity, while it was successfully used as cell-penetrating peptide. sC18 was used during this work and is a 16 amino acids long C-terminal fragment of the CAP18 peptide, which belongs to the group of cathelicidines and is known to bind to lipopolysaccharides (LPS) (75). Previous studies already illustrated that parts of the CAP18 peptide exhibit high antimicrobial effects. Within CAP18, the fragment C18, which contains residues 106-125, was highlighted as an antimicrobial peptide, exhibiting an amphipathic  $\alpha$ -helix (76). Since the C18 peptide was also used as a gene delivery system (77), our group developed a four amino acids shorter version of the C18 peptide in 2009, called sC18 (residues 106-121), in order to develop a potential drug carrier system (78). Since sC18 showed very efficient cell-penetrating activities and no toxicity against human cell lines, it was further optimized via cyclisation or truncation, to ensure an efficient cellular uptake (79-82).

### 1.3. Antibacterial AMPs – mechanism of action

As already mentioned, the most common mechanism of antibacterial AMPs is the permeation of bacterial membranes followed by their disruption. The amphipathic character of AMPs, especially their positively charged sites, leads to a highly selective interaction with the outer microbial membrane. Due to lipoteichoic acids (gram-negative bacteria) and lipopolysaccharides (gram-positive bacteria), these membranes show characteristically a negatively charged environment (83, 84). Bacterial death occurs only when AMPs are completely saturated on the bacterial cell membrane. Nevertheless, the interaction of AMPs with lipopolysaccharides or anionic lipoteichoic acids may reduce the AMP concentration needed for destabilization of the bacterial membrane and pore formation (85). The hydrophobic part of the peptides enables them to insert into bacterial membranes (86). The disruption of the bacterial membrane induces the breakdown of the membrane potential as well as the leakage of intracellular components and is finally leading to cell death (87). The membrane disrupting mechanism is highly complex but can roughly be divided into three main models, namely the barrel-stave, the toroidal pore and the carpet-like model (Figure 2) (72). In the barrel-stave model, the AMPs aggregate and attach to the outer membrane with their hydrophobic part aligning to the lipid bilayer. During the following pore forming process, the hydrophobic part of the AMP is oriented to the cell membrane while the hydrophilic part is exposed to the pores (54). In the toroidal model, the mechanism also starts with an aggregation of the peptides on the membrane surface. In this way, the hydrophilic residues of the AMPs interact with the lipid head groups inducing a pore built up by inserted peptides as well as lipid head groups (88). The last model, the carpet-like model, depicts the formation of micelles instead of pores. AMPs are oriented parallel to the membrane, covering the whole membrane surface resulting in a carpet formation, which then disrupts the membrane structure in a detergent-like manner (89, 90). Due to the differences in membrane composition of bacteria and mammalian cells, antimicrobial peptides exhibit a selective cytotoxicity against microorganisms. In contrast to bacterial membranes, mammalian cell surfaces consist additionally of sphingomyelin and cholesterol (91).

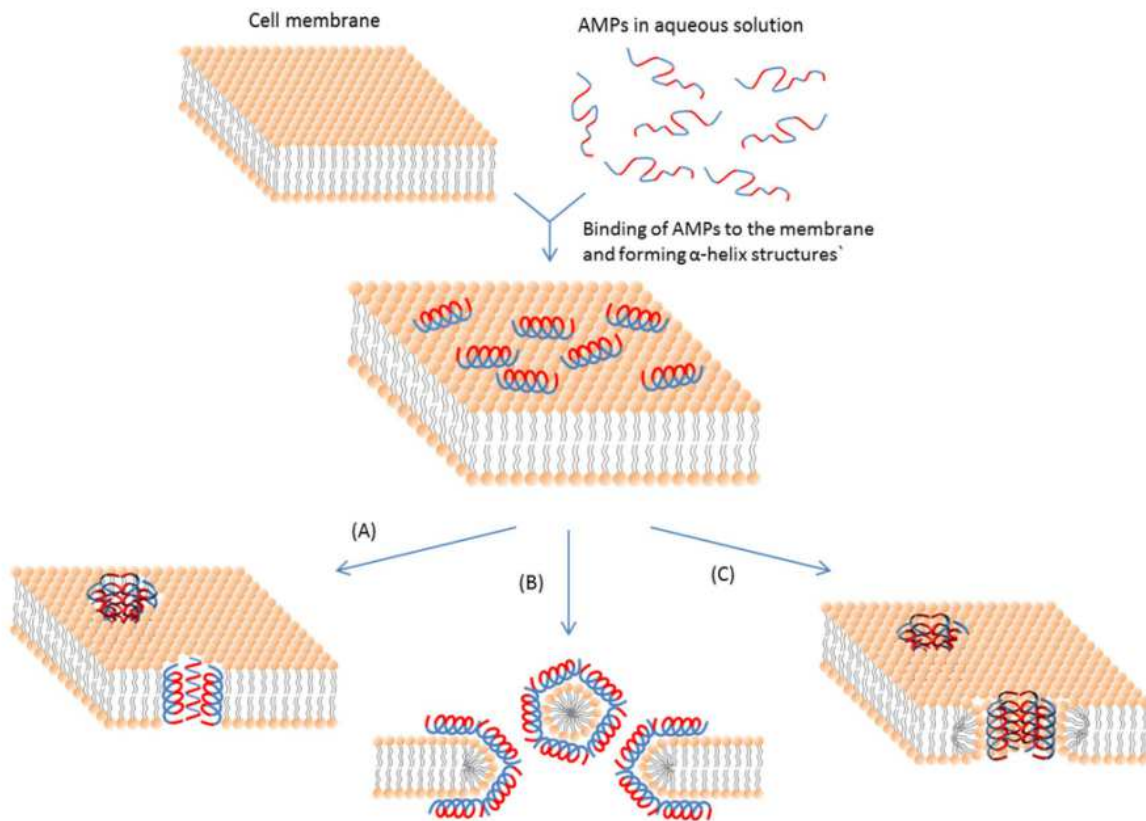


**Figure 2: Membrane disrupting mechanism of AMPs.** In blue: hydrophobic regions, in red: hydrophilic regions. Peptides attach to the lipid head groups of the cell membrane (A) The barrel-stave model: Hydrophobic sides of the peptides are at the outside while hydrophilic sides build the channel inside. (B) The carpet-like model: Peptides disrupt the cell membrane forming a carpet around the membrane. (C) The toroidal model: The peptide pore is built by the inserted peptides and the lipid head groups of the cell membrane (92).

AMPs are not limited to operate just via membrane permeation, because there also exist AMPs with intracellular targets (93, 94). These translocate across the membrane and are able to target a wide range of intracellular processes (72). One major intracellular target for AMPs is DNA or the protein machinery. For example, the AMP buforin II translocates across the cell membrane and binds to DNA and RNA inhibiting both (95-97). The AMP apidaecin is another peptide, which blocks the pore forming ability of bacteria (Table 2). However, this AMP is only able to act against gram-negative bacteria. It is suggested that apidaecin is carried inside the cell by a transporter protein, which is specific for gram-negative bacteria (98). On the other hand, there exist AMPs, which can inhibit enzymatic activity like histatin-5 or phyrocidin. Histatin-5 inhibits a protease from *Bacteriocides gingivalis*, while phyrocidin inhibits the ATPase activity of the heat shock protein DnaK that is

involved in protein folding (99, 100). Some AMPs are only active against bacteria in a certain growth stage, proposing an interaction with a specific metabolic pathway, which is activated during bacterial growth (101). The cytoplasmic localization of AMPs leads to the presumption of existing cellular uptake mechanisms. Two mechanisms for cellular uptake of AMPs are reported. The uptake is either accomplished via endocytosis, including micropinocytosis or receptor-mediated endocytosis or by direct penetration (86).

#### 1.4. Structural properties of antimicrobial peptides

The structural properties of antimicrobial peptides are essential for their antimicrobial activity and cell selectivity. Although a structure related prediction about the mode of action cannot be proposed, the conformation, charge, hydrophobicity and solubility are important aspects for antimicrobial peptides. The structure of  $\alpha$ -helical AMPs is often formed during the interaction with the amphipathic bacterial membrane. It was reported that for an  $\alpha$ -helical AMP a length of at least 22 amino acids is required to transverse the bacterial bilayer via the barrel-stave model (102). By the introduction of D-amino acids in the hydrophobic face, the secondary structure is affected, which results in a hemolytic effect and improved selectivity (103). As the secondary structure of peptides is predicted by the amino acid sequence, the introduction of amino acids like proline and glycine hinders the helix-formation and the flexibility (104). Nevertheless, there exist proline-arginine rich peptides inducing polyproline helical type II structures, which are comparable to an alpha helix (105, 106).

The positive net charge of AMPs is an important property because the electrostatic interactions between AMPs and bacterial cell membranes are the major force for the first contact (72, 107, 108). Since bacterial membranes are rich in acidic phospholipids and human cell membranes contain acidic phospholipids only on the inner side, the net charge plays a crucial role for selectivity, too (109). An increasing positive net charge often leads to an increased antimicrobial but also hemolytic activity (110).

Another essential structural property of AMPs is the content of hydrophobic amino acids, which for most antimicrobial peptides is in the range of approximately 50% (111). Increasing hydrophobicity on the positively charged side of the AMPs up to a

certain point leads to an increased antimicrobial activity. Nevertheless, increasing hydrophobicity is often connected to mammalian cell toxicity and loss of selectivity (109). Furthermore, an augmented hydrophobicity can alter the range of targets for the AMP. The AMP magainin, which is only active against gram-negative bacteria, can also be effective against gram-positive bacteria by the insertion of hydrophobic amino acids (112).

### 1.5. Bacterial resistance mechanisms against antimicrobial peptides

In order to find new and useful antibiotic compounds, some AMPs have already been investigated in clinical research. The understanding of bacterial resistance against these AMPs is the next, crucial step (113). Therefore, research groups focus on the identification of different bacterial resistance mechanisms. Membrane alterations represent one major tool for bacteria to develop resistances. It was shown, that changes in the membrane lipid composition by the inclusion of cardiolipin or other positively charged phospholipids avoid the insertion of positively charged AMPs (114) (Figure 3A). Moreover, bacteria are able to overexpress genes encoding for transmembrane transporters like the efflux pumps, which allow the displacement of AMPs back into the periplasm (115) (Figure 3B). Another example for the development of resistances against gram-positive bacteria, is the modification of their teichoic acids through D-alanylation resulting in the reduction of their anionic charge (116) (Figure 3C). On the other hand, gram-negative bacteria can make use of lipid A modifications to incorporate positive charges into lipopolysaccharides, which decreases the binding affinity of antimicrobial peptides (117) (Figure 3D). Furthermore, bacteria are able to alter their cellular metabolism and regulate the expression of proteases, biofilm formation and modifications of surface structures to avoid the uptake of AMPs (109).

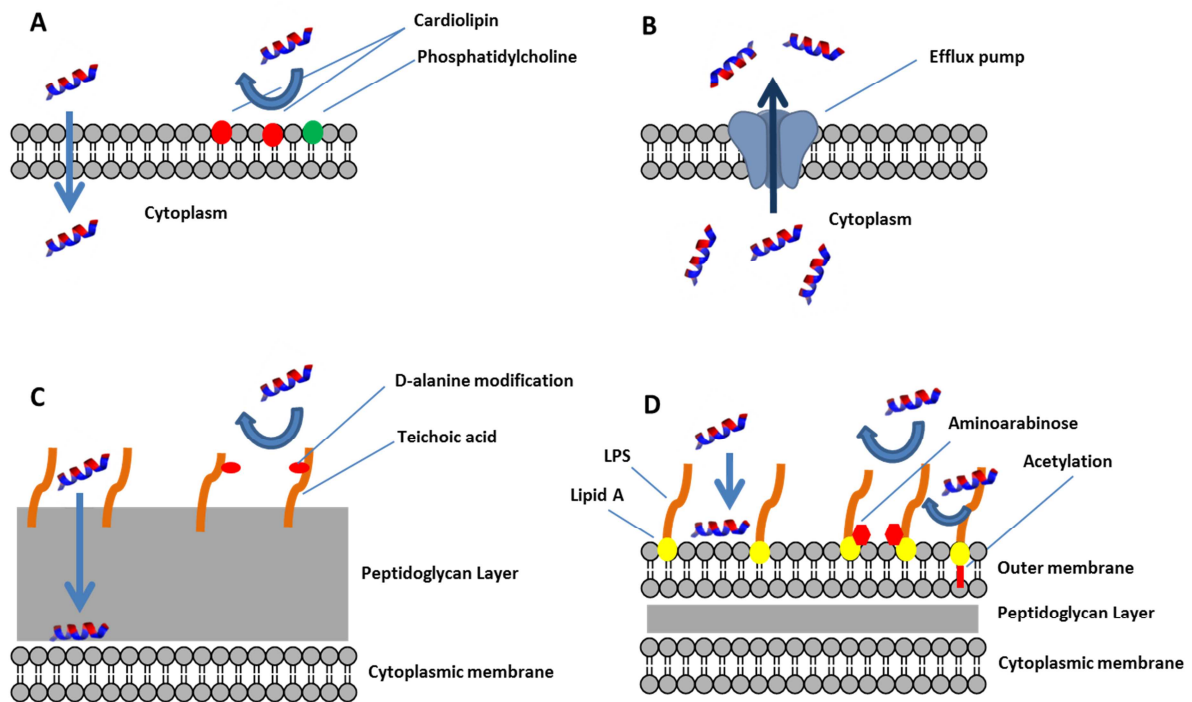


**Figure 3: Schematic overview of AMP resistance mechanism.** (A) Insertion of cardiolipin or phosphatidylcholine leads to an increased positive charge. (B) Membrane transporter like the efflux pump are overexpressed and transport the AMPs outside the cell. (C) D-alanylation of teichoic acids in gram-positive bacteria. (D) Lipid A modifications through positive charges in gram-negative bacteria (modified from (92)).

## 1.6. Biofilms – a problem of bacterial infections

Biofilms consist of single or multiple organism species in a wide range of physiological states and are mostly attached to tissue or abiotic surfaces. Formation of such biofilms and their upcoming resistance to antimicrobial agents are one of the main reasons for many chronic bacterial infections (118). Moreover, it was estimated that 80% of human bacterial infections are caused by biofilm formation on implants, catheters and heart valves (119). Biofilm formation itself can be divided into four stages, starting with the adherence of microorganisms to a tissue or abiotic surface. The second state is initiated by the generation of an extracellular polymeric substance containing proteins, extracellular DNA and polysaccharides. During biofilm maturation, the formation of water channels and other complex structures occurs and is pronounced as the third stage of biofilm formation. As a final step, biofilm spreading takes place, in which adjacent regions are colonized (120-122). A biofilm consists, as already mentioned, of single or multiple organisms, such as fungi, bacteria and viruses. With the generation of biofilm matrices, the organisms

are able to protect themselves against environmental stresses such as UV-radiation, pH variation and osmotic shock. Interactions like horizontal gene transfer, metabolic cooperation as well as a competition between bacteria result in an improved survivability (123, 124). Heterogeneity is an important property of biofilms, too (125). A biofilm produces gradients of oxygen, pH value and redox conditions leading to a multilayered biofilm (126). Due to the presence of oxygen in the water phase, the upper layer of the biofilm is aerobic. The present oxygen is consumed rapidly by aerobic bacteria, resulting in the formation of anaerobic zones in deeper layers (127). In a biofilm, cooperative interactions between bacteria are observable. During the process of nitrification, ammonia-oxidizing bacteria convert ammonium into nitrite, which is then consumed by nitrite-oxidizing bacteria (128). As a result of these cooperative interactions, a 10-1,000 fold higher resistance against antibiotics is observed within biofilms compared to the planktonic state of the same bacteria (129, 130). However, also competitive interactions, caused by bacteriocins, extracellular vesicles or the application of antibiotics, can be observed within biofilms and lead to the prevention of adhesion (131).

To avoid biofilm formation, several methods, including the generation of antimicrobial peptides on surfaces were reported (132-134). Moreover, colonizing surfaces with non-pathogenic bacteria (129), and/or coating them with biocidal substances like triclosal or polyquaternary amines might also avoid biofilm formation (135, 136). Another common way is the direct coating or immobilization of surfaces with antibiotic compounds, such as vancomycin, penicillin or ampicillin (137-139).

## 1.7. General structure of bacterial membranes

The main purpose of the bacterial cell membrane is the protection against osmotic lysis. In 1884, Christian Gram developed a staining procedure to classify the bacteria into two groups, namely gram-positive and gram-negative bacteria. Gram-positive bacteria retain the stain, while gram-negative bacteria do not.

Gram-negative bacterial membranes consist of three layers: the outer membrane (OM), the peptidoglycan and the cytoplasmic or inner membrane (IM) (Figure 4). The composition of the OM can be described asymmetrically with the inner leaflet containing phospholipids and the outer leaflet composed of glycolipids, mostly lipopolysaccharides (LPS) (140, 141). Furthermore, the OM is enriched in

phosphatidylethanolamine (142, 143). LPS consists of lipid A, a core oligosaccharide and an O-antigen, and play a critical role in the barrier function of the OM (144, 145). The core oligosaccharide can be further distinguished into the inner and the outer region. Moreover, two protein types, lipoproteins and  $\beta$ -barrel proteins, can be detected in the OM. While lipoproteins are attached to the inner leaflet of the OM,  $\beta$ -barrel proteins function as transmembrane proteins, which span the outer membrane (146, 147). Peptidoglycan consists of *N*-acetylglucosamine and *N*-acetylmuramic acid, which are connected by  $\beta$ -1,4 glycosidic bonds (148) and are important for the characteristic shape of bacteria. The aqueous compartment surrounded by the outer and the inner membrane is called periplasm and contains the peptidoglycan and various proteins and chaperons (149). The inner membrane of gram-negative bacteria can be described as a phospholipid bilayer with inner membrane proteins (150).

In contrast to gram-negative bacteria, gram-positive bacteria possess no outer membrane. To compensate this disadvantage, gram-positive bacteria consist of a thicker peptidoglycan layer (151). Long anionic polymers called teichoic acids are localized within this peptidoglycan layer. These, so-called wall-teichoic acids, are covalently attached to the peptidoglycan while the lipoteichoic acids are anchored to the lipid head groups of the membrane (152). Since gram-positive bacteria miss the outer membrane, the surface of the peptidoglycan is decorated with lots of proteins, which are similar to proteins found in the periplasm of gram-negative bacteria (153). Additionally to gram-positive and gram-negative bacteria, there exists a further class of special bacteria in nature, called mycobacteria. Due to the complex structure of their cell wall, mycobacteria are more resistant against antibiotics and virulences (154). The peptidoglycan of mycobacteria is more cross-linked than in *E. coli* or *B. subtilis*, as 80% of the peptidoglycan contains 3-3 peptide crosslinks (155). The peptidoglycan is surrounded by a layer of arabinogalactan (156), which further is ligated with mycolic acids. (157). These mycolic acids, composed of long carbon chains, form the characteristic thick waxy lipid layer of mycobacteria and are primarily responsible for the impermeability of the cell membrane (158).

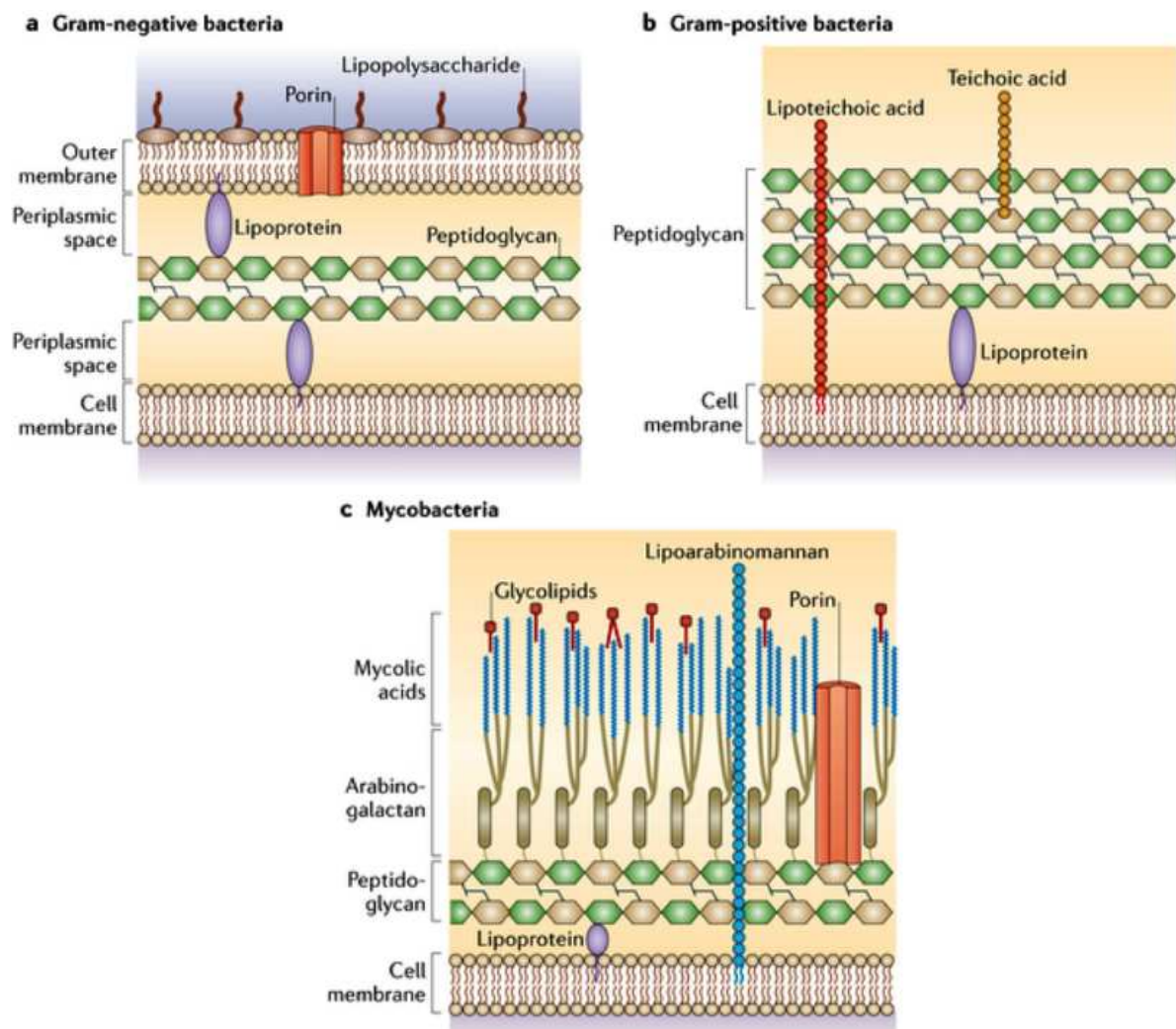


**Figure 4: Cell-wall structure of gram-negative, gram-positive and mycobacteria.** (a) Gram-negative bacteria consist of a cell membrane with a periplasmic space and an outer membrane. In the periplasmic space localizes a thin peptidoglycan layer. The outer membrane contains LPS and porins. (b) Gram-positive bacteria have a cell membrane and a thicker peptidoglycan layer than gram-negative bacteria. The peptidoglycan consists of teichoic acids and lipoteichoic acids. (c) Mycobacteria consist of a cell membrane, a thin layer of peptidoglycan and arabinogalactan and a thicker layer of mycolic acids. Glycolipids and porins are detected in the cell walls (159).

## 1.8. Ionic liquids

Due to their potential antimicrobial activity, ionic liquids (ILs) have gained much interest. ILs represent a class of liquid materials consisting of an amphiphilic cation and an inorganic or organic anion (160). Depending on the structure of ILs, they are applied in various fields like synthetic chemistry, enzyme stabilization, or as

pharmaceutical compounds in pharmaceutical industry (161-163). ILs are extremely interesting due to their flexibility of altering composition and structure of cation and anion, their thermal stability and their solvating potential (164-166). Usually, ILs can be divided into four classes, namely dialkylimidazolium-, alkylammonium-, phosphonium- and *N*-alkylpyridinium-based ILs. A well-studied class are imidazolium-based ionic liquids, which are used as solvents in bioorganic transformations (167) (Figure 5). The imidazolium cations show high stability within oxidative and reductive conditions (168) and are relatively easy to synthesize (169). This class of ionic liquids also improves the solubility of proteins and thus, prevents them from aggregation (170). In 1999, Welton *et al.* designed special ionic liquids with toxic effects against microorganisms (165). Further studies demonstrated that ionic liquids with a charged hydrophilic head group and hydrophilic tail have an amphiphilic character, which especially is true for imidazolium and pyrimidinium-based ionic liquids (171). The amphiphilic character and the length of the alkyl-chain are the major requirements for their toxic effects against microorganisms (172). However, also non-specific toxic side effects resulting in cell toxicity against host cells were observed (173). Consequently, in the next step researchers focus on the development of new ionic liquid compounds and conjugates with reduced host cell toxicity.

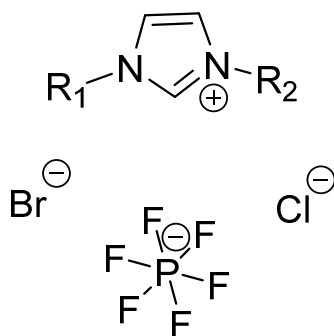


**Figure 5: The imidazolium cation with different anions.** R = methyl, ethyl or butyl groups.

## 1.9. Preliminary work

The preceding paragraphs have described the difficulty about increasing antimicrobial resistances and the connected health problem. Due to this, the development of new antibiotic substances is crucial. Antimicrobial peptides represent an alternative antibiotic class, which holds for a comprehensive analysis.

One of my main goals during my master thesis was therefore the identification of future lead structures, demonstrating high antimicrobial activity and selectivity. Therefore, imidazolium-salt cations were covalently coupled to AMPs and the influence on the antimicrobial activity was investigated. Conjugates containing one imidazolium-salt cation and a branched conjugate consisting of an AMP and four ionic liquids (namely IL-KKA) were already synthesized and tested during my master thesis (Figure 6).

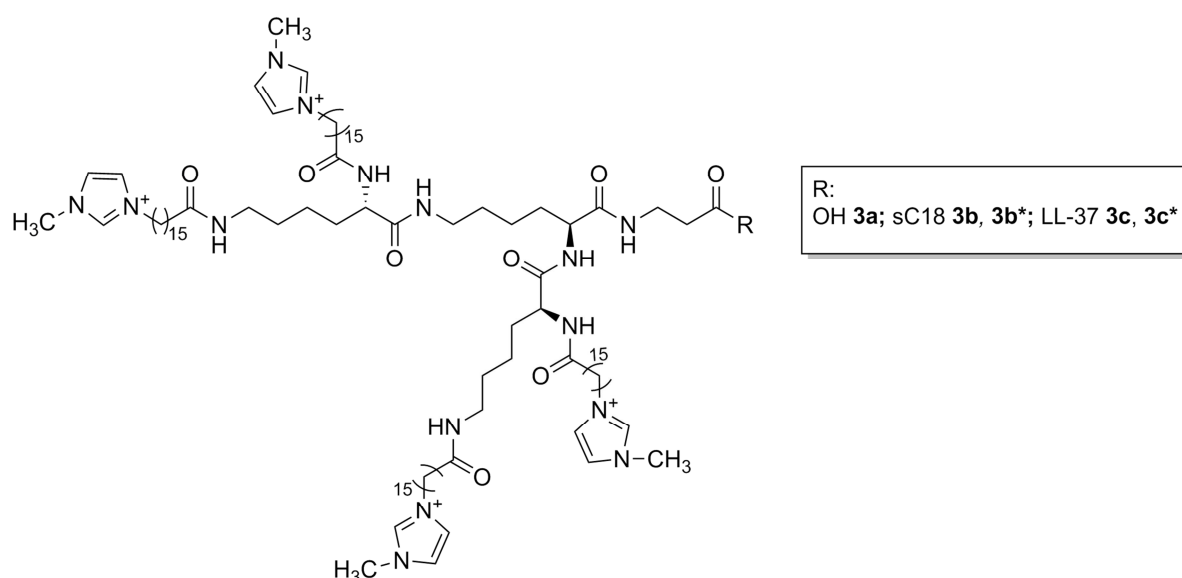


**Figure 6: Final structure of 3a, 3b and 3c.** \* CF-labelled peptides at the  $\epsilon$ -amino group of lysine (Table 6).

The results showed that four molecules of imidazolium-salts coupled to AMPs increased the antimicrobial activity dramatically compared to the mono imidazolium salt conjugate. Antimicrobial activity for **3a**, **3b** and **3c**, peptide conjugates containing four imidazolium salts (see table 6 for peptide sequences), is shown in Figure 7.  $[(C_{16}C_1)im]Br^-$  was used as a negative control. **3a** showed a toxic effect against all bacterial strains in particular against *B. subtilis*. An increase of the antimicrobial activity could be reached by coupling sC18 to compound **3a**, leading to compound **3b**. Against *B. subtilis* the three peptides demonstrated a relevant toxic effect since after treatment with 5  $\mu$ M concentration only 5% of bacteria survived, while using *E. coli* only **3a** and **3b** reached this high toxic effect at 5  $\mu$ M concentrations. Contrarily, the highest toxicity against *M. phlei* is already reached at 1  $\mu$ M for all peptides with 30% living bacteria and no further increase after enhanced peptide concentration.

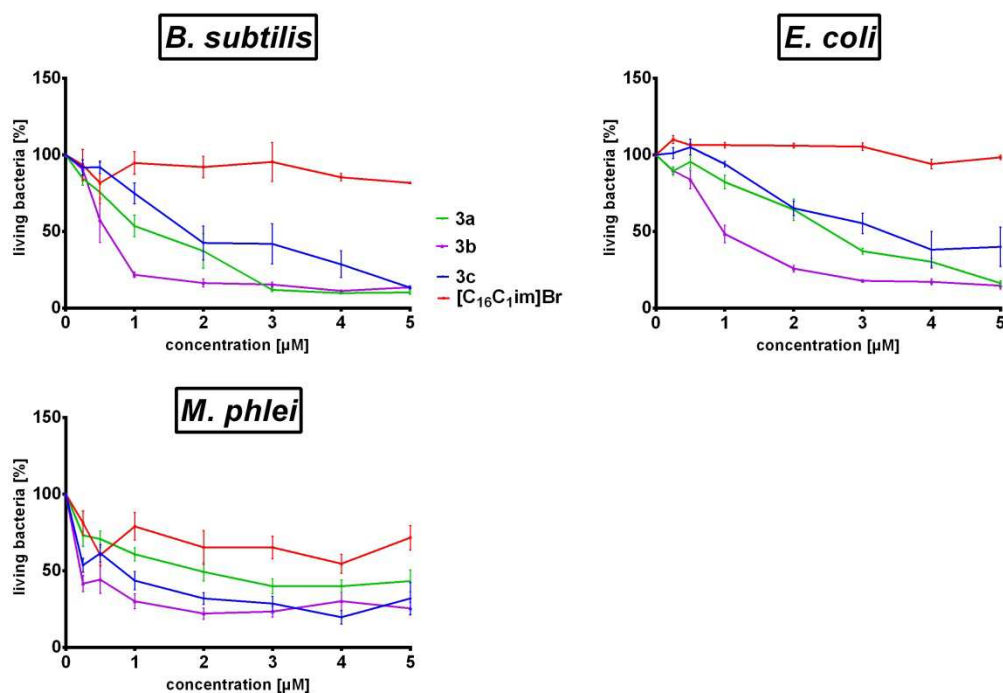


**Figure 7: Antimicrobial activity of 3a, 3b and 3c.** INT-assay was performed against *B. subtilis*, *E. coli* and *M. phlei*. Negative control was set up to 100%.

Besides the peptide sC18, already described in chapter 1.2., also the LL-37 peptide was investigated during this work. The LL-37 peptide is a 37 amino acids long segment of the FALL-39 peptide, which is known as the only human cathelicidin-derived AMP. LL-37 was identified as an antimicrobial peptide, expressed in the bone marrow, with activity against gram-positive as well as gram-negative bacteria (174). The proposed mechanism for LL-37 is the carpet-like mechanism (175).

## 1.10. Aim of the thesis

Aim of this work was to design new and more potent antimicrobial peptides as well as conjugates thereof, and to elucidate their antimicrobial activity spectrum as well as their mechanism of action.

The first part of the thesis deals with further modification of imidazolium salt-peptide conjugates to improve their antimicrobial activity and selectivity. Therefore, conjugates already developed during my master thesis, including the peptides sC18 and LL-37, should be further evaluated concerning their activity against resistant bacterial strains, as well as their activity mechanism.

Further work should then investigate the potential of the short IL-KKA peptide to act as an anti-biofilm compound when immobilized on polyether sulfone (PES) membranes. Different coating strategies should be used and the activity of the functionalized membranes should be characterized by different physical as well as biological techniques.

The second goal of this work was to improve the antimicrobial activity of sC18. Since the parent C18 peptide already showed antimicrobial activity it should be tested if the introduction of hydrophobic amino acids could return this antimicrobial activity to the shorter sC18 peptide. Therefore, several amino acids within the sequence of sC18 should be exchanged with either isoleucine or phenylalanine, respectively, and the antimicrobial activity should be tested. To verify the influence of the amino acid exchange, structural characteristics and antimicrobial activity against different bacterial strains should be determined.

## 2. Materials and methods

### 2.1. Materials

All chemicals, reagents and consumables, which were used during this work, were obtained from Fluka (Taufkirchen, Germany), Merck (Darmstadt, Germany), Sarstedt (Nümbrecht, Germany), Sigma-Aldrich (Taufkirchen, Germany) and VWR (Darmstadt, Germany).

For peptide synthesis, all N<sup>α</sup>-Fmoc protected amino acids were achieved from Iris Biotech (Marktredwitz, Germany). The side-chains of the trifunctional amino acids were equipped with acid-labeled protection groups to make use of the orthogonal Fmoc/tBu strategy for peptide synthesis. Protection groups for the regular amino acids were Pbf (Arg), Trt (Asn, Gln, His, Cys), Boc (Trp, Lys) and *tert*-butyl (Asp, Glu, Ser, Thr, Tyr). For branched peptide compounds, Fmoc-L-Lys(Fmoc)-OH was used while for CF-labeled peptides Fmoc-L-Lys(Dde)-OH was used.

For the calculation of the peptide concentrations, the binding of TFA anions to positively charged amino acid side chains and free amino groups was taken into consideration.

## 2.1.1. Equipment

**Table 3: Equipment used during this work.**

<b>Equipment</b>	<b>Producer</b>
<b>CD spectrometer</b>	Jasco Corp. J715
<b>Centrifuges</b>	Thermo Scientific; Multifuge X1R Thermo Scientific; PicO 17
<b>ELISA-mircoplate reader</b>	Biotek – EL 808
<b>Heating block</b>	Eppendorf – Thermomixer compact
<b>HPLC (analytic)</b>	Hewlett Packard Series 1100, Agilent 1100 Series; Column: Machery-Nagel, 2,6 u, C18, 100 A, 125 x 4.6 mm Elite Lachrom Hitachi Pump L-2130, Elite
<b>HPLC (preparative)</b>	Lachrom Hitachi Autosampler L-2200, Elite Lachrom Hitachi Diode Array Detector L-2455, Teoedyne ISCO Fraction Collector Foxy R1, Column: Machery-Nagel, 2,6 u, C18, 100 A, 250 x 16 mm, 4 micron
<b>Mass spectrometer</b>	Thermo Scientific LTQ-XL
<b>Lyophilizer</b>	Leybold Christ; Alpha 2-4 LDplus
<b>Spectral photometer</b>	Thermo Scientific Genesys 10S UV-Vis
<b>Speed-Vac</b>	Thermo Scientific Speedvac Concentrator Savant SC210A, RVT5105 Refrigerated Vapor Trap VLP80 Vacuum Pump
<b>Synthesis roboter</b>	MultiSynTech Syro I

<b>Vortex</b>	Scientific Industries – Vortex Genie 2
<b>Xcel Vap</b>	Horizon Technology

## 2.1.2. Buffers

**Table 4: Buffers used during this work.**

<b>Giant unilamellar vesicle buffer</b>	10 mM HEPES buffer, pH 7.4 50 mM KCl 50 mM NaCl 1mg/mL dextran (from <i>Leuconostoc spp.</i> , 6 kDA) 5 µM Oyster 405
<b>Iodnitrotetrazolium violet solution</b>	10 mg Iodnitrotetrazolium-chloride 10 mL DMSO (cell culture quality)
<b>Kaiser test solutions</b>	Solution I (1 g ninhydrin in 20 mL EtOH) Solution II (80 g phenol in 20 mL EtOH) Solution III (0.4 mL aqu. KCN-solution (1mM) in 20 mL pyridine)
<b>Mueller-Hinton medium (Pronadisa-Conda)</b>	2.0 g/L Beef Infusion 1.5 g/L Corn Starch 17.5 g/L Casein Peptone (acidic hydrolysate) pH 7.4 21 g/L Mueller-Hinton Broth in deionized water
<b>Mueller-Hinton agar plates</b>	21 g/L Mueller-Hinton Broth 15 g bacteriologic Agar

### 2.1.3. Bacterial strains

*Bacillus subtilis* (ATTC 6633)

*Corynebacterium glutamicum* (ATCC 13032)

*Escherichia coli* K12 (MG 1625)

*Micrococcus luteus* (DSM 20030)

*Mycobacterium phlei* (DSM 48214)

*Pseudomonas fluorescens* (DSM 50090)

*Salmonella typhimurium* (TA 100)

Methicillin-resistant *Staphylococcus aureus*

Vancomycin-resistant *Enterococci*

### 2.1.4. Peptide sequences

**Table 5: Peptides synthesized during this work.**

Peptide	Sequence
<b>1a (sC18)</b>	GLRKRLRKFRNKIKEK-NH <sub>2</sub>
<b>2a (LL-37)</b>	LLGDFFRKSKEKIGKEFKRIVQRIKDFLRNLVPRTES-NH <sub>2</sub>
<b>3a (IL-KKA)</b>	IL <sub>4</sub> -KK(εK)βA-OH
<b>3b (IL-KKA-sC18)</b>	IL <sub>4</sub> -KK(εK)βA-GLRKRLRKFRNKIKEK-NH <sub>2</sub>
<b>3b* (IL-KKA-sC18)</b>	IL <sub>4</sub> -KK(εK)βA- GLRKRLRKFRNKIKEK(CF)-NH <sub>2</sub>
<b>3c (IL-KKA-LL-37)</b>	IL <sub>4</sub> -KK(εK)βA- LLGDFFRKSKEKIGKEFKRIVQRIKDFLRNLVPRTES-NH <sub>2</sub>
<b>3c* (IL-KKA-LL-37)</b>	IL <sub>4</sub> -KK(εK)βA- LLGDFFRKSKEKIGKEFKRIVQRIK(CF)DFLRNLVPRTES-NH <sub>2</sub>
<b>3d (IL-KKA-Ahx-Ahx-G)</b>	IL <sub>4</sub> -KK(εK)βA -Ahx-Ahx-G-OH
<b>3e (IL-KKA-FF)</b>	IL <sub>4</sub> -KK(εK)βA -FF-OH

<b>3f (IL-KKA-WLLKW)</b>	IL <sub>4</sub> -KK(εK)βA -WLLKW-OH
<b>sC18I1</b>	ILRKRLRKFRNKIKEK-NH <sub>2</sub>
<b>sC18I2</b>	GIRKRLRKFRNKIKEK-NH <sub>2</sub>
<b>sC18I3</b>	GLIKRLRKFRNKIKEK-NH <sub>2</sub>
<b>sC18I4</b>	GLRIRLRKFRNKIKEK-NH <sub>2</sub>
<b>sC18I5</b>	GLRKILRKFRNKIKEK-NH <sub>2</sub>
<b>sC18I6</b>	GLRKIRKFRNKIKEK-NH <sub>2</sub>
<b>sC18I7</b>	GLRKRLIKFRNKIKEK-NH <sub>2</sub>
<b>sC18I8</b>	GLRKRLRIFRNKIKEK-NH <sub>2</sub>
<b>sC18I9</b>	GLRKRLRKIRNKIKEK-NH <sub>2</sub>
<b>sC18I10</b>	GLRKRLRKFINIKIKEK-NH <sub>2</sub>
<b>sC18I11</b>	GLRKRLRKFRNIKIKEK-NH <sub>2</sub>
<b>sC18I12</b>	GLRKRLRKFRNIIKEK-NH <sub>2</sub>
<b>sC18I14</b>	GLRKRLRKFRNKIIIEK-NH <sub>2</sub>
<b>sC18I15</b>	GLRKRLRKFRNKIKIK-NH <sub>2</sub>
<b>sC18I16</b>	GLRKRLRKFRNKIKEI-NH <sub>2</sub>
<b>sC18I10I15</b>	GLRKRLRKFINKIKIK-NH <sub>2</sub>

<b>sC18I10I16</b>	GLRKRLRKFINIKI EI-NH <sub>2</sub>
<b>sC18I15I16</b>	GLRKRLRKFRNKIKII-NH <sub>2</sub>
<b>sC18I10I15I16</b>	GLRKRLRKFINIKIKII-NH <sub>2</sub>
<b>sC18F10</b>	GLRKRLRKFFNIIKIEK-NH <sub>2</sub>
<b>sC18F15</b>	GLRKRLRKFRNKIKFK-NH <sub>2</sub>
<b>sC18F16</b>	GLRKRLRKFRNKIIEF-NH <sub>2</sub>
<b>sC18F10F15</b>	GLRKRLRKFFNIIKFK-NH <sub>2</sub>
<b>sC18F10F16</b>	GLRKRLRKFFNIIIEF-NH <sub>2</sub>
<b>sC18F15F16</b>	GLRKRLRKFRNKIKFF-NH <sub>2</sub>
<b>sC18F10F15F16</b>	GLRKRLRKFFNIIKFF-NH <sub>2</sub>

\* Peptides were labeled with 5(6)-carboxyfluorescein (CF).

## 2.2. Solid phase peptide synthesis (SPPS)

### 2.2.1. Loading of Wang-resin with the first amino acid

For the peptides **3a**, **3d**, **3e** and **3f**, the first amino acid had to be preloaded to a Wang resin. Therefore, 30 mg Wang resin (loading 1.1 mmol/g) was swollen for 15 min in dimethylformamide (DMF). DMF was removed and 5 eq. Fmoc-amino acid, 5 eq. Oxyma Pure and 5 eq. N',N'-diisopropylcarbodiimide (DIC) were dissolved in 500 mL DMF and added to the resin beads. The solution was shaken over night at room temperature (RT). On the next day, the resins were washed five-times with DMF, dichloromethane (DCM), methanol and diethylether. Afterwards, the resins were dried using a SpeedVac.

### 2.2.2. Determination of the first residue attachment

To quantify the coupling of the first amino acid toward the Wang resin, the Fmoc-group was cleaved and the absorption was measured.

Therefore, 500  $\mu\text{L}$  30% piperidine in DMF was incubated with 3 mg Wang resin beads for 30 min at RT. 250  $\mu\text{L}$  of the solution were mixed with 1.5 mL DMF and the absorbance at 301 nm was measured. As blank 250  $\mu\text{L}$  30% piperidine in DMF was added to 1.5 mL DMF. The loading was calculated using the following equation (Formula 1):

$$L_{301\text{ nm}} \left[ \frac{\text{mmol}}{\text{g}} \right] = \frac{E_{301\text{ nm}}}{\epsilon [M^{-1}\text{cm}^{-1}] \times D[\text{cm}]} \times \frac{2 \times V[\text{ml}]}{m_{\text{Harz}}[\text{g}]} \quad (1)$$

E = extinction at 301 nm

V = volume

$\epsilon$  = extinction coefficient of Fmoc (7800)

m = mass of weight resin (g)

D = density of cuvette.

### 2.2.3. Automated peptide synthesis

To generate longer peptides, a synthesis robot from MultiSynTech was used. The required amino acid solutions and reaction reagents were prepared manually. Rink amid resin (substitution 0.48 mmol/g, 0.015 mmol scale) or preloaded Wang resin (0.015 mmol scale) were swollen for 10 min in 800  $\mu\text{L}$  DMF and after that, the deprotection of the Fmoc group was performed using 40% piperidine for 3 min and 20% piperidine for 10 min in DMF. Resins were washed four times with 600 mL DMF and the coupling of the N <sup>$\alpha$</sup> -Fmoc-protected amino acid was performed. Hereby, 8 eq. (300  $\mu\text{L}$ ) of the amino acid and 2.4 M (50  $\mu\text{L}$ ) Oxyma Pure were mixed and incubated for 3 min. Then, 2.4 M (50  $\mu\text{L}$ ) DIC was added to the solution and incubated for 40 min at RT. (Due to Oxyma Pure and DIC, the carboxyl group of the amino acid gets activated.) The resins were washed twice with 800  $\mu\text{L}$  DMF. Each coupling was performed as a double coupling step. The synthesis robot repeats this procedure until the peptide is synthesized. Then, resins were washed

manually five times with DCM, methanol and diethylether and dried in the SpeedVac.

#### 2.2.4. Manual coupling of ionic liquids and 5(6)-carboxyfluorescein

For manual coupling, the resin was swollen for 15 min in 1 mL DMF. Then, 5 eq. ionic liquid, or 3 eq. 5(6)-carboxyfluorescein (CF), respectively, was added with 5 eq. or 3 eq. HATU in 300  $\mu$ L DMF. After that, diisopropylethylamine (DIPEA) (5 eq. for ionic liquids and 3 eq. for CF) were added to the mixture and incubated for 2 min. The solution was added for 2 h to the resin at RT. The resin was washed five times with DMF and again incubated with IL or CF, HATU and DIPEA for 2 h at RT. After the second coupling, the resin was washed five times with DMF, DCM, methanol and diethylether and dried using a SpeedVac.

#### 2.2.5. Endcapping

To block free reactive groups and amino acid side-chains during a peptide synthesis, an endcapping was performed.

Therefore, the resin was swollen for 15 min in 1 mL DCM. After the DCM was removed, 50  $\mu$ L acetic anhydride and 50  $\mu$ L DIPEA were dissolved in 500  $\mu$ L DCM and added to the resin. The resin was shaken for 15 min at RT. In the end, the resin was washed five times with DCM, methanol and diethylether and dried using a SpeedVac.

#### 2.2.6. Fmoc cleavage

To couple the next amino acid towards a peptide sequence, first, the Fmoc-protection group had to be removed.

Therefore, the resin was swollen in 300  $\mu$ L DMF for 15 min. Then, 300  $\mu$ L 20% piperidine (in DMF) were added to the resin and incubated for 5 min. Afterwards the resin was washed five times with DMF, 300  $\mu$ L 20% piperidine were added again to the resin for 15 min. In the end, the resin was washed five times with DMF, DCM, methanol and diethylether and dried using a SpeedVac.

### 2.2.7. Cleavage of the Dde-protection group

For CF-labeled peptides, Fmoc-Lys(Dde)-OH was used to couple the CF at the  $\epsilon$ -side chain of the lysine.

For the cleavage of the Dde-protection group, the resin was swollen in 1 mL DMF for 15 min. After removing the DMF, 1 mL of 3% hydrazine in DMF was added to the resin and incubated for 10 min at RT. The flow through was collected in a falcon and the resin was washed two times with 1 mL DMF. The washing solution was added to the flow through into the falcon. Then again, 1 mL of 3% hydrazine in DMF was added. This procedure was repeated ten times and the amount of cleaved Dde in step 1 and step 10 was determined measuring the absorption at 301 nm. As a blank 2 mL DMF with 1 mL of 3% hydrazine in DMF were used. If the  $OD_{301nm}$  was less than 0.1, the deprotection was successful. After the cleavage, the resin was washed five times with DMF, DCM, methanol and diethylether and dried using a SpeedVac.

### 2.2.8. Kaiser test

To check the completion of an amino acid coupling to the peptide sequence, a visual test was used indicating the presence or absence of free amino groups.

One drop of each solution was added to a few resin beads: solution I (1 g ninhydrin in 20 mL EtOH); solution II (80 g phenol in 20 mL EtOH) and solution III (0.4 mL aqu. KCN solution (1 mM) in 20 mL pyridine). As negative control, a sample without resin beads was used and as positive control, N-ethyl-diisopropylamine was used. The samples were incubated for 5 min at 95 °C. If the solution turned yellow, no free amino groups were present, while a blue color is a hint for free amino groups.

### 2.2.9. Sample cleavage

The sample cleavage was performed to verify the coupling success and to analyze the composition of the products.

2.5  $\mu$ L triisopropylsilane (TIS) and 2.5  $\mu$ L  $H_2O_{dd}$ , working as scavenger, were added to a small amount of dry resin beads. For peptide **3d**, 7  $\mu$ L thioanisole and 3  $\mu$ L 1,2-ethanedithiol were used as scavenger due to the presence of tryptophan in the peptide sequence. The mixture was filled up to 100  $\mu$ L with trifluoroacetic acid

(TFA). After 3 h shaking at RT, 1 mL ice-cold diethylether was added for at least 20 min at -20 °C to precipitate the peptide. The peptide was washed five times with diethylether by centrifugation at 10,000 x g for 5 min. After each centrifugation step, the supernatant was discarded and the pellet again resuspended in diethylether. The pellet was dried using a SpeedVac and dissolved in 100 µL H<sub>2</sub>O<sub>dd</sub> or 100 µL H<sub>2</sub>O<sub>dd</sub> /tBuOH (3:1). The peptide solution was diluted in either 10% acetonitrile/ 90% H<sub>2</sub>O<sub>dd</sub> + 0.1% formic acid (FA) or 10% acetonitrile/ 90% H<sub>2</sub>O<sub>dd</sub> + 0.1% TFA for qualitative and quantitative analysis, respectively.

### 2.2.10. Full cleavage

With the full cleavage, all protection groups were removed from the peptide and the peptide was cleaved from the resin.

25 µL TIS and 25 µL H<sub>2</sub>O<sub>dd</sub> were added to the dry resin. For peptide **3d**, 70 µL thioanisole and 30 µL 1,2-ethanedithiol were used due to the tryptophan in the peptide sequence. The mixture was filled up to 1 mL with TFA and shaken for 3 h at RT. After that, the peptide was precipitated in 10 mL ice-cold diethylether. The resin was washed with 200 µL TFA and the solution was added to diethylether. The mixture was stored for at least 20 min at -20 °C to precipitate the peptide. Afterwards, the peptide was washed five times with 10 mL diethylether by centrifugation at 5,000 x g for 5 min. After every centrifugation step, the supernatant was discarded and the pellet was resuspended in 10 mL diethylether. The pellet was dried using a SpeedVac and dissolved in 2-3 mL H<sub>2</sub>O<sub>dd</sub> or 2-3 mL H<sub>2</sub>O/tBuOH (3:1). One part of the peptide solution was diluted with either 10% acetonitrile/ 90% H<sub>2</sub>O<sub>dd</sub> + 0.1% formic acid (FA) or 10% acetonitrile / 90% H<sub>2</sub>O<sub>dd</sub> + 0.1% TFA for qualitative and quantitative analysis, respectively. The rest of the peptide solution was lyophilized.

### 2.2.11. LC-mass spectrometry with 0.1% FA for qualitative analysis

The peptide solution was analyzed qualitatively by reverse-phase liquid chromatography mass spectrometry (RP-HPLC-MS) using a Nucleodur column (100-5; C18ec; 4.6 x 125 mm) from Macherey-Nagel. 10 µL of the diluted peptide solution were injected into the RP-HPLC and separated by an acetonitrile gradient increasing from 10% up to 60% in 15 min. The flow rate was set to 0.6 mL/min.

After HPLC, the eluent was injected into a LTQ-XL ESI-MS. Pseudo molecular ions were generated and a full mass spectrum was acquired.

#### 2.2.12. RP-HPLC with 0.1% TFA for purity analysis

The purity of the peptides was determined by reverse-phase liquid chromatography (RP-HPLC) using a Nucleodur column (100-5; C18ec; 4.6 x 125 mm) from Macherey-Nagel. 10  $\mu$ L of the diluted peptide solution were injected into the RP-HPLC and separated by an acetonitrile gradient increasing from 10% up to 60% in 15 min. The flow rate was set to 0.6 mL/min. The UV-chromatogram was used to determine the percentage of the peptide purity.

#### 2.2.13. Preparative RP-HPLC with 0.1% TFA

The preparative RP-HPLC was used to purify the peptide. A Nucleodur column (1005; C18ec; 16 x 250 mm) from Macherey-Nagel was used. The column was equilibrated with 10% acetonitrile in H<sub>2</sub>O<sub>dd</sub> + 0.1% TFA for 15 min. For purification, an acetonitrile gradient from 10% to 60% in 45 min was used. The flow rate was 6 mL/min and the peptide was detected at 220 nm. Acetonitrile was removed with the Xcel Vap and the sample was lyophilized.

#### 2.2.14. Synthesis of ionic liquids

Ionic liquids were synthesized by the group of AG Giernoth by Julie Piper gen. Schmauck (176).

### 2.3. Characterization methods

#### 2.3.1. Circular dichroism spectroscopy

Circular dichroism (CD) spectroscopy was used to determine the secondary structure of the synthesized peptides. All CD spectra were measured with a Jasco Corp. J715 spectrometer at 20 °C. A 20  $\mu$ M peptide solution in 10 mM phosphate buffer, pH 7.0 or 10 mM phosphate buffer/TFE (1:1 v/v), pH 7.0 was prepared. Peptide solutions were filled into a 0.1 cm quartz cell and a spectrum was recorded from wavelength 180 to 260 nm in 0.2 nm intervals. The measurement was

performed in triplicate. The scanning speed was 50 nm/min and the sensitivity 100 mdegrees.

### 2.3.2. Preparation of large unilamellar vesicle (LUVs)

LUVs were prepared combining either 1,2-dioleoyl-sn-glycero-3-phosphoethanolamine (DOPE) and 1,2-dioleoyl-sn-glycero-3-[phospho-rac-(1-glycerol)] (DOPG) (DOPE/DOPG 80:20) to imitate a gram-negative bacterial membrane, or by combination of DOPE, DOPG and cardiolipin (CL) (DOPE/DOPG/CL 15:80:5) to imitate a gram-positive bacterial membrane. Lipid mixtures were dissolved in 1 mL chloroform and the chloroform was evaporated under reduced pressure. Then, the lipid film was dissolved in 1 mL 10 mM phosphate buffer, pH 7.0 and ten times frozen and melted in liquid nitrogen. In a next step, the suspension was passed 21 times through a mini-extruder equipped with a 0.4  $\mu\text{m}$  polycarbonate track-etch membrane (Avanti Polar Lipids, Alabaster, USA). The size of the vesicle was determined via dynamic light scattering.

### 2.3.3. Circular dichroism with LUVs

20  $\mu\text{M}$  peptide solution was added to 1 mM LUVs in 10 mM phosphate buffer, pH 7.0. The CD measurement was performed as written above.

### 2.3.4. Preparation of giant unilamellar vesicle (GUVs)

The preparation of giant unilamellar vesicles (GUVs) was performed by Mareike Horn. In brief, GUVs were prepared combining 1,2-dioleoyl-sn-glycero-3-phosphocholine (DOPC), Atto550 labeled DOPE and different amounts of cholesterol. In a first step, super low melting agarose (1% w/v) was coated on a glass slide and dried for 30 min at 50 °C. After that, 10  $\mu\text{L}$  of DOPC and DOPE solution were spread on the agarose layer and dried *in vacuo* for at least 1 h. In a next step, a seal ring was placed on the lipid coated agarose film. For the preparation of GUVs with encapsulated Oyster 405, a 10 mM HEPES buffer, pH 7.4, 50 mM KCl, 50mM NaCl, 1mg/mL dextran (from *Leuconostoc spp.*, 6 kDA) and 5  $\mu\text{M}$  Oyster 405 was used. After adding the buffer into the seal ring, the glass slide

was left for 2 h in the dark to allow the lipids to swell. For harvesting the GUVs, the glass slide was tilted gently in all directions. The GUVs were used within three days.

### 2.3.5. CLSM observation of GUVs treated with peptide conjugates

The CLSM observation with GUVs and peptides were performed by Mareike Horn. In brief, GUVs were centrifuged at 14.000 x g for 10 min at RT to remove untrapped Oyster 405. 40  $\mu$ L GUV solution was diluted with 50  $\mu$ L of the respective HEPES buffer described above and transferred into a tissue culture vessel. CF-labeled peptide conjugates were added to the GUVs with a final concentration of 5  $\mu$ M.

The GUV-peptide interaction was analyzed using a confocal laser scanning system (Nikon D-Eclipse C1) containing an inverted microscope (Nikon Eclipse Ti) with an 20x objective (N.A. 0.45, Plan Flour; Nikon). The fluorescence intensity was determined using ImageJ.

## 2.4. Biological methods

### 2.4.1. Antimicrobial activity

The iodnitrotetrazolium-purple assay was performed to determine the viability of different bacteria. Only viable bacteria convert tetrazolium to formazan, therefore, the absorption is proportional to the bacterial number.

*For imidazolium-salt conjugates:* Each bacterial strain was incubated overnight in Müller-Hinton medium at 30 °C. The next day, the optical density (OD) at 600 nm was determined and the bacteria culture was diluted to an  $OD_{600nm} = 0.7$ . In each well of a 96-well plate, 180  $\mu$ L Müller-Hinton medium, 10  $\mu$ L bacteria suspension and 10  $\mu$ L of peptide conjugates (concentration 5  $\mu$ M, 4  $\mu$ M, 3  $\mu$ M, 2  $\mu$ M, 1  $\mu$ M, 0.5  $\mu$ M and 0.25  $\mu$ M) were added. As positive control, gentamicin (for *B. subtilis*), streptomycin (for *M. phlei*) and tetracycline (*E. coli*) and as negative control, H<sub>2</sub>O<sub>dd</sub> was used. Bacteria were incubated with peptide-conjugates for 6 h at 30 °C. Then, 10  $\mu$ L INT solution (iodnitrotetrazolium-chloride 1 mg/mL in DMSO) were added to each well and incubated for 30 min at 37 °C. The viability was analyzed measuring the absorption at 540 nm. Negative control was set to 100%.

*For sC18 variants:* Each bacterial strain was incubated in a subculture overnight at 37 °C. The next day, the sub culture was given to 100 mL fresh Müller-Hinton

medium and bacteria were grown to an  $OD_{600nm} = 0.7$ . Then, the INT-assay was performed as written above with the difference that everything was performed at 37 °C.

#### 2.4.2. Killing assay using resistant bacterial strains

The killing assay was performed by Dr. Andreas Schubert at the Fraunhofer Institute for Cell Therapy and Immunology, Leipzig. It was performed against vancomycin-resistant *Enterococci* (VRE) and methicillin-resistant *Staphylococcus aureus* (MRSA). In brief, an overnight bacteria culture was diluted to an  $OD_{600nm} = 0.05$  in Trypticase-Soya-Bouillon and incubated for 2 h at 37 °C. After an  $OD_{600nm} = 0.3$  was reached, VRE bacteria were diluted to 700 cfu/180  $\mu$ L in 10 mM PPB and 0.5% LB-medium (MRSA bacteria to 500 cfu/180  $\mu$ L in 10 mM PPB and 2% LB-medium). 180  $\mu$ L of the solution was transferred to 20  $\mu$ L peptide solution at different concentrations and shaken at 37 °C for 1 h. Then, bacteria were plated on Bacto Brain Heart Infusion (BD) agar plates and incubated overnight at 37 °C. The next day, the bacteria colonies were counted.

#### 2.4.3. Hemolytic activity

Human red blood cells (h-RBCs) were used to determine the hemolytic activity based on the release of hemoglobin. H-RBCs were centrifuged at 5,000 x g at 4 °C for 10 min and three times washed with PBS by centrifugation at 4,000 x g at 4 °C for 10 min. After each washing step, h-RBCs were resuspended in PBS. 50  $\mu$ L peptide solution were added to 50  $\mu$ L of h-RBCs in PBS to a final concentration of 4% v/v. The solution was incubated for 60 min at 37 °C and centrifuged at 1,000 x g for 5 min. The supernatant was added into 96-well plates and the absorbance of the released hemoglobin was measured at 550 nm. As negative control, only PBS was used, while 0.1% Triton X-100 acts as positive control. Percentage of hemolysis was calculated (Formula 2):

$$\% \text{ hemolysis} = \frac{(A_{550nm} \text{ of erythrocytes plus peptide} - A_{550nm} \text{ of erythrocytes in PBS})}{(A_{550nm} \text{ of erythrocytes in 0.1 \% Triton - X 100} - A_{550nm} \text{ of erythrocytes in PBS})} \times 100 \quad (2)$$

#### 2.4.4. Immobilization and characterization of polyether sulfone membranes (PES)

Immobilization and characterization of polyether sulfone membranes were performed by Dr. Agnes Schulze at the Institute for Surface Modifications in Leipzig. For peptide immobilization, the PES membrane disc ( $\varnothing$  10 mm) was immersed into a peptide solution (2.5 mg/mL in ultrapure water) for 5 min followed by electron beam irradiation (E-Beam) with a dose of 50, 100 or 150 kGy. Irradiation was performed in N<sub>2</sub> atmosphere with O<sub>2</sub> quantities < 10 ppm. The voltage and the current were set to 160 kV and 10 mA, respectively. Then, the irradiated membrane was rinsed three times for 30 min with ultrapure water and dried at ambient temperature.

Alternatively, peptides were immobilized by a chemical linker system. For this purpose, the membranes had first to be functionalized with amino groups at the surface. The PES membrane disc ( $\varnothing$  47 mm) was immersed into a solution of 2-aminoethyl methacrylate hydrochloride (AEMA) (0.5 wt. % in water) for 30 min followed by E-Beam irradiation (150 kGy). Then, the samples were washed with water (three times for 30 min) and dried at ambient temperature. The membranes were cut into 10 mm discs and were treated with an aqueous solution of the peptide (2.5 mg/mL), N-hydroxysuccinimide (NHS) (5 mg/mL), and 1-ethyl-3-(3-dimethylaminopropyl)carbodiimide (EDC) (5 mg/mL). The coupling was allowed to react overnight at RT. Then, membranes were washed three times for 30 min with ultrapure water and dried at ambient temperature.

The membrane morphology was investigated by scanning electron microscopy (SEM, Ultra 55, Carl Zeiss SMT, Jena, Germany).

The chemical surface composition was analyzed with X-ray photoelectron spectroscopy (AXIS Ultra, Kratos Analytical, Manchester, England). The kinetic energy of the electrons was analyzed with a pass energy of 160 eV for the survey spectra and 40 eV for the energy resolved spectra, respectively.

#### 2.4.5. Antimicrobial activity with immobilized PES membranes

For antimicrobial activity tests, the gram-positive bacterium *Bacillus subtilis* (ATCC 6633) was used as test strain. The bacteria were cultured in Mueller-Hinton Broth (MHB) medium overnight at 37 °C and diluted to an OD<sub>600nm</sub> = 0.001 (correspond to

10<sup>6</sup> bacteria/mL). PES membranes immobilized with peptides (control: membrane without peptide) were placed at the bottom of a 48 well-plate. In each well, 50 µL of bacteria suspension were added and the solution was incubated for 3 h at 37 °C. Bacteria suspensions were diluted 1:100 with PBS and 10 µL were exposed onto Mueller-Hinton agar plates. The next day, the grown bacteria colonies were counted. Additionally, to the membranes with the bacteria solution, 600 µL Mueller-Hinton medium were added and incubated for 24 h at 37 °C. Membranes were removed and 20 µL INT-solution were added for 30 min at 37 °C to the bacteria suspension. The 48-well plate was subsequently placed in an ELISA plate reader to measure absorption at 540 nm. Negative control was set up to 100%. All experiments were done in triplicate or duplicate with  $n=3$ .

### 3. Results and discussion

#### 3.1. Improvement of imidazolium salt-peptide conjugates and their mechanism of action

During my master thesis, the covalent combination of imidazolium salts and the peptides sC18 and LL-37 yielded new compounds with high antimicrobial activity against different bacterial strains. To further investigate the antimicrobial activity, the designed compounds should be tested against multi-resistant strains, which are heavy to threat with common antibiotics. Moreover, experiments were performed in order to investigate selectivity and mechanism of action of the newly designed compounds.

##### 3.1.1. Synthesis of imidazolium salt-peptide conjugates

For the new sets of experiment, the conjugates first had to be synthesized again. Table 6 gives an overview of all the synthesized imidazolium-salt peptide compounds. Remarkable is that the yield of all peptides containing IL<sub>4</sub>-KK(εK)βA in their sequence (**3b**, **3b\***, **3c** and **3c\***) was low (only 5-10%). A reason for this low peptide amount could be the fact, that as last coupling step, four imidazolium salts had to be simultaneously coupled to the already branched peptide sequence. Therefore, also side products with less than four imidazolium salts were obtained. Nevertheless, after purification via preparative HPLC all peptides showed a satisfying purity of around 98%.

**Table 6: Analytical and synthetic data of all imidazolium salt compounds.** Net-charge was determined by counting all lysine and arginine residues and the N-terminus. Calculated molecular weight was determined using a calculation software, while the experimental molecular weight, retention time and purity was determined using the UV-chromatograms und ESI-MS-spectra. The acetonitrile gradient was 10-60% acetonitrile in water in 15 min with 0.1% TFA.

Peptide	Sequence	Net charge	MW <sub>calc</sub> [Da]	MW <sub>exp</sub> [Da]	RT [min]	Purity [%]	Yield [%]
<b>1a (sC18)</b>	GLRKRLRKFRNKIKEK-NH <sub>2</sub>	+9	2069.6	2069.5	7.20	98	48
<b>2a (LL-37)</b>	LLGDFFRKSKEKIGKEFKRIVQRIKDFLRNLVPRTES-NH <sub>2</sub>	+7	4492.4	2234.8	8.40	98	54
<b>3a (IL-KKA)</b>	IL <sub>4</sub> -KK(εK)βA-OH	+4	1751.7	1752.1	18.78	98	20
<b>3b (IL-KKA-sC18)</b>	IL <sub>4</sub> -KK(εK)βA-GLRKRLRKFRNKIKEK-NH <sub>2</sub>	+14	3803.3	3802.8	17.27	97	20
<b>3b* (IL-KKA-sC18)</b>	IL <sub>4</sub> -KK(εK)βA- GLRKRLRKFRNKIKEK(CF)-NH <sub>2</sub>	+13	4161.6	4160.9	18.35	96	18
<b>3c (IL-KKA-LL-37)</b>	IL <sub>4</sub> -KK(εK)βA-LLGDFFRKSKEKIGKEFKRIVQRIKDFLRNLVPRTES-NH <sub>2</sub>	+11	6226.1	6226.0	18.62	98	12
<b>3c* (IL-KKA-LL-37)</b>	IL <sub>4</sub> -KK(εK)βA-LLGDFFRKSKEKIGKEFKRIVQRIK(CF)DFLRNLVPRTES-NH <sub>2</sub>	+10	6584.4	6584.5	18.81	97	10

The synthesis of the unmodified peptides **1a** and **2a** was performed by standard solid phase peptide synthesis. For peptides **3a**, **3b** and **3c** the imidazolium salt (Figure 8) was coupled on solid phase to the N-terminus of the peptide sequence. The final conjugates are depicted in Figure 8. Moreover, peptides **3b** and **3c** were also labeled with the fluorophore (**3b\*** and **3c\***) 5,(6)-carboxyfluorescein (CF). The CF-fluorophore was coupled to the  $\epsilon$ -amino group of the last lysine residue, to avoid steric hindrance with the imidazolium salts. The peptides were cleaved from the resin and fully deprotected using TFA and a scavenger cocktail. After purification with a preparative HPLC, all peptides were isolated as trifluoroacetate salts.

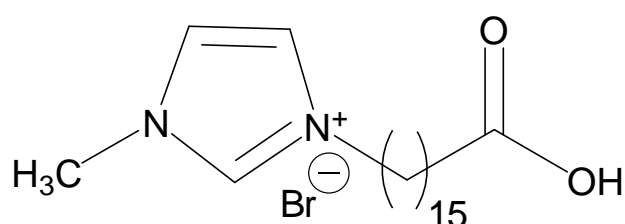


**Figure 8: Structure of the imidazolium salt used for peptide 3a, 3b and 3c.**

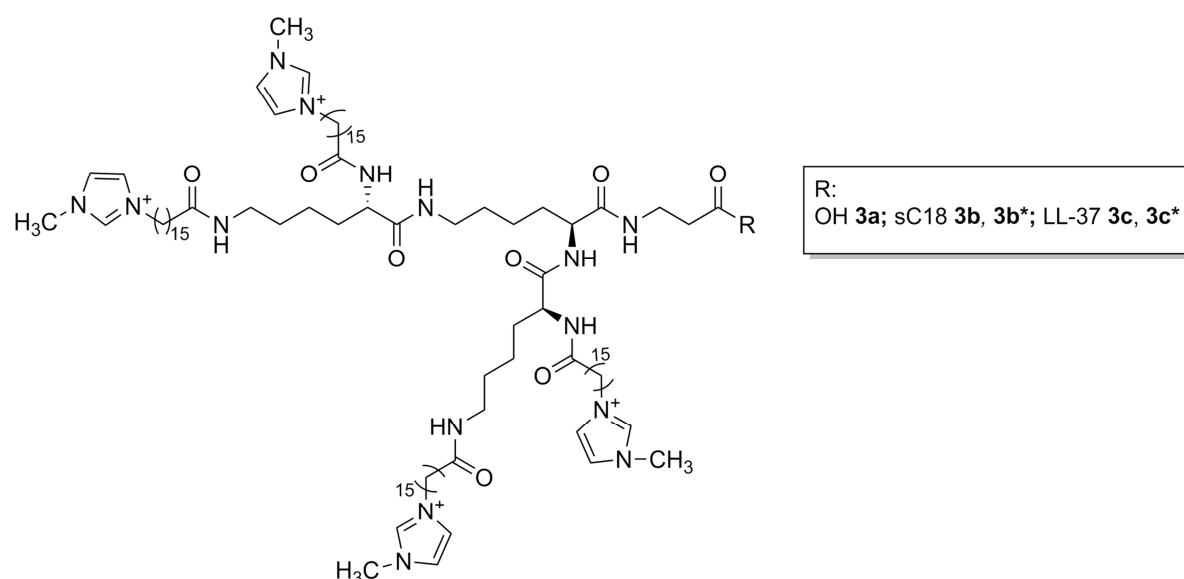


**Figure 9: Final structure of 3a, 3b and 3c.** \* CF-labeled peptides at the  $\epsilon$ -amino group of lysine (Table 6).

Figure 10 shows the UV-chromatogram and ESI-MS-spectrum of **3a** before and after the purification step via HPLC. The ESI-MS spectrum shows the 4-fold ( $[M]^{4+} = 438.06$ ), 3-fold ( $[M-H]^{3+} = 583.63$ ) and 2-fold ( $[M-2H]^{2+} = 931.30$ ) charged molecular peaks, corresponding to the peptide mass of **3a**

( $MW_{\text{calc}} = 1751.7$ ). After the purification step (Figure 10, right side), all impurities were removed and only the peak of the desired compound is detectable, again with the 4-fold, 3-fold and 2-fold charged molecular peaks. The reason why the 4-fold charged molecular peak contains no additional  $H^+$  ion can be explained through the four positive charges of the four imidazolium cations (Figure 9).

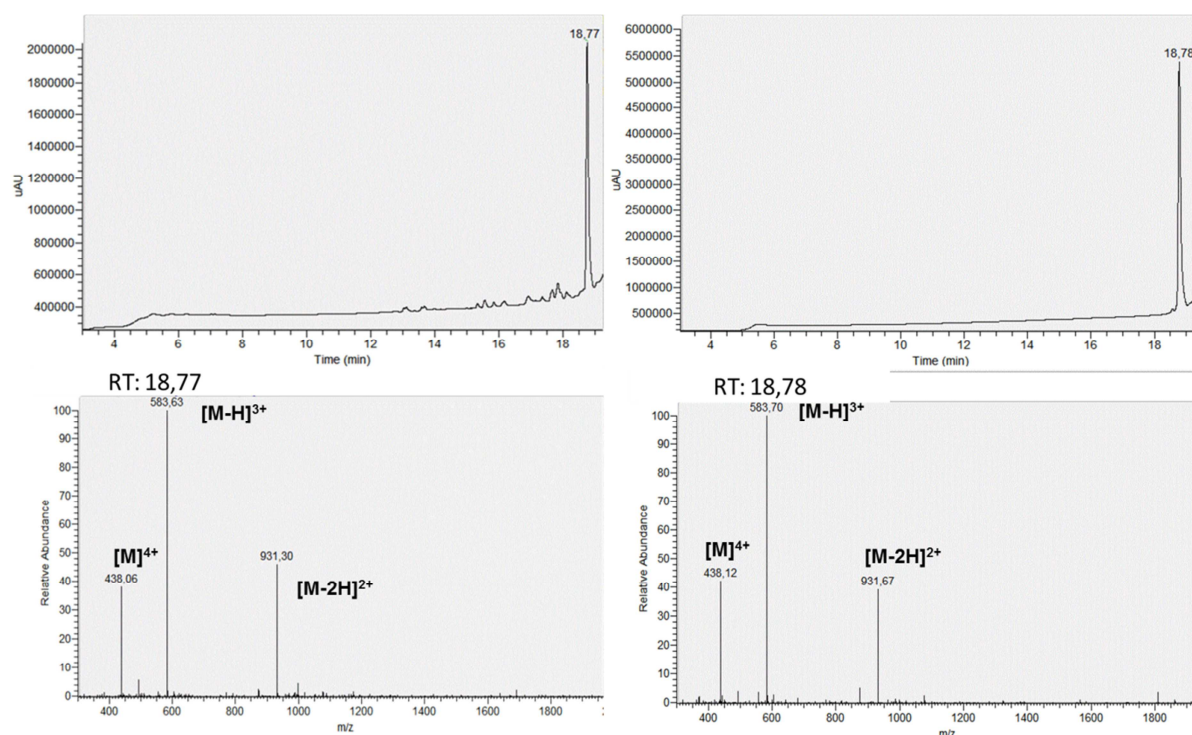


**Figure 10: HPLC-MS analysis of **3a** before and after purification via preparative HPLC.** Used gradient: acetonitrile in water 10-60% in 15 min. UV-chromatogram (above) and full scan ESI-MS were both performed with 0.1% TFA. On the left side the UV and ESI-spectrum before purification is shown with the product **3a** at a RT of 18.77 min. On the right side the UV and ESI-spectrum after purification is shown with the product **3a** at a RT of 18.78 min.

The purification of **3c** looks pretty similar to the one of **3a**. Before the purification (Figure 11, left side), a small side product can be detected in the UV-chromatogram, visible as a shoulder of the main product peak. This side product corresponds to an uncomplete coupling of the imidazolium salts to the peptide. After the purification (Figure 11, right side), this impurity is eliminated and only the main product peak is visible. In both spectra, before and after the purification, charged molecular peaks from the 8-fold ( $[M+4H]^{8+} = 778.89$ ) to the 4-fold ( $[M]^{4+} = 1556.12$ ) are detectable, which correspond to peptide **3c** ( $MW_{\text{calc}} = 6224.5$ ).

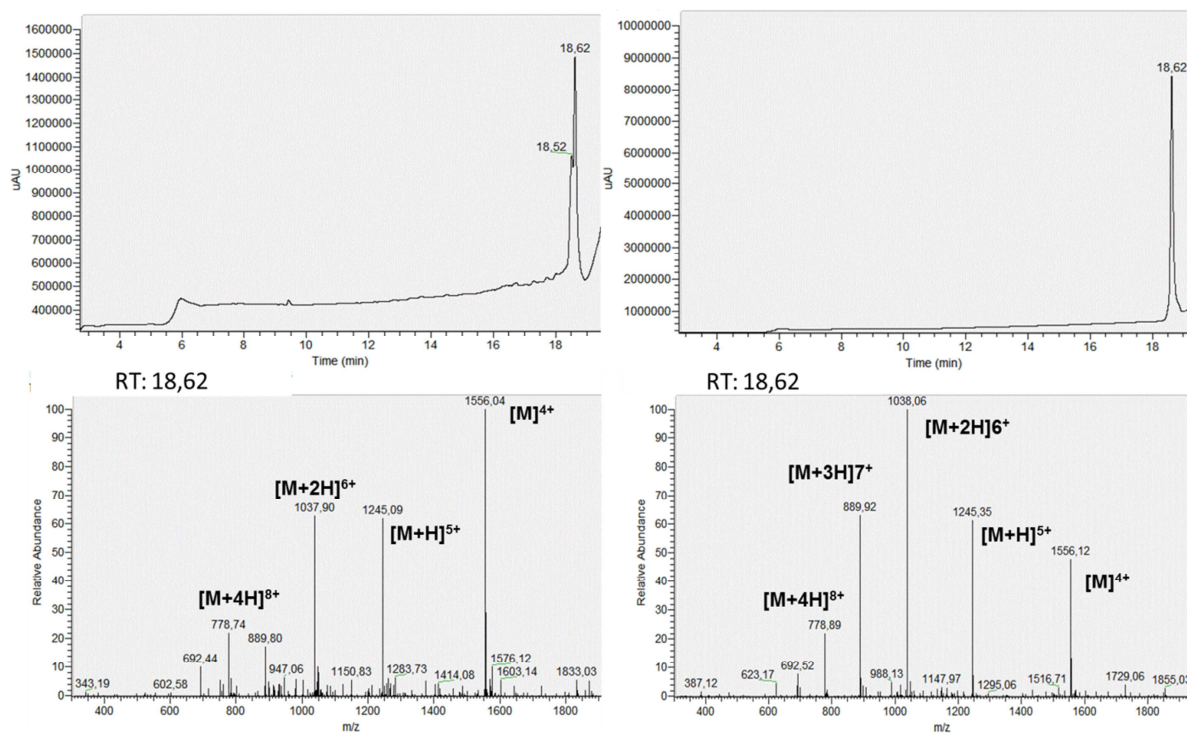


**Figure 11: HPLC-MS analysis of **3c** before and after purification via preparative HPLC.** Used gradient: acetonitrile in water 10-60% in 15 min. UV-spectrum (above) and full scan ESI-MS were both performed with 0.1% TFA. On the left side the UV and ESI-spectrum before purification is shown with the product **3c** at a RT of 18.62 min. On the right side the UV and ESI-spectrum after purification is shown with the product **3c** at a RT of 18.62 min.

### 3.1.2. pH influence on the secondary structure of compound **3c**

The secondary structure analysis of all imidazolium salt-peptide conjugates already showed that peptides **2a** and **3c** form an alpha helical structure in the absence of TFE. This is due to the presence of the LL-37 peptide (176). To verify the influence of different pH values on the secondary structure of **3c**, the pH value of 10 mM phosphate buffer + 50% TFE was changed to an acidic and basic milieu. This experiment was performed to test, if an acidic or basic milieu leads to structural changes or aggregation of the peptide. At this point, only peptide **3c** was checked exemplarily, since it showed an  $\alpha$ -helix without the use of TFE in comparison to **3b** (176). All pH-values minima at 222 nm and 208 nm were present in the spectrum (Figure 12). To analyze the spectra further, the  $\alpha$ -helical content was determined by calculating the ratio between the molar ellipticity at 222 nm and 208 nm ( $R = [\theta]_{222 \text{ nm}} / [\theta]_{208 \text{ nm}}$ ). The R-value of 1 stands for a perfect formed  $\alpha$ -helix. Comparing the R-values, no conformational shifts can be detected for the different pH values, demonstrating that a basic or acidic milieu has no influence on the secondary structure of **3c**.

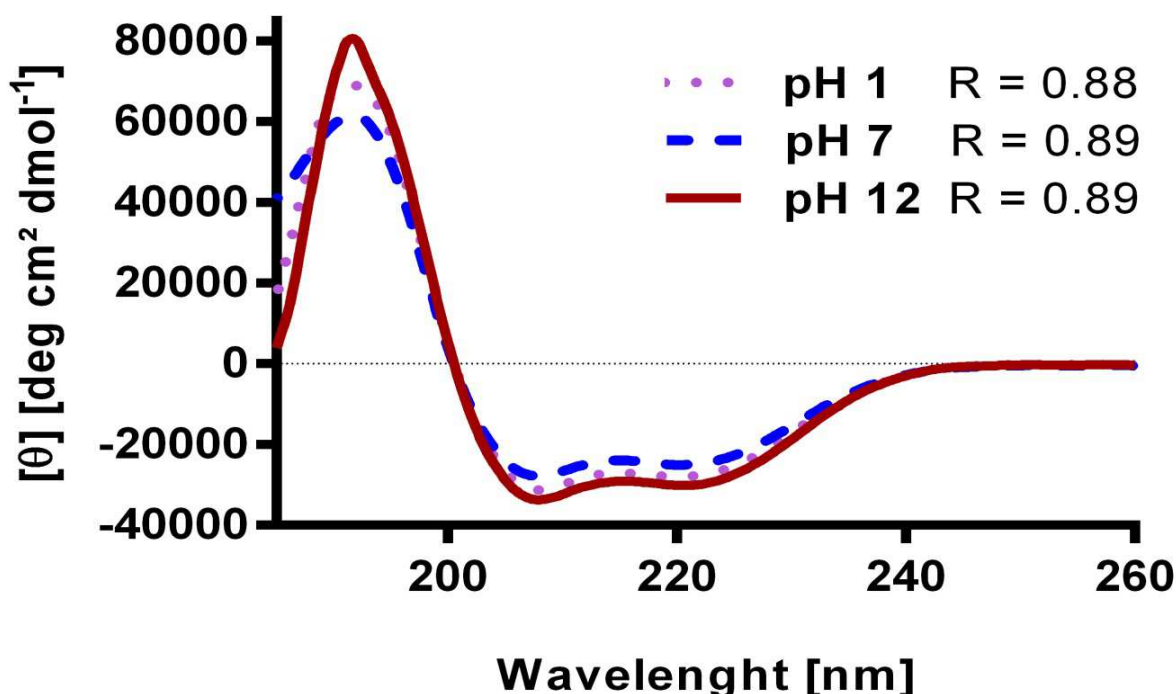


**Figure 12: Circular dichroism spectra of 3c at different pH values.** The spectrum was measured with 20  $\mu$ M peptide concentration in 10 mM phosphate buffer + 50% TFE. R-values (R) represent the ratio between the molar ellipticity values at 222 nm and 208 nm.

### 3.1.3. Antimicrobial activity against resistant bacterial strains

To further investigate the antimicrobial activity of all compounds, the activity against methicillin-resistant *Staphylococcus aureus* (MRSA) and vancomycin-resistant *Enterococci* (VRE) were determined. Figure 13 shows the results of the killing assays, which were performed by the Fraunhofer Institute for Cell Therapy and Immunology in Leipzig. While the control peptide **1a**, without imidazolium salts, showed no activity up to 5  $\mu\text{M}$  against both bacterial strains, the other control peptide **2a** exhibited a minimal inhibitory concentration of 50% ( $\text{MIC}_{50}$  value of 2  $\mu\text{M}$ ) for both bacteria. All imidazolium salt-peptide conjugates displayed very promising activities with  $\text{MIC}_{50}$  values in the lower molecular range and the lowest  $\text{MIC}_{50}$  value of 0.3  $\mu\text{M}$  for compound **3b**. However, the  $\text{MIC}_{50}$  values of **3a** and **3c** were nearly as low as for **3b**, with **3a** being more active against MRSA and **3c** against VRE bacteria.

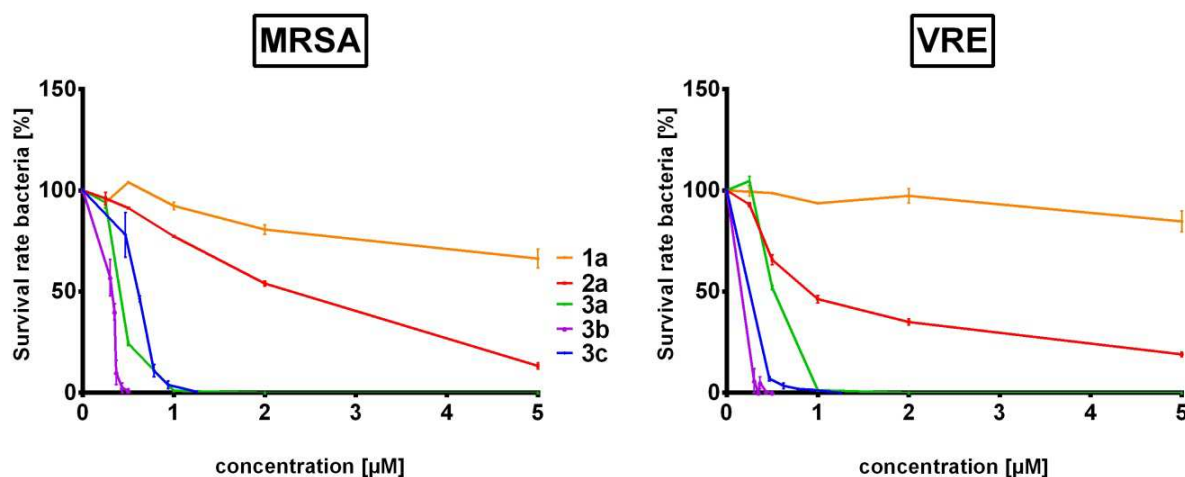


**Figure 13: Antimicrobial activity against resistant bacterial strains.** All compounds were tested against methicillin-resistant *Staphylococcus aureus* and vancomycin-resistant *Enterococci*.  $n=3$  in triplicate.

A comparison of all  $\text{MIC}_{50}$  values is shown in Table 7. The  $\text{MIC}_{50}$  values were manually defined from the individual graphs of each compound.  $\text{MIC}_{50}$  values for *B. subtilis*, *E. coli* and *M. phlei* had been already calculated during my master work. The unmodified peptide **1a** showed no activity against all bacteria strains, while **2a** was inactive only against the gram-negative bacterium *E. coli*. Against all other gram-positive bacteria and the acid-fast bacterium *M. phlei*, a slightly increased activity was visible. The fact that **2a** is more active than **1a**, can be explained comparing their length. **2a** is twice as long as **1a** and, therefore, is probably better

integrated into the bacterial membrane. Furthermore, **1a** is maybe too short to span the whole peptidoglycan of the bacteria. Interestingly, the short compound **3a** exhibited a high activity ( $MIC_{50} = 0.4 - 2.5 \mu M$ ) against all bacterial strains tested, with the exception of *M. phlei*. Generally, *M. phlei* is very hard to be affected by antibiotics due to its additional waxy mycolic layer. The antimicrobial peptide coupled to the imidazolium salts led to a further increased antimicrobial activity for nearly all bacterial strains. Notably, the sC18 conjugate **3b** exhibited a slightly increased toxicity compared to the LL-37 conjugate **3c**. This result can be explained by the fact that the LL-37 conjugate **3c** is bigger and longer than the sC18 conjugate **3b** and maybe cannot permeate the bacteria membrane as good as **3b**. All conjugates **3a**, **3b** and **3c** were the most active against the resistant bacteria, which makes them very interesting for further investigation. Additionally, it can be noticed that these three compounds were the most active against the gram-positive bacteria *B. subtilis*, *MRSA* and *VRE* and exhibited only low activity against the gram-negative bacterium *E.coli*. This is mainly because gram-positive bacteria miss the outer membrane compared to gram-negative bacteria. Another point is that the composition of both bacteria membranes is different: gram-negative bacterial membranes contain more phosphatidylethanolamine, while in gram-positive bacteria membranes phosphatidylglycerol is the main component (177). Since phosphatidylglycerol is negatively charged, while phosphatidylethanolamine is neutral, the positive charged imidazolium salt compounds interact better with the gram-positive bacterial membranes.

**Table 7: Minimal inhibitory concentration ( $MIC_{50}$ ) of all tested compounds.**

Compound	Organism				
	<i>B. subtilis</i> (ATTC 6633)	<i>E. coli</i> K12 (MG 1625)	<i>M. phlei</i> (DSM 48214)	<i>MRSA</i>	<i>VRE</i>
<b>1a</b>	-	5.0 $\mu M$	5.0 $\mu M$	-	-
<b>2a</b>	3.0 $\mu M$	5.0 $\mu M$	1.0 $\mu M$	2.3 $\mu M$	0.9 $\mu M$
<b>3a</b>	1.1 $\mu M$	2.5 $\mu M$	5.0 $\mu M$	0.4 $\mu M$	0.5 $\mu M$
<b>3b</b>	0.5 $\mu M$	1.0 $\mu M$	0.3 $\mu M$	0.3 $\mu M$	0.2 $\mu M$
<b>3c</b>	1.8 $\mu M$	3.5 $\mu M$	0.8 $\mu M$	0.6 $\mu M$	0.3 $\mu M$

- :no activity detected at the highest concentration of 5  $\mu M$  .  $MIC_{50}$  values of control compounds: gentamicin (*B. subtilis* 2.1  $\mu M$ ), tetracycline (*E. coli* 32.8  $\mu M$ ) and streptomycin (*M. phlei* 17  $\mu M$ ).

Compared with commonly used antibiotics, the tested MIC<sub>50</sub> values of the compounds were between 0.3 – 0.6 µM, which is similar to values of vancomycin (MIC<sub>50</sub> = 0.32 µM against MRSA (178, 179)) and linezolid (MIC<sub>50</sub> = 0.59 µM against VRE (179)), highlighting again their high antimicrobial potential.

#### 3.1.4. Hemolytic activity studies

To get a first impression of every compound's selectivity, the hemolytic activity against human erythrocytes was determined and a selectivity index (SI) was calculated. Therefore, human red blood cells (h-RBCs) from a healthy volunteer were used and the HC<sub>20</sub> values were defined. The HC<sub>20</sub> represents the value where 20% hemolytic activity was detected. For peptides **1a** and **2a**, as well as the conjugate **3a** no hemolytic activity below 5 µM was detected (Figure 14); therefore the HC<sub>20</sub> value was set to 5. Notably, the coupling of four imidazolium salts to the sC18 and LL-37 peptides led to a highly increased hemolytic activity with HC<sub>20</sub> values of 1 µM for **3b** and 0.5 µM for **3c**. To further investigate the selectivity, the SI index (HC<sub>20</sub>/MIC<sub>50</sub>) was calculated, considering that a high SI index is a hint for good selectivity (Table 8). **3a** exhibited the highest SI, except for *M. phlei*, because no high hemolysis against red blood cells was detected. To increase the antimicrobial activity of **3a** further with consistent selectivity, some additional positive amino acids like arginine and lysine could be added at the C-terminus of this small compound until the point the selectivity decreases. On the other hand, conjugates **3b** and **3c** showed low SI due to their high hemolytic activity. These results can be explained by the higher hydrophobicity and increased amount of positive charges of compounds **3b** and **3c**, which can be correlated to a strong hemolytic activity. It was additionally shown that the peptides alone were not that active against erythrocytes compared to the conjugates.

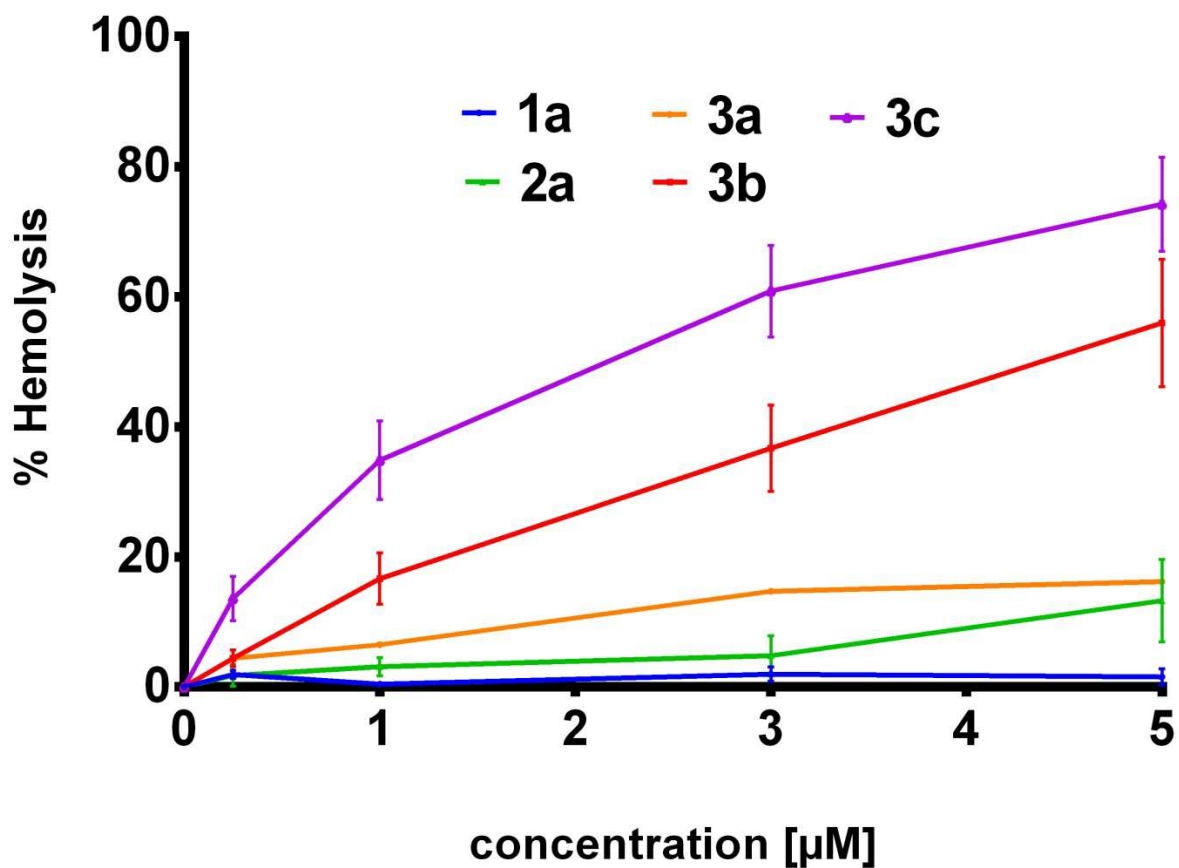


**Figure 14: Hemolytic activity of all novel conjugates against human red blood cells.** The activity was measured against peptide concentrations from 0.25 to 5 µM. Triton-X 100 and water were used as positive and negative control, respectively. HC<sub>20</sub> value was determined from this Figure; *n*=2.

**Table 8: Selectivity index (SI) of all conjugates calculated with HC<sub>20</sub>/MIC<sub>50</sub>**

Organism	1a	2a	3a	3b	3c
<i>B. subtilis</i>	-	1.7	4.5	2	0.3
<i>E. coli</i>	1	1	2	1	0,3
<i>M. phlei</i>	1	5	1	3.3	0.6
<i>MRSA</i>	-	2.2	12.5	3.3	2.5
<i>VRE</i>	-	5.6	10	1.7	1.7

- : denotes no activity at the highest concentration of 5 µM detected

### 3.1.5. Interaction with model membrane systems

To get a first hint about the membrane disturbing processes of the tested compounds, the interaction of **3b** and **3c** with giant unilamellar vesicles (GUVs) were studied. AMPs get usually attracted to a membrane through electrostatic interactions. However, membrane interactions are lower for eukaryotic membranes than for bacterial membranes due to the presence of cholesterol in eukaryotic membranes (180). It is assumed, that the binding of AMPs to eukaryotic membranes is prevented by cholesterol, which increases membrane cohesion and membrane stiffness to stabilize the membrane resulting in a liquid ordered state. The experiments were performed with the CF-labeled versions of **3b\*** and **3c\***, since **3b** and **3c** showed the highest antimicrobial activity in the previous tests.

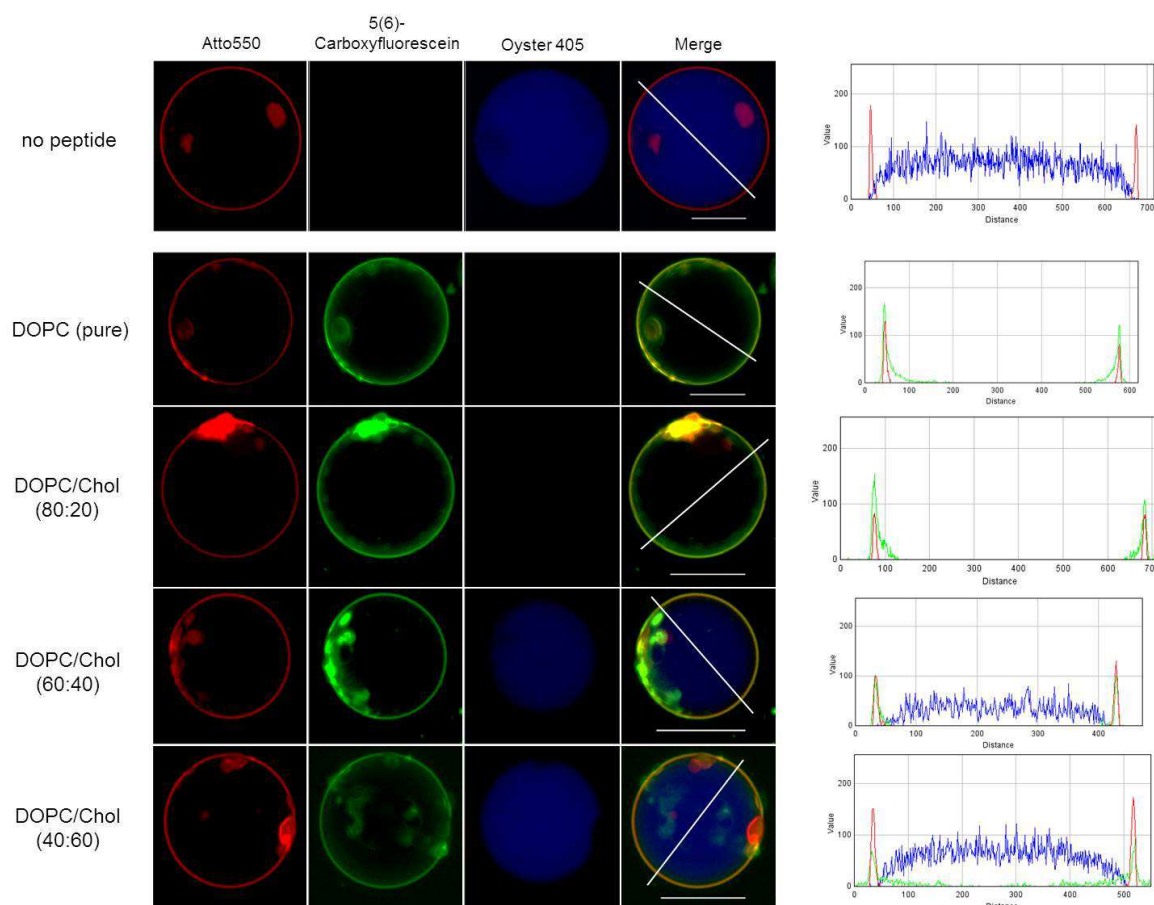


**Figure 15: Interaction of peptide **3b\*** with GUVs and different DOPC/cholesterol compositions.** GUVs were incubated with 5  $\mu$ M **3b\*** for 90 min and analyzed by CLSM. On the right side the intensity profiles of Atto550 (red), 5(6)-carboxyfluorescein (green) and Oyster 405 (blue) along the lines of the merge confocal picture were depicted. GUVs contain 0.2 mol% Atto550-DOPE as lipid marker and 5  $\mu$ M Oyster 405 inside the vesicles. Scale bar, 30  $\mu$ M.

GUVs with different amounts of cholesterol ranging from 0 – 60 mol% were prepared (181). For GUV preparation DOPC and 0.2 mol% Atto550 labeled DOPE were used to visualize the membrane (Figure 15/16 red channel). To visualize a possible membrane leakage by dye outflow, Oyster 405 was encapsulated inside the vesicles. Compound **3b**\* showed strong interactions with the GUV membrane, as it could be seen in the microscope pictures and the intensity profile (Figure 15). A complete dye outflow was visible for GUVs with 20% cholesterol and without cholesterol suggesting that the mode of action of **3b** is a pore-forming mechanism. The intensity profile of these GUVs further showed that the green dye is detectable in and outside the vesicle suggesting that the peptide had crossed the vesicle membrane. However, increasing the cholesterol content led to an increased dye outflow.

In Figure 16 the results for compound **3c** were shown. In this case, no membrane disrupting mechanism could be identified, since no dye outflow was visible. This result was unexpected because in the antimicrobial experiments it seems that **3b** and **3c** act both via strong membrane interactions. The intensity profile depicted some green fluorescence inside the vesicle, suggesting that some peptides of **3c** already crossed the membrane. For the LL-37, which is a part of **3c**, the carpet-like mechanism had already been proposed (182). Maybe our compound also acts in a detergent-like manner and the concentration was too low to detect micelles, which were aroused from the membrane. The extreme clusters of the red green fluorescence dye, especially visible in Figure 16, might be caused by the high presence of cholesterol. Especially at 60%, it seemed that the cholesterol was not homogenously distributed over the GUV membrane and built these clusters.

This experiment exposed that compounds **3b** and **3c** have different mode of actions.

For **3b** a pore-forming mechanism is proposed, where the conjugate in a first step interacts with the lipid membrane, which could be identified by the green accumulation at the lipid membrane, and in a second step builds pores leading to the outflow of the blue dye. To differentiate better between the first and the second step, this experiment could be performed with different concentrations or at different time points. In contrast, **3c** seems to act in a detergent-like manner, since no outflow of the blue dye could be detected. Nevertheless, an interaction of peptide and lipid membrane is visible.

Previous studies with AMPs Citropin, Aurein and Maculatin also showed differences between pore-forming and detergent-like mechanism while interacting with lipid bilayers. Citropin and Aurein, both acting in a detergent-like manner (183), indicate that these peptides need a higher lipid-to-peptide ratio to achieve a dye leakage compared to the pore-forming Maculatin. Therefore, it seems that more peptide molecules are required to disrupt the membrane in a detergent-like manner compared to a pore-forming mechanism. This observation could explain the different results seen for the pore forming **3b** and the detergent-like acting **3c**.

Furthermore, an inhibitory effect of cholesterol was visible for compound **3b**. Hereby, not the interaction between cholesterol and compound led to this inhibitory effect, but an indirect effect of cholesterol on the membrane properties (184). The presence of cholesterol results in an enhanced membrane cohesion and mechanical stiffness, which is explained by an increased acyl chain order in the liquid ordered phase of membranes containing cholesterol (180).

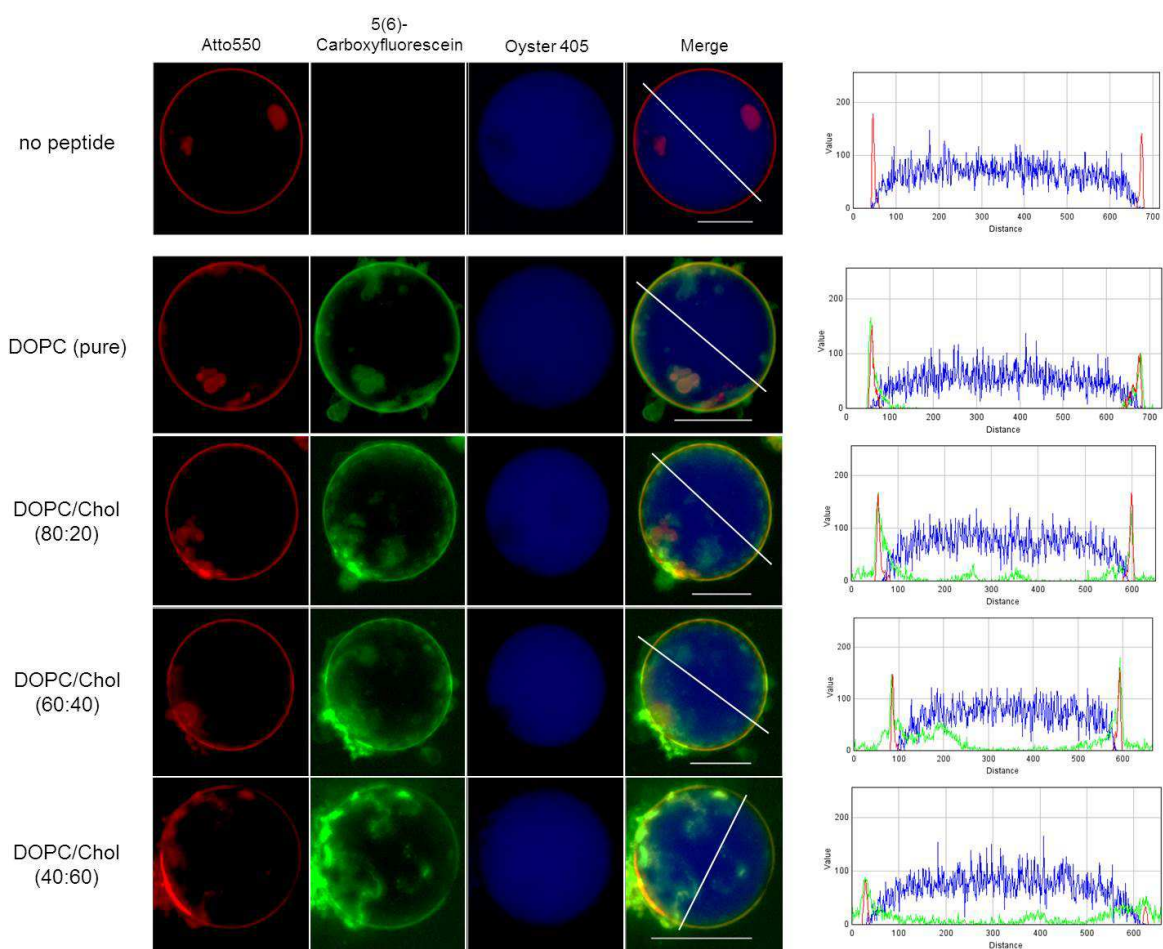


**Figure 16: Interaction of peptide 3c\* with GUVs and different DOPC/cholesterol compositions.** GUVs were incubated with 5  $\mu\text{M}$  3c\* for 90 min and analyzed by CLSM. On the right side the intensity profiles of Atto550 (red), 5,6-carboxyfluorescein (green) and Oyster 405 (blue) along the lines of the merge confocal picture were depicted. GUVs contain 0.2 mol% Atto550-DOPE as lipid marker and 5  $\mu\text{M}$  Oyster 405 inside the vesicles. Scale bar, 30  $\mu\text{M}$ .

In conclusion, all imidazolium salt-peptide conjugates showed an increased antimicrobial activity. Their highly potent activity, especially against drug-resistant strains, and their ease of preparation could make them possible future lead compounds. Compound **3a** is the most interesting one demonstrating the best selectivity, with high antimicrobial activity. The content of cholesterol and different membrane composition could be a critical factor for this compound's selectivity, which has to be further investigated. To further increase the antimicrobial activity of the imidazolium-salt-peptide conjugates, the C-chain length of the imidazolium cation could be extended to a C-18 or C-20 chain. In literature, it was already demonstrated that the antimicrobial activity of imidazolium salts is mainly driven by the length of the C-chain (185, 186). However, a too long C-chain may hinder the

antimicrobial effect, too. This observation is named “cut-off” effect and can be explained based on inadequate solubility (187). Another reason could be that too long C-chains mimic the components of lipid bilayer which leads to an decreased perturbation and disruption within the membrane (188). Moreover, in this work, the long C-16 chain was located between the antimicrobial peptide and the imidazolium cation, while a shorter methyl group was at the end of the conjugate. To further increase the antimicrobial activity, the methyl group can be replaced with an 8 to 16 long C-chain. This additionally C-chain can strengthen the interaction with the lipid tails of the membrane, which promotes the integration into the membrane layer. Nevertheless, the C-chain should not be too long on the basis of the problems mentioned above.

### 3.2. Electron beam immobilization of novel antimicrobial, short peptide motifs leads to membrane surfaces with promising anti-biofilm properties

Biofilm formation is a major problem: 80% of human bacterial infections are caused by biofilm infections and upcoming resistance is steadily increasing. Therefore compound **3a**, which showed potent antimicrobial activity and selectivity, was coupled to polyethersulfone (PES) membranes with different linkers and different coating strategies. PES is a high temperature resistant polymer, which is often used in biological and pharmaceutical applications due to its advantages in oxidative, thermal and hydrolytic stability as well as mechanical property (189). One disadvantage of the PES membranes is the very hydrophobic character, resulting in membrane fouling. (190). Since alternative membrane materials are often unstable and expensive, PES membranes are a good alternative. Furthermore, they can be easily modified to decrease their hydrophobicity (191). In the following experiments PES membranes were functionalized with the hydrophilic compound **3a**, characterized and their antimicrobial activities were investigated. On the one hand electron beam radiation was used as novel an easy method for surface coating ((192, 193)). Electron beam radiation is a high-energy dependent process which is used for cross-linking molecules with the membrane surface. The advantage of cross-linking is the locking effect of the compounds leading to thermal resistance, mechanical strength and chemical stress (194). This method was then compared to a chemical coupling method of peptide immobilization.

### 3.2.1. Synthesis of **3a** and its derivatives **3d**, **3e** and **3f**

In addition to compound **3a** (Figure 8), three derivatives with different linkers at the C-terminus were synthesized (**3d**, **3e** and **3f**). Compound **3d** contained a flexible Ahx-Ahx-Gly linker, consisting of two 6-(amino)hexanoic acids (Ahx) and one glycine. The glycine was important, because the direct coupling of Ahx to the Wang resin was not very successful. To increase the hydrophobicity, two additionally phenylalanine residues were used as linker for peptide **3e**. The last compound **3f** contained a short antimicrobial peptide as linker with the amino acid sequence Trp-Leu-Leu-Lys-Trp. The three novel C-terminal linkers should promote a better integration into the PES membranes during the irradiation process, either by an increased distance (**3d**), by supporting hydrophobic interaction with the membranes (**3e**), or by the introduction of a hydrophobic AMP to increase the overall antimicrobial activity (**3f**). Table 9 shows that the synthesis of all peptides was very successful.

**Table 9: Analytical und synthetic data of all peptide derivates.** Net-charge was determined by counting all lysine and arginine residues and the N-terminus as positive charges and aspartic acid and glutamic acid residues as negative charges. Calculated molecular weight was determined using a calculation software, while the experimental molecular weight, retention time and purity was determined using the UV-chromatograms und ESI-MS-spectra. The gradient was 10-60% acetonitrile in water in 15 min with 0.1% FA except for **3a** where the gradient was 10-60% in 15 min with 0.1% TFA.

Peptide	Sequence	Net charge	MW <sub>calc</sub> [Da]	MW <sub>exp</sub> [Da]	RT [min]	Purity [%]	Yield [%]
<b>3a</b>	IL <sub>4</sub> -KK(εK)βA-OH	+4	1751.74	1752.24	18.78	98	20
<b>3d</b>	IL <sub>4</sub> -KK(εK)βA-Ahx-Ahx-Gly-OH	+4	2035.13	2035.68	15.63	98	33
<b>3e</b>	IL <sub>4</sub> -KK(εK)βA-Phe-Phe-OH	+4	2046.11	2046.84	15.08	95	21
<b>3f</b>	IL <sub>4</sub> -KK(εK)βA-Trp-Leu-Leu-Lys-Trp-OH	+5	2478.68	2479.6	13.75	97	17

### 3.2.2. Membrane immobilization and characterization

Membrane immobilization and characterization was performed by Dr. Agnes Schulze at the Institute for Surface Modifications in Leipzig. The four peptides **3a**, **3d**, **3e** and **3f** were immobilized onto PES membranes using either electron beam radiation with 50 kGy, 100 kGy or 150 kGy, or chemical immobilization via a peptide bond. For this, the C-terminus of the peptides was introduced on the membrane by NHS/EDC activation. Successful immobilization on the PES membrane was proven by X-ray photoelectron spectroscopy (XPS) (Table 10). The unmodified PES membranes were used as reference. XPS data show that they contain 70% carbon, 26% oxygen and 4% sulfur. After the immobilization of all peptides on the membrane, a significant increase of nitrogen on the membrane surface could be detected. Since the PES membrane reference contains no nitrogen, the nitrogen increase let conclude a successful peptide immobilization.

A comparison of the four different peptides was difficult because the values of nitrogen seem to be pretty variable. However, the highest nitrogen amount (0.72 – 1.73%) could be detected for **3f** compared with the other peptides. All in all, the electron beam radiation seemed to be a successful method to immobilize peptides on a PES membrane.

Scanning electron microscopy (SEM) pictures were taken to further characterize the membrane morphology after immobilization. The reference PES membrane depicted in Figure 17 is highly porous with a pore-like structure. After electron radiation, immobilization and EDC/NHS immobilization of the peptides, the pore structure remained the same as for the reference leading to the conclusion that no pore blocking or structural defects were caused by both immobilization methods.

**Table 10: Atomic composition of the membranes (as determined by XPS analysis).**

Label	Elemental ratio (relative atom-%)			
	C	N	O	S
PES Membrane (reference)	69.95	-	26.12	3.93
Membrane + 3a 50kGy	67.81	0.36	28.17	3.33
Membrane + 3a 100kGy	69.25	0.73	26.87	3.62
Membrane + 3a 150kGy	69.39	0.61	27.05	3.56
Membrane + 3a (NHS/EDC)	69.61	0.98	26.61	3.78
Membrane + 3d 50kGy	69.28	0.71	26.85	3.17
Membrane + 3d 100kGy	69.44	0.69	26.61	3.27
Membrane + 3d 150kGy	68.79	0.17	27.47	3.56
Membrane + 3d (NHS/EDC)	69.42	1.03	26.50	3.06
Membrane + 3e 50kGy	68.38	0.81	27.53	3.28
Membrane + 3e 100kGy	67.84	0.59	28.20	3.37
Membrane + 3e 150kGy	69.55	1.34	25.86	3.25
Membrane + 3e (NHS/EDC)	68.95	0.33	27.06	3.65
Membrane + 3f 50kGy	68.81	0.72	27.12	3.35
Membrane + 3f 100kGy	68.60	0.73	27.34	3.33
Membrane + 3f 150kGy	70.51	1.73	24.93	2.85
Membrane + 3f (NHS/EDC)	69.15	0.73	26.79	3.33

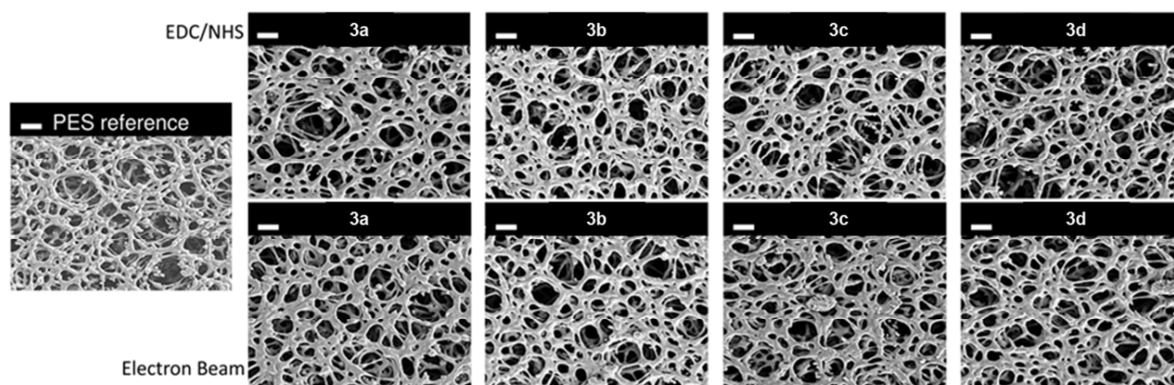


**Figure 17: SEM images of immobilized PES membranes.** PES reference membrane without peptide. Membranes with peptides **3a**, **3d**, **3e** and **3f** after coupling with EDC/NHS (upper row) and after electron beam radiation (lower row). All membranes images are in top view.

### 3.2.3. Antimicrobial activity of the functionalized PES membranes

To investigate the antimicrobial activity of the functionalized PES membranes, an INT-assay was performed after 24 h incubation of *B. subtilis*, a gram-positive bacterium, with functionalized membranes (Figure 18). Hereby, the peptide **3a** showed the best antimicrobial activity when immobilized via covalent coupling, while **3d** had the highest effect on *B. subtilis* when the membrane radiated with 150 kGy was tested. An explanation for these results could be that the peptide **3a** without linker is closer to the membrane than the tested compounds with linker. Since the bacteria build their bacterial film on the membranes, the peptide **3a** was closer to the bacteria than the other compounds. On the other side, the good results for **3d** radiated with 150 kGy could be explained by the fact that the aliphatic chain of aminohexanoic acid could be better integrated in the membrane compared to phenylalanine. However, when **3a** was incorporated by radiation, it showed no activity at all, may be due to the fact that it got integrated too deep into the membrane and subsequently lost its antimicrobial activity. In contrast, the bulky aromatic groups of **3e** and **3f** may hinder the integration of these peptides into the membrane leading to lower antimicrobial effects.

Most of the time, the antimicrobial activity of immobilized peptides was reduced compared to soluble peptide activity (196). To check, if this statement also is true for the results of compound **3a** the concentration in  $\mu\text{M}$  had to be compared. On the one hand, *B. subtilis* **3a** exhibited a  $\text{MIC}_{50}$  value of  $1.1 \mu\text{M}$ ; on the other hand, 0.25 mg of **3a** was immobilized on the PES membrane which equals approximately

142  $\mu\text{M}$ . Therefore, it is very hard to predict, if the soluble peptide activity is higher than the immobilized peptide activity, but it seems very plausible that some antimicrobial activity was lost during the immobilization step. To solve this problem Gabriel *et al.* used a more flexible hydrophilic poly(ethylene glycol) linker and retain antimicrobial activity (197). In literature, it was further shown that immobilization of peptides led to an higher stability in physiological environment (195).

Further insides should give a time-dependent INT-assay (Figure 19). Antimicrobial activity was detected after 17 h, 19 h, 21 h and 23 h. No differences between the control membranes and peptide-immobilized membranes could be measured except for **3a** at 100 kGy. Thus, it was concluded that this method was not suitable for measuring the anti-biofilm effects.

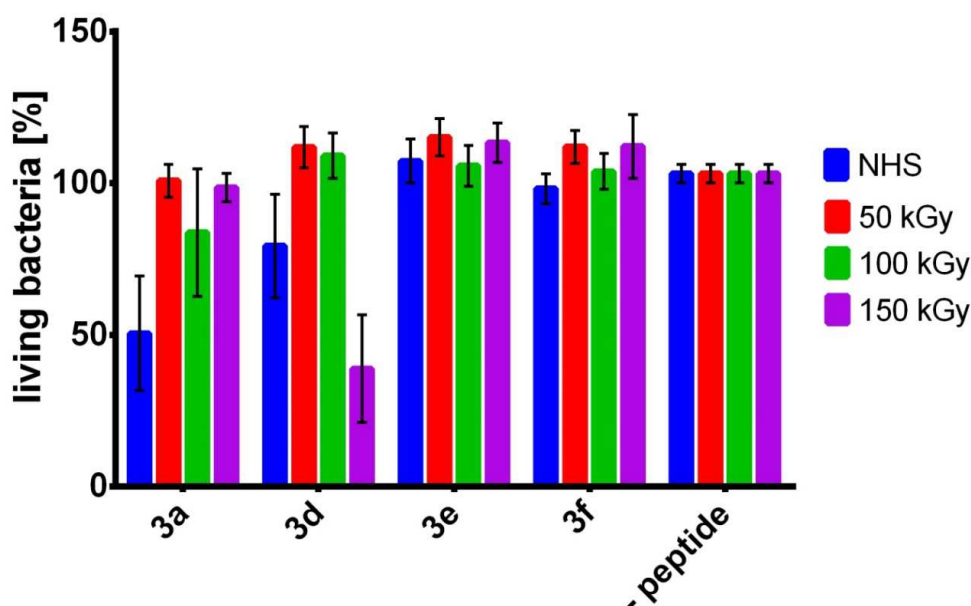


**Figure 18: INT-assay of immobilized membranes.** Membranes were incubated for 24 h at 37°C with bacteria. Membranes were removed and 20  $\mu\text{l}$  INT-solution were added for 30 min at 37°C to the bacteria suspension. The 48-well plate was subsequently put in an ELISA plate reader to measure absorption at 540 nm. Negative control was set up to 100% ( $n=4$ ).

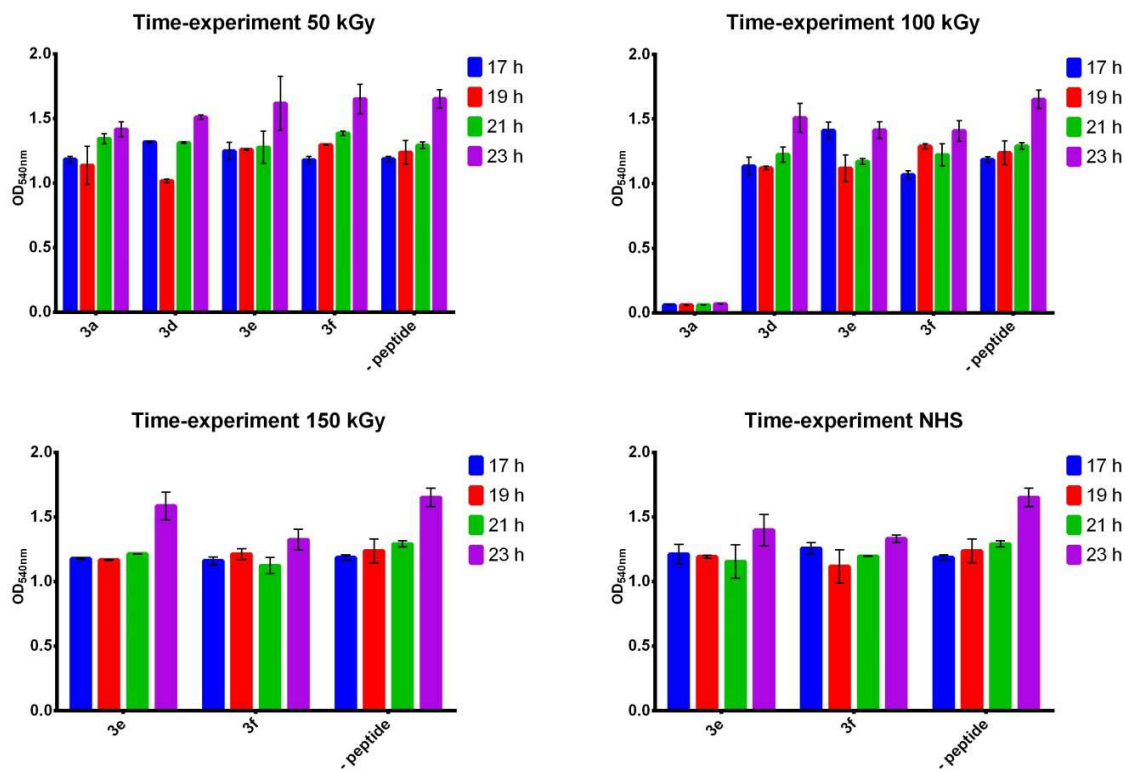


**Figure 19: Time-experiments of immobilized membranes.** Membranes were incubated for 17 h, 19 h, 21 h and 23 h at 37°C with bacteria. OD<sub>540nm</sub> was measured at each time-point. The 48-well plate was subsequently put in an ELISA plate reader to measure absorption at 540 nm. Negative control was set up to 100% ( $n=2$ ).

Therefore, as an additional experiment, an agar plate assay was performed using *B. subtilis*. The respective membranes were incubated for 3 h with a solution containing *B. subtilis*, and then a small amount of this solution was exposed on agar plates (Figure 20). Figure 20 depicts that for peptide **3a** only one agar plate containing some single bacteria colonies could be detected using electron beam radiation of 150 kGy. Covalent coupling of peptide **3d** exhibited no bacteria at the agar plates, while for the control without peptide lots of bacteria were visible. The amount of bacteria colonies for all linker variants and immobilization methods are illustrated in Figure 21. It is displayed that **3a** and **3d** dramatically inhibited the bacterial growth independently from the immobilization method used. On the contrary, the activity of **3e** and **3f** seemed to be dependent on the immobilization technique used, but the results were not statistically significant to confirm this assumption.

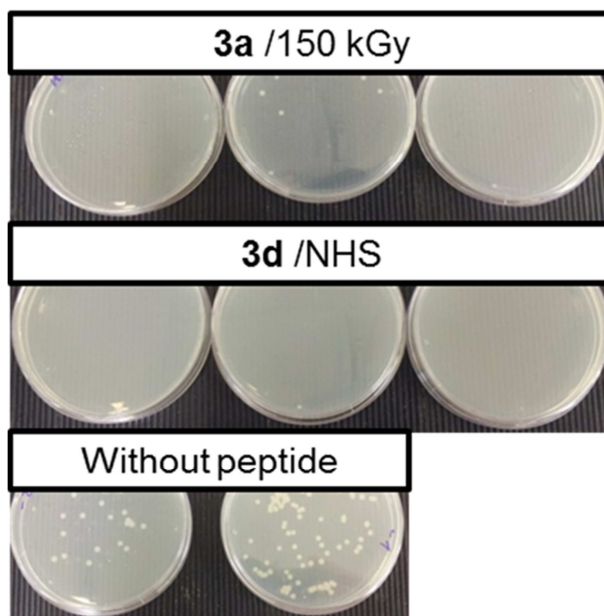


**Figure 20: Grown bacteria after incubation with immobilized membranes.** Immobilized membranes were incubated for 3 h with *B. subtilis* and some drops of the solution were exposed on agar plates. This Figure shows the results for peptide **3a** with electron beam radiation of 150 kGy, for **3d** using covalent coupling and the control agar plates without peptide.

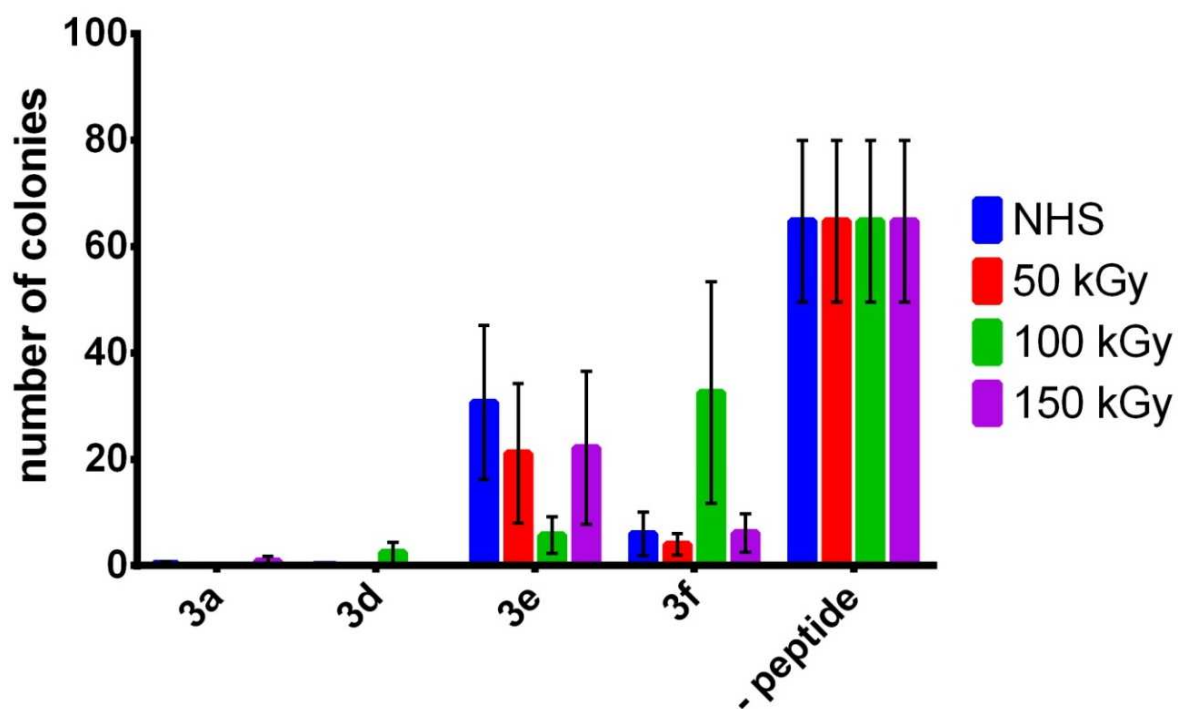


**Figure 21: Agar plate assay of immobilized membranes.** Membranes modified with peptide were incubated with *B. subtilis*. After 3 h incubation at 37°C 1  $\mu$ L of bacteria solution were mixed with 99  $\mu$ L PBS and scratched out on Mueller-Hinton Agar plates. The day after grown bacteria colonies were counted. As negative control membrane without peptide was used ( $n = 4$ ).

In conclusion, bacteria growing experiments showed antimicrobial activity of **3a** and **3d**, while within the INT-assays, no antimicrobial effect was detected. The difference between these two experiments might be the volume of the bacterial solution, which is 10-fold higher in the INT-assay than in the agar plate assay. Additionally, the incubation time for the agar plate assay is with 3 h shorter than the 6 h for the INT-assays. It can be concluded that the small compounds **3a** and **3d** are very active in the first 3 h and have only a limited range with their branched side chains. However, all coated membranes exhibited an increased activity against *B. subtilis* compared to membranes without peptide. Taken together, the electron beam radiation method demonstrated as high antimicrobial activity as the chemical coupled method. This lead to the assumption that peptides can be immobilized successfully on PES membranes using the electron beam radiation method.

### 3.3. Optimizing the antimicrobial activity of the CPP sC18

sC18 is originally derived from CAP18, a cathelicidin peptide with antimicrobial activity. sC18 was studied and developed in our research group and is mostly used as cell-penetrating peptide in the delivery of cytostatic drugs or imagine probes. (80, 196). sC18 is mostly taken up in cells via endocytosis, but an direct entry seems also possible (55, 81, 82). In chapter one of this work, it was already shown, that sC18 as a peptide conjugate exhibited high antimicrobial activity. Besides sC18 other well-known CPPs were found to exhibit antimicrobial activity as well, for example TAT(48-60), penetratin or Pep-1 (55, 197-199). The lastly named peptide Pep-1 was already modified to an antimicrobial Peptide Pep-1-k through increase of the cationic character (200). Since the sC18 peptide already has a cationic character, the idea was to increase the antimicrobial activity and selectivity through the integration of hydrophobic amino acids. Kim *et al.* revealed that an introduction of isoleucine or leucine in the AMP sequence led to an increase in antimicrobial activity (201). Isoleucine was chosen because its hydrophobicity is a little bit higher than the hydrophobicity of leucine (202). Furthermore, the hydrophobicity index of Monera *et al.* exhibited that phenylalanine is the most hydrophobic amino acid. Therefore, isoleucine and phenylalanine exchanges were performed and their influence was tested towards activity and selectivity.

### 3.3.1. Synthesis of sC18 variants

In a first set of experiments, an isoleucine full scan was performed. Further on, the isoleucine exchanges at position 10, 15 and 16 showed the best antimicrobial activity, and so they were combined to three double and one triple mutants (Table 11) (Antimicrobial activity is shown in 3.3.2). To investigate, if phenylalanine exhibits the same influence on the antimicrobial activity as isoleucine did, the same amino acid exchanges at position 10, 15 and 16 as well as the double and triple mutants were accomplished for phenylalanine, too (Table 11). The synthesis of all these peptides was performed successfully. Peptides **sC18I1** – **sC18I9** and **sC18I11** – **sC18I14** were only used in the preliminary full scan to investigate which amino acid substitution position showed the highest increase in antimicrobial activity. For the preliminary tests, these peptides were synthesized in small amounts and were not further purified via preparative HPLC. However, the obtained yields were above 70%, what was sufficient for a first row of biological testing. The peptides **sC18**, **sC18I10**, **sC18I15**, **sC18I16**, **sC18F10**, **sC18F15**, **sC18F16** and all double and triple mutants were purified and showed high purity between 91-98%. The yield of these peptides was around 30%, except for the double and triple mutants of isoleucine, which were obtained in a yield of only 10%. This can be explained by the formation of a side-product, which was detected in the UV-chromatogram before HPLC purification (Figure 22). The side-product at a retention time of 5.56 min exhibited a 6-fold charged molecular peak of 342.24 m/z, corresponding to a peptide mass of 1939.26 Da. The molecular weight of this side-product was 113 m/z fewer compared to the product peak at a retention time of 6.79 min. This mass difference can be explained by the loss of an isoleucine at position 15. Similar side products were detected for all peptides containing an isoleucine at position 15. A closer look at the peptide sequence suggested that the KIKIK (**sC18I15**) or similar motifs at the N-terminus of the peptide were very difficult to synthesize resulting in a low yield of the final product. As already mentioned, the main product was detected in the UV-chromatogram at 6.79 min. The ESI-MS spectrum displays the 3-fold ( $[M+3H]^{3+} = 685.58$ ) to 6-fold ( $[M+6H]^{6+} = 343.29$ ) charged molecular ions. After purification via preparative HPLC, a sharp peak could be detected in the UV-chromatogram with 0.1% TFA (Figure 23). Again, the 3-fold ( $[M+3H]^{3+} = 685.66$ ) to 6-fold ( $[M+6H]^{6+} = 343.22$ ) charged molecular ions were visible with the corresponding molecular mass of 2054.70 Da which was assigned to **sC18I15**.

**Table 11: Analytic data of all synthesized sC18 variants.** Net-charge was determined by counting all lysine, arginine and the N-terminus as positive charge and aspartic acid and glutamic acid as negative charge. Calculated molecular weight was determined using a calculation software, while the experimental molecular weight, retention time and purity was determined using the UV-chromatograms und ESI-MS-spectra. The acetonitrile gradient was 10-60% in 15 min with 0.1% FA for molecular weight calculation. To calculate the retention time and purity an acetonitrile gradient 10-60% in 15 min with 0.1% TFA was used.

Peptide	Sequence	Net charge	MW <sub>calc</sub> [Da]	MW <sub>exp</sub> [Da]	RT [min]	Purity [%]	Yield [%]
sC18	GLRKRLRKFRNKIKEK-NH <sub>2</sub>	+9	2069.60	2070.54	7.8	> 99	35
sC18I1	ILRKRLRKFRNKIKEK-NH <sub>2</sub>	+9	2125.70	2126.82	-	> 75*	80
sC18I2	GIRKRLRKFRNKIKEK-NH <sub>2</sub>	+9	2069.60	2070.33	-	> 70*	81
sC18I3	GLIKRLRKFRNKIKEK-NH <sub>2</sub>	+8	2026.57	2027.28	-	> 80*	72
sC18I4	GLRIRLRKFRNKIKEK-NH <sub>2</sub>	+8	2054.58	2055.78	-	> 80*	91
sC18I5	GLRKILRKFRNKIKEK-NH <sub>2</sub>	+8	2026.57	2027.25	-	> 80*	66
sC18I6	GLRKRIRKFRNKIKEK-NH <sub>2</sub>	+9	2069.60	2069.94	-	> 85*	62
sC18I7	GLRKRLIKFRNKIKEK-NH <sub>2</sub>	+8	2026.57	2027.70	-	> 85*	92
sC18I8	GLRKRLRIFRNKIKEK-NH <sub>2</sub>	+8	2054.58	2055.78	-	> 80*	97

sC18I9	GLRKRLRKIRNKIKEK-NH <sub>2</sub>	+9	2035.58	2036.01	-	> 80*	88
sC18I10	GLRKRLRKFINNKIKEK-NH <sub>2</sub>	+8	2026.57	2027.70	9.2	95	37
sC18I11	GLRKRLRKFRINKIKEK-NH <sub>2</sub>	+9	2068.65	2069.88	-	> 90*	95
sC18I12	GLRKRLRKFRNIIKEK-NH <sub>2</sub>	+8	2054.58	2055.78	-	> 75*	65
sC18I14	GLRKRLRKFRNKIIEK-NH <sub>2</sub>	+8	2054.58	2055.84	-	> 80*	71
sC18I15	GLRKRLRKFRNKIKIK-NH <sub>2</sub>	+10	2053.64	2054.70	7.6	98	24
sC18I16	GLRKRLRKFRNKIKEI-NH <sub>2</sub>	+8	2054.58	2055.90	8.6	95	28
sC18I10I15	GLRKRLRKFINKIKIK-NH <sub>2</sub>	+9	2010.61	2011.00	9.2	90	11
sC18I10I16	GLRKRLRKFINKIKEI-NH <sub>2</sub>	+7	2011.55	2012.5	10.1	95	8
sC18I15I16	GLRKRLRKFRNKIKII-NH <sub>2</sub>	+9	2038.63	2038.85	8.3	95	9
sC18I10I15I16	GLRKRLRKFINKIKII-NH <sub>2</sub>	+8	1995.60	1996.05	9.3	95	6
sC18F10	GLRKRLRKFFNKIKEK-NH <sub>2</sub>	+8	2060.59	2060.76	9.3	94	37
sC18F15	GLRKRLRKFRNKIKFK-NH <sub>2</sub>	+10	2087.66	2087.96	8.3	93	31

sC18F16	GLRKRLRKFRNKIKEF-NH <sub>2</sub>	+8	2088.60	2888,75	8.7	92	32
sC18F10F15	GLRKRLRKFFNKIKFK-NH <sub>2</sub>	+9	2078.65	2079,02	9.6	98	28
sC18F10F16	GLRKRLRKFFNKIKEF-NH <sub>2</sub>	+7	2079.59	2079,93	10.3.	98	29
sC18F15F16	GLRKRLRKFRNKIKFF-NH <sub>2</sub>	+9	2106.66	2107,06	9.3	92	32
sC18F10F15F16	GLRKRLRKFFNKIKFF-NH <sub>2</sub>	+8	2097.65	2097,95	10.6	91	16

- : no retention time and purity investigated. \* : purity was determinend via the UV-spectrum containing 0.1% FA.

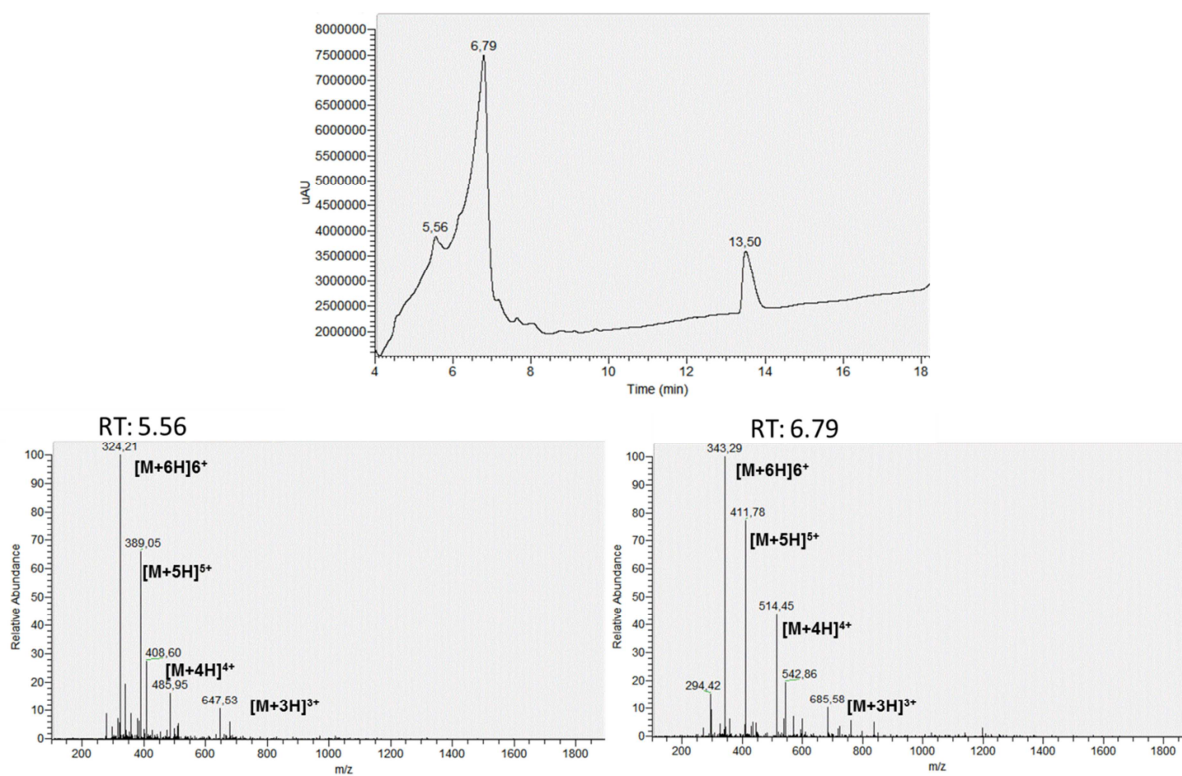


**Figure 22: HPLC-MS analysis of sC18I15 before purification via preparative HPLC.** Used gradient: acetonitrile in water 10-60% in 15 min UV-spectrum (above) and full scan ESI-MS were both performed with 0.1% FA. At the top the UV chromatogram is shown with the product **sC18I15** at a RT of 6.79 min and a side-product (-113 m/z) at 5.56 min. On the bottom the ESI-spectra of product side product (5.56 min) and product (6.79 min) are shown.

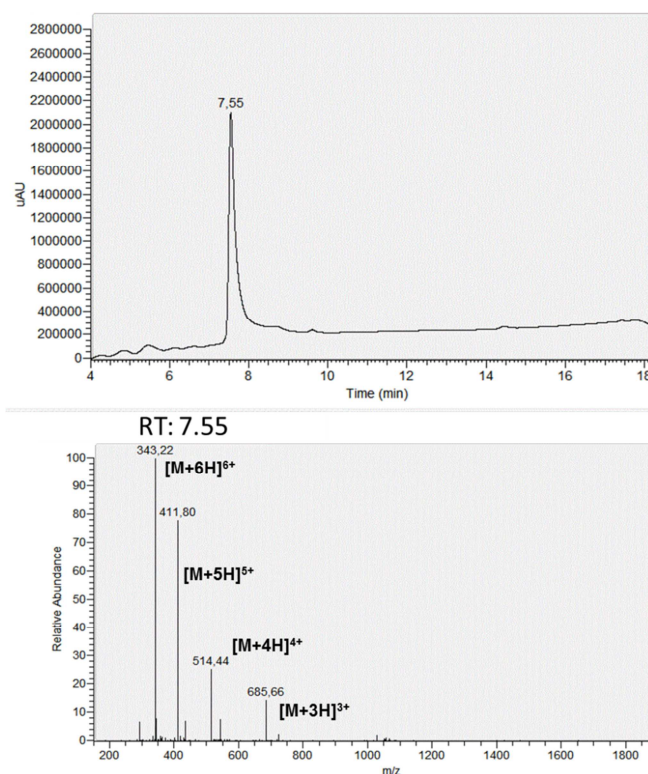


**Figure 23 HPLC-MS analysis of sC18I15 after purification via preparative HPLC.** Used acetonitrile gradient was 10-60% in 15 min. UV-spectrum (above) was performed with 0.1% TFA while full scan ESI-MS was performed with 0.1% FA. At the top the UV chromatogram is shown with the product **sC18I15** at a RT of 7.55 min. On the bottom the ESI-spectra of the purified **sC18I15** is shown.

### 3.3.2. Antimicrobial activity of sC18 isoleucine variants

To get a hint which amino acid positions are best to exchange with isoleucine, the antimicrobial activity of **sC18** and **sC18I1 – sC18I16** was tested at 50  $\mu\text{M}$  and 25  $\mu\text{M}$  against seven different bacteria strains (*B. subtilis*, *E. coli*, *P. fluorescens*, *S. typhimurium*, *M. phlei*, *C. glutamicum* and *M. luteus*) using the INT-assay. Bacteria were divided into three subgroups: (1) bacillus, (2) proteobacteria and (3) actinobacteria. From each subgroup one bacterium is shown exemplarily, namely (1) *B. subtilis*, (2) *P. fluorescens*, (3) *M. luteus* (Figure 24). Against *B. subtilis*, all sC18 variants showed high antimicrobial activity. The highest effect was detected for **sC18I1**, **sC18I3**, **sC18I5**, **sC18I8**, **sC18I10** and **sC18I12 – sC18I16**. All of these variants had an exchange of a basic amino acid residue, either arginine or lysine, with isoleucine leading to an increased hydrophobic effect of the whole peptide and therefore maybe a better integration into the membrane of *B. subtilis*. An exception

was **sC18I15**, where the deletion of the acidic glutamic acid led to an increased activity compared to **sC18**.

For *P. fluorescens*, a proteobacterium, the results looked a little bit different. Not all sC18 isoleucine variants exhibited an increased antimicrobial activity. The most toxic effects were determined for **sC18I4**, **sC18I10** and **sC18I16** with only 20% living bacteria at 25  $\mu$ M. Again for these three variants isoleucine substituted a basic amino acid.

The Results for the actinobacterium *M. luteus* were similar to the results of *P. fluorescens*. Again **sC18I10** and **sC18I16** showed the highest antimicrobial activity with 30% and 20% living bacteria, respectively. Furthermore, also **sC18I15** displayed a moderate antimicrobial activity.

A comparison of the antimicrobial activity of all seven bacteria strains (not all data shown) led to the conclusion that isoleucine exchanges at position 10, 15 and 16 increased the antimicrobial activity. Figure 25 depicts the helical wheel projections of **sC18** as well as **sC18I10**, **sC18I15** and **sC18I16** indicating that an expansion of the hydrophobic face (**sC18I10** and **sC18I16**) or the deletion of the negatively charged glutamic acid (**sC18I15**) led to better antimicrobial activity effects. Furthermore, the isoleucine scan revealed that a hydrophobic isoleucine inside a high positive area (**sC18I7**) as well as the replacement of the high hydrophobic phenylalanine (**sC18I9**) or asparagine (**sC18I11**) decreased the antimicrobial activity.

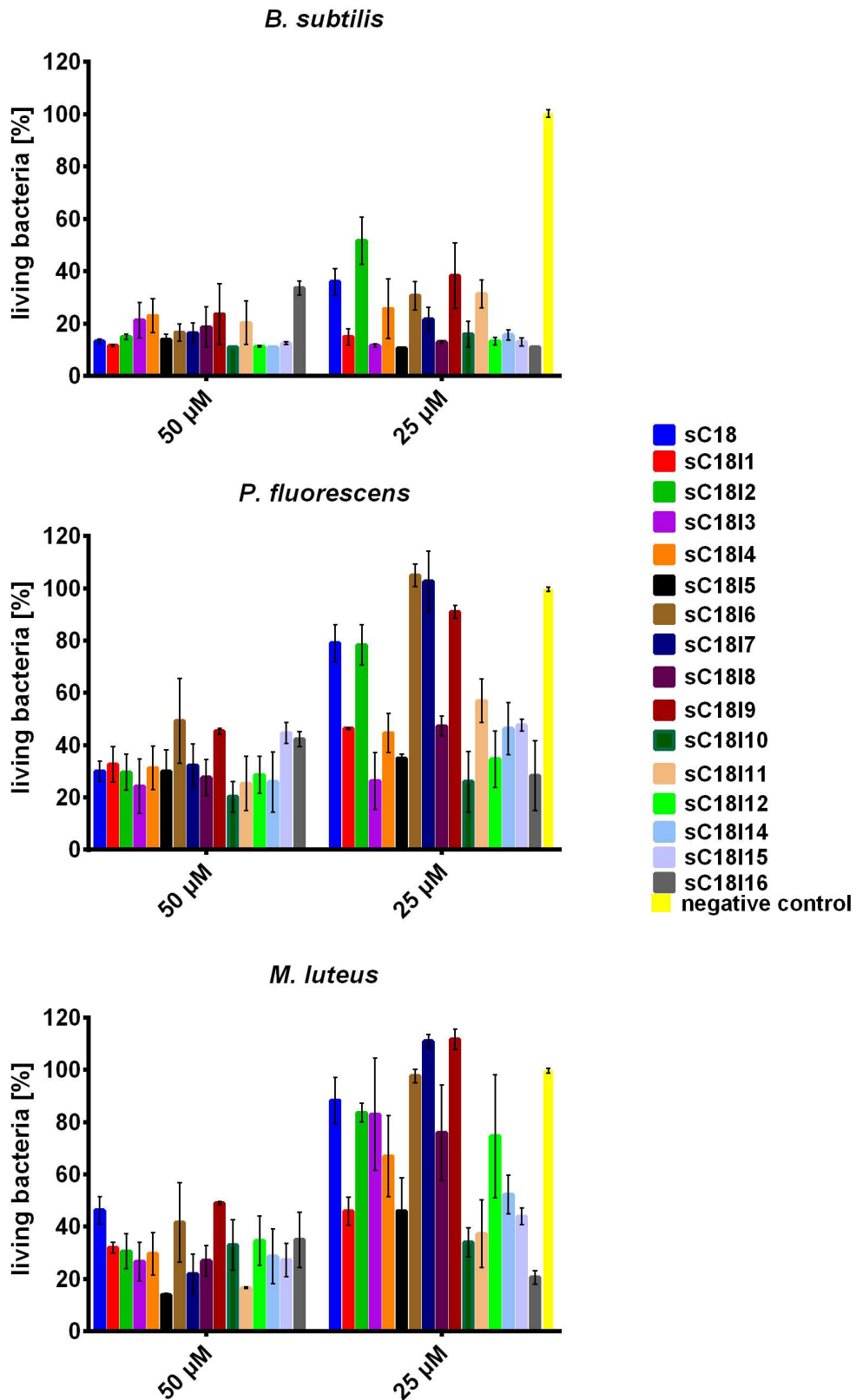


**Figure 24: Antimicrobial activity of sC18 isoleucine variants.** Antimicrobial activity was tested against *B. subtilis*, *P. fluorescens* and *M. luteus*. Each value represents the mean  $\pm$  SEM ( $n=1$  in triplicate). Negative control (water) was set up to 100%.

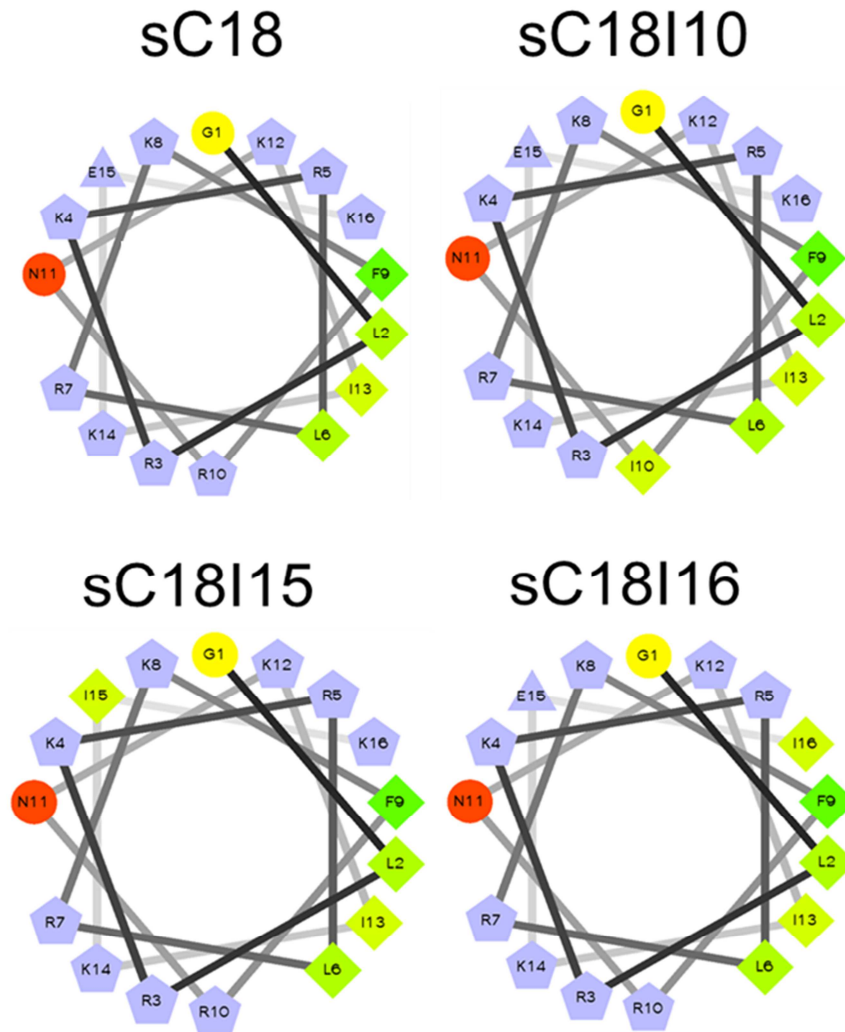


**Figure 25: Helical wheel projection of sC18, sC18I10, sC18I15 and sC18I16.** Hydrophilic residues are shown as circles, hydrophobic residues as diamonds, potentially negatively charged residues as triangles and potentially positively charged residues as pentagons. Hydrophobicity is color coded as well: the most hydrophobic residue is green, and the amount of green is decreasing proportionally to the hydrophobicity, with zero hydrophobicity coded as yellow. Hydrophilic residues are coded red with pure red being the most hydrophilic (uncharged) residue, and the amount of red decreasing proportionally to the hydrophilicity. The potentially charged residues are light blue. The program of the website <http://r2lab.ucr.edu> was used for helical wheel projections.

In a next set of experiments, **sC18, sC18I10, sC18I15, sC18I16, sC18I10I15, sC18I10I16, sC18I15I16** and **sC18I10I15I16** were tested again against seven different bacterial strains, but this time in a concentration range of 2.5  $\mu\text{M}$  – 25  $\mu\text{M}$ . For a better overview, the bacteria were again divided into bacillus, proteobacteria and actinobacteria. Compared to the pretests, this time bacteria were first grown in a preculture and the next day diluted and grown to an  $\text{OD}_{600} = 0.7$ . Figure 26

depicts the results of the antimicrobial activity for *B. subtilis*. For **sC18**, no activity could be detected; on the contrary at 5  $\mu\text{M}$  and 10  $\mu\text{M}$  the percentage of living bacteria increases. A reason for this increase could be that bacteria were stressed by the presence of the peptide in the solution, but peptide concentration was not high enough to kill the bacteria. The highest activity of a single exchanged peptide was shown by **sC18I16** with only 15% living bacteria at 10  $\mu\text{M}$ . **SC18I10** also exhibited a high activity but was not as potent as **sC18I16**. It seems that an extension of the hydrophobic area is more effective than the deletion of glutamic acid, since **sC18I15** only showed a low activity against *B. subtilis*. However, all double and triple mutants displayed a very high antimicrobial activity already at 5  $\mu\text{M}$ . The mutant **sC18I10I16** was the most active one and confirms that the hydrophobic face is more important for *B. subtilis* than the deletion of the negative charge.

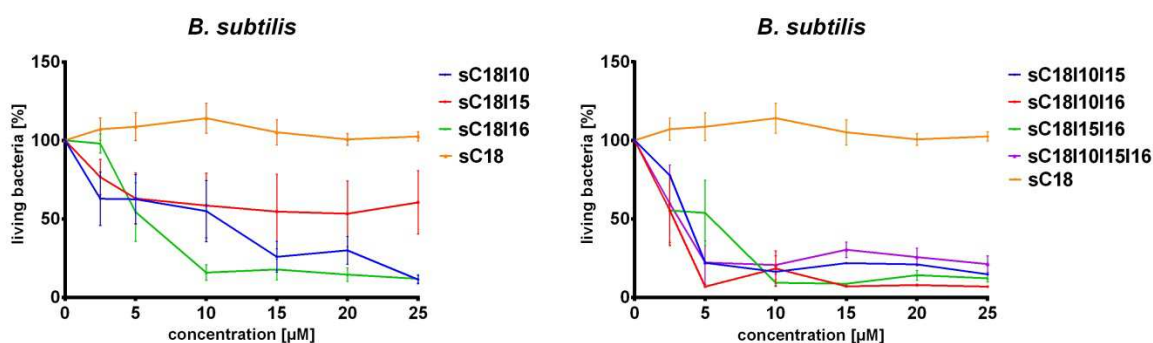


**Figure 26: Antimicrobial activity of sC18 isoleucine variants against *B. subtilis*.** Antimicrobial activity was tested against *B. subtilis* (2.5, 5, 10, 15, 20 and 25  $\mu\text{M}$ ). On the left site, the single isoleucine exchanges were depicted, while the right site shows the double and triple isoleucine exchanges. Each value represents the mean  $\pm$  SEM ( $n=2$  in triplicate). Negative control (water) was set up to 100%.

The results for the antimicrobial activity of the sC18 variants against the proteobacteria *C. glutamicum* and *M. luteus* are depicted in Figure 27. Against *M. phlei*, no activity was detected for any of the sC18 variants (Data not shown), which could be explained by the fact that *M. phlei* was very hard to threat with antibiotics due to its additional mycolic acid layer. The control peptide **sC18** showed a slightly increased percentage of living bacteria for *M. luteus* at 2.5  $\mu\text{M}$  and 5  $\mu\text{M}$ , which was also detected for *B. subtilis* (Figure 26). Moreover, **sC18** exhibited no toxic effects against *C. glutamicum* and *M. luteus*. The single isoleucine exchange

**sC18I10** showed the highest toxic effect even though no significant differences between **sC18**, **sC18I10**, **sC18I15** and **sC18I16** could be detected. Having a closer look to the double mutants, no differences between **sC18I10I15**, **sC18I10I16** and **sC18I15I16** could be observed. However, the triple exchange of **sC18I10I15I16** was a little bit less active than the double mutants, which could be explained by the high hydrophobicity content that is too high with 38% of hydrophobic residues in the CPP sequence. Another explanation could be that the steric hindrance of the many isoleucine residues did not permit the formation of an alpha helix, resulting in the loss of activity.

The most active single-exchanged peptide against *M. luteus* was again **sC18I10**. **sC18I16** was the second most active compound. A closer look at the combination of these single exchanges (**sC18I10I16**) showed a high increased antimicrobial effect at 5  $\mu\text{M}$  – 15  $\mu\text{M}$ . The triple exchanged peptide **sC18I10I15I16** was again less active at 5  $\mu\text{M}$  – 15  $\mu\text{M}$  than all double exchanges.

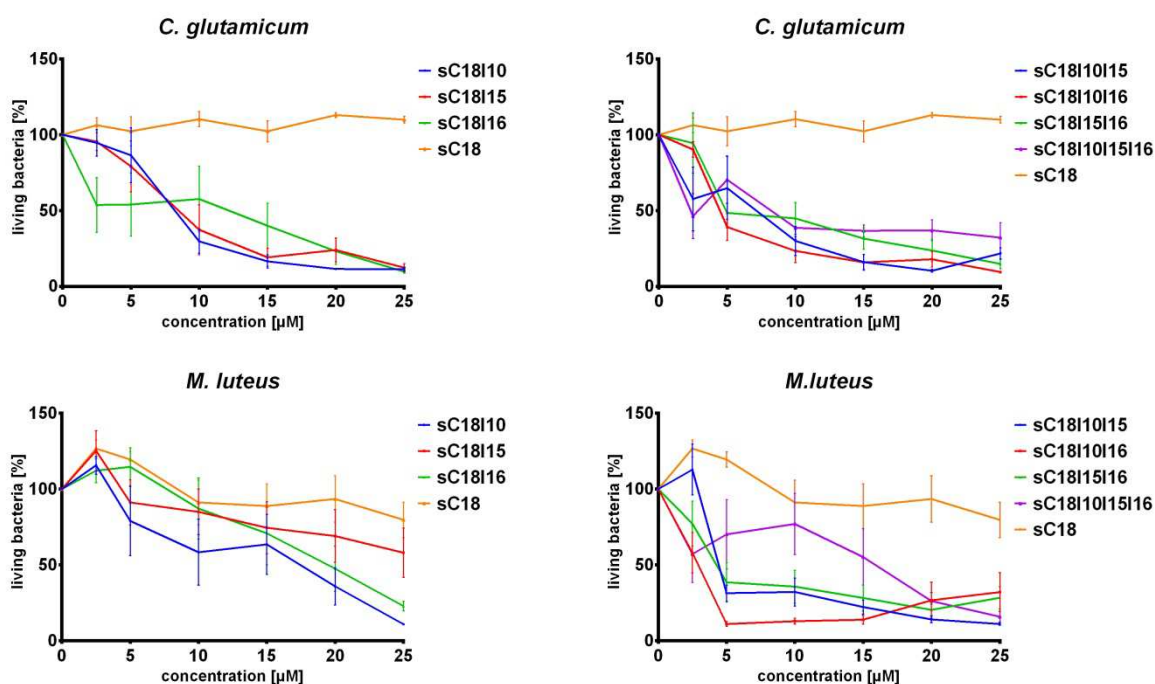


**Figure 27: Antimicrobial activity of sC18 isoleucine variants against *C. glutamicum* and *M. luteus*.** Antimicrobial activity was tested against *C. glutamicum* and *M. luteus* (2.5, 5, 10, 15, 20 and 25  $\mu\text{M}$ ). On the left site the single isoleucine exchanges were depicted, while the right site shows the double and triple isoleucine exchanges. Each value represents the mean  $\pm$  SEM ( $n=2$  in triplicate). Negative control (water) was set up to 100%.

Within the third group of tested bacteria were the gram-negative actinobacteria *P. fluorescens*, *S. typhimurium* and *E. coli*. The results for *E. coli* were not displayed because no antimicrobial effect was detected for any compound. The results for *P. fluorescens* and *S. typhimurium* depicted in Figure 28 exhibited similar results than obtained for the other bacteria. The single exchange at position 10 showed the highest increase in activity with MIC<sub>50</sub> values of around 5  $\mu$ M. Moreover, **sC18I10I15I16** did not increase the activity compared to **sC18I10**, **sC18I15** and **sC18I16**.

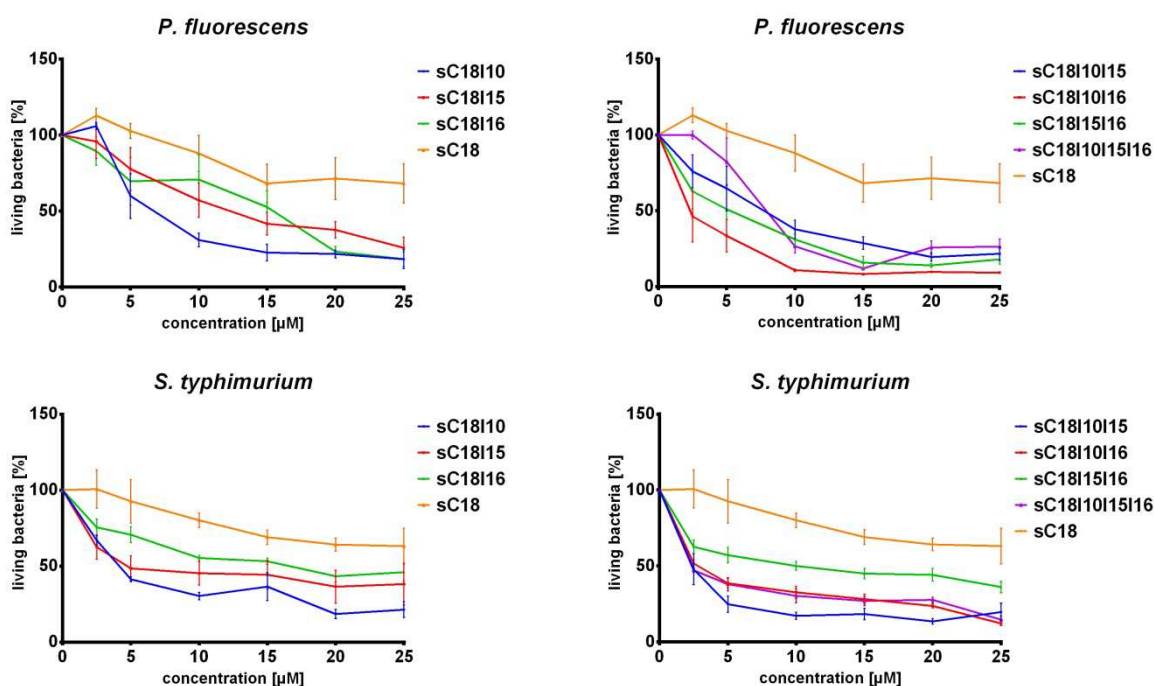


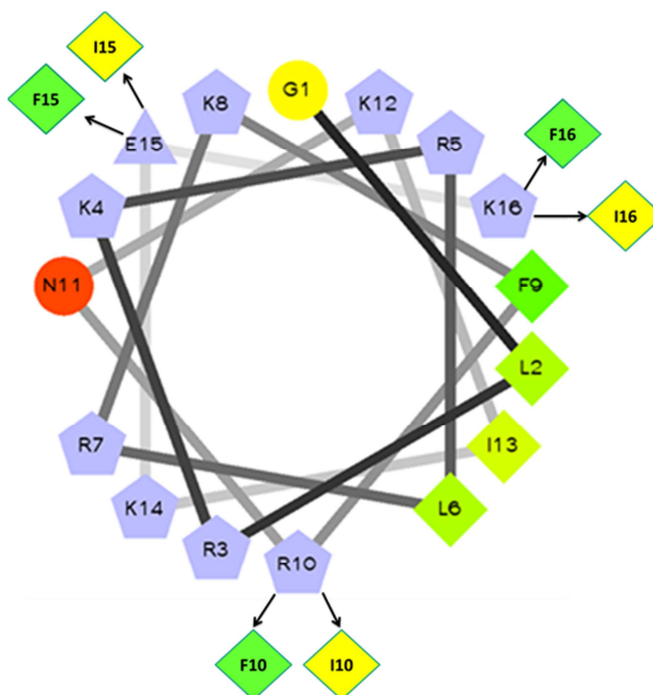
**Figure 28: Antimicrobial activity of sC18 isoleucine variants against *P. fluorescens* and *S. typhimurium*.** Antimicrobial activity was tested against *P. fluorescens* and *S. typhimurium* (2.5, 5, 10, 15, 20 and 25  $\mu$ M). On the left site the single isoleucine exchanges were depicted, while the right site shows the double and triple isoleucine exchanges. Each value represents the mean  $\pm$  SEM ( $n=2$  in triplicate). Negative control (water) was set up to 100%.

In comparison, the results showed that an increase of the hydrophobic faces (**sC18I10** and **sC18I16**) affects the antimicrobial activity more than the deletion of the acidic glutamic acid. Nevertheless, the combination of these variations to the double exchange variant **sC18I10I16** led to an increased antimicrobial effect. On the contrary, this was not the case for the triple exchange variant **sC18I10I15I16** compared to the double exchanged ones. The observation that position 10 seemed

to be the most important one can be explained as follows. First, the variant **sC18I10** expands the hydrophobic face more compared to **sC18I16** due to the loss of an amino acid between arginine 10 and leucine 6, which can be seen in the helical wheel projection (Figure 24). Secondly, the sC18 peptide contains 16 amino acids and position 16 is direct at the C-terminus. Therefore, this position is not as important as position 10 in the  $\alpha$ -helical secondary structure.

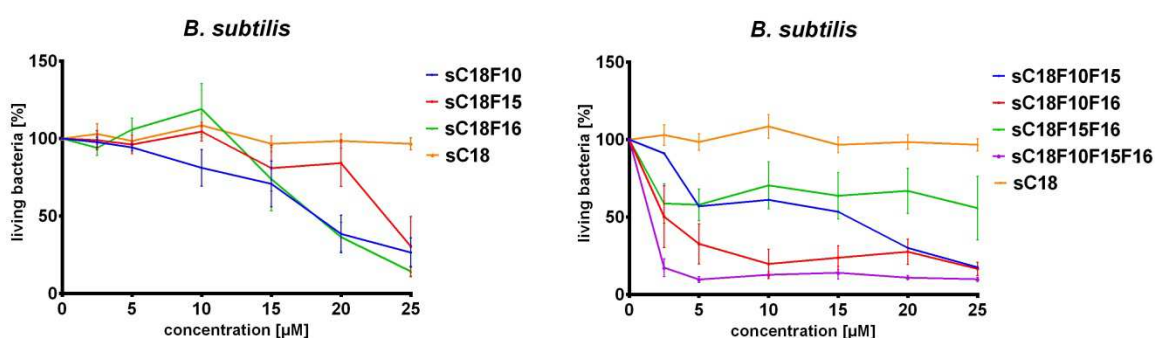
### 3.3.3. Antimicrobial activity of phenylalanine variants

To investigate further the influence of hydrophobic amino acids to the antimicrobial activity of antimicrobial peptides phenylalanine exchanges were performed because phenylalanine is more hydrophobic than isoleucine. The positions chosen were the same than for the isoleucine scan, namely **sC18F10**, **sC18F15**, **sC18F16**, **sC18F10F15**, **sC18F10F16**, **sC18F15F16** and **sC18F10F15F16** (Figure 29). Again, all variants were tested against the seven bacterial strains mentioned above.



**Figure 29: Helical wheel projection.** Helical wheel projection with amino acid exchanges at position 10, 15 and 16. Hydrophilic residues are shown as circles, hydrophobic residues as diamonds, potentially negatively charged residues as triangles and potentially positively charged residues as pentagons. The most hydrophobic residue is green, and the amount of green is decreasing proportionally to the hydrophobicity, with zero hydrophobicity coded as yellow while hydrophilic residues are coded in red. The potentially charged residues are light blue. The program of the website <http://r2lab.ucr.edu> was used for helical wheel projections.

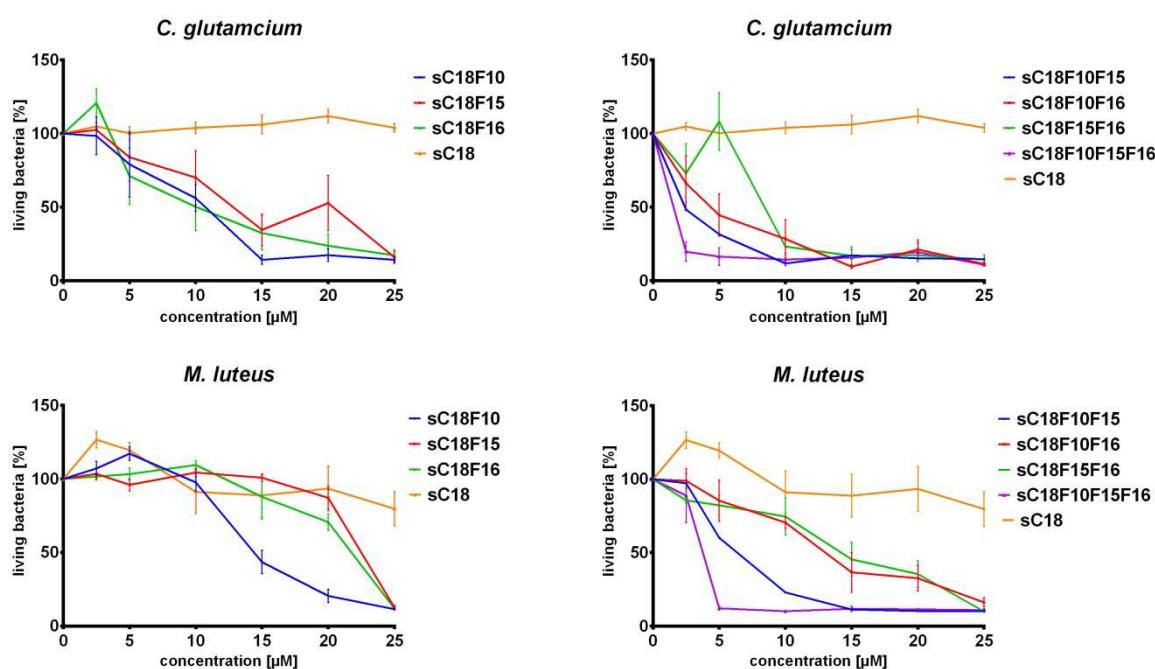
Figure 30 illustrates the results of the antimicrobial activity against the gram-positive bacterium *B. subtilis*. The highest activity of the single mutants was detectable for **sC18F10** with an MIC<sub>50</sub> value of 15 µM followed by **sC18F16**. Compared to the isoleucine single mutants, the MIC<sub>50</sub> values exhibited higher values (Figure 26), and were therefore, less active. However, at 25 µM the percentage of living bacteria was the same for isoleucine and phenylalanine single mutants. Combination of mutation F10 and mutation F16 with mutation F15 to **sC18F10F15** and **sC18F15F16** did not increase the antimicrobial activity compared to the single mutants, amplifying the argument that position 15 did not play an important role in improving the antimicrobial activity of the peptides. However, **sC18F10F16** showed an increased activity with a MIC<sub>50</sub> of 2 µM, which was further increased through the triple mutant **sC18F10F15F16** to a MIC<sub>50</sub> of 1.5 µM.



**Figure 30: Antimicrobial activity of sC18 phenylalanine variants against *B. subtilis*.** Antimicrobial activity was tested against *B. subtilis* (2.5, 5, 10, 15, 20 and 25 µM). On the left site the single isoleucine exchanges were depicted, while on the right site the double and triple isoleucine exchanges are shown. Each value represents the mean ± SEM ( $n=2$  in triplicates). Negative control (water) was set up to 100%.

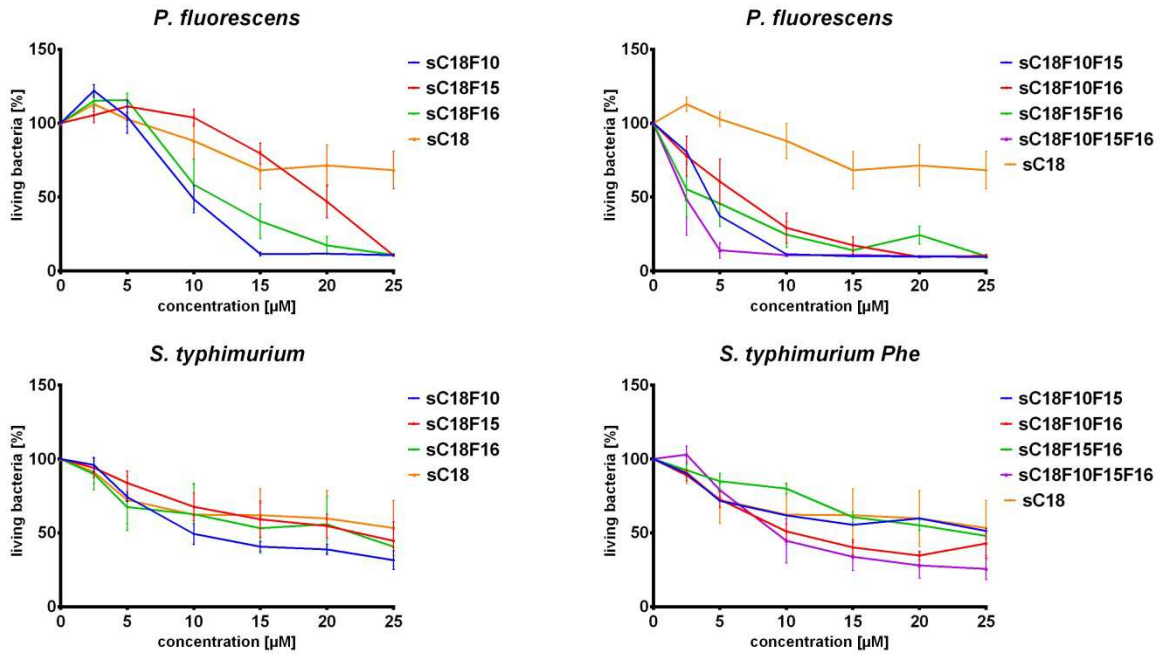
The results of the antimicrobial activity against the gram-positive bacteria *C. glutamicum* and *M. luteus* are shown in Figure 31. Again, no activity could be detected for the **sC18** peptide. Moreover, for both bacterial strains the peptide **sC18F10** was the mono mutant with the highest antimicrobial activity. For *C. glutamicum* the difference between the double mutants was not very high. In contrast, **sC18F15** and **sC18F16** only exhibited an antimicrobial activity at 25 µM, while at 20 µM nearly 90% living bacteria were detected. As already seen for *B. subtilis*, the triple mutant **sC18F10F15F16** also increased the antimicrobial

activity against *C. glutamicum* and *M. luteus* compared to all mono and double mutants.



**Figure 31: Antimicrobial activity of sC18 phenylalanine variants against *C. glutamicum* and *M. luteus*.** Antimicrobial activity was tested against *C. glutamicum* and *M. luteus* (2.5, 5, 10, 15, 20 and 25 µM). On the left site, the single isoleucine exchanges were depicted, while on the right site the double and triple isoleucine exchanges are shown. Each value represents the mean  $\pm$  SEM ( $n=2$  in triplicate). Negative control (water) was set up to 100%.

Finally, the results of the phenylalanine variants against the actinobacteria *P. fluorescens* and *S. typhimurium* are shown in Figure 32. Again **sC18F10** exhibited the highest antimicrobial activity as single mutant with only 15 % living bacteria at 15 µM against *P. fluorescens*. Examining the double and triple mutants, only the triple mutant **sC18F10F15F16** displayed an increased antimicrobial activity with only 15 % living bacteria at 5 µM. The results for *S. typhimurium* were a little bit different, since only minor alterations in the antimicrobial activity could be detected for all sC18 variants. Nevertheless, the double mutant **sC18F10F16** and the triple mutant **sC18F10F15F16** showed a slightly increased activity compared to the other variants.



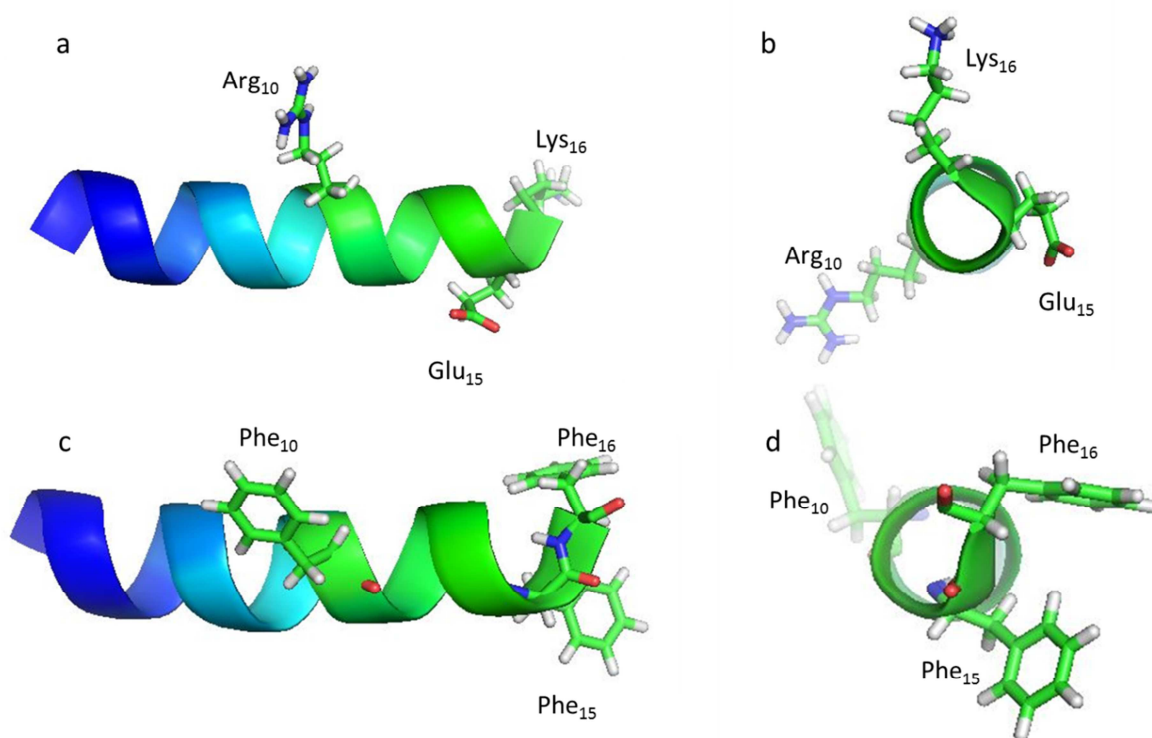
**Figure 32: Antimicrobial activity of sC18 phenylalanine variants against *P. fluorescens* and *S. typhimurium*.** Antimicrobial activity was tested against *P. fluorescens* and *S. typhimurium* (2.5, 5, 10, 15, 20 and 25 µM). On the left site, the single isoleucine exchanges were depicted, while the right site shows the double and triple isoleucine exchanges. Each value represents the mean ± SEM ( $n=2$  in triplicate). Negative control (water) was set up to 100%.

Table 12 summarizes the MIC<sub>50</sub> values against every bacterial strain tested. The results indicate that the isoleucine mono variants were more active than the phenylalanine mono variants. Peptides with exchanges at position 10 were the most active ones. As already mentioned, the reason for this could be that position 10 is located in the middle of the α-helix, while position 15 and 16 are the last amino acids at the C-terminus. Therefore, it might be that positions 15 and 16 are less important for the formation of an α-helix. Comparing the results of the double and triple mutants, the phenylalanine double and triple variants were more active than the isoleucine double and triple variants. Comparing phenylalanine double and triple mutations, more phenylalanine mutations resulted in a higher antimicrobial activity. In contrast, the antimicrobial activity of the isoleucine triple mutant decreased compared to **sC18I10I15**, **sC18I10I16** and **sC18I15I16**. To explain why a synergetic effect was detected for the phenylalanine mutations, the 3D-structures of **sC18** and **sC18F10F15F16** are depicted in Figure 33. While for sC18 the glutamic acid at position 15 and the lysine at position 16 point into opposite directions (Figure 33 b), the phenylalanine at position 15 and 16 of the **sC18F10F15F16** peptide are close

nearby for hydrophobic and pi-interactions of the benzyl rings. In 1985, Singh *et al.* reported that parallel structures of phenylalanine rings exhibit the highest interaction in proteins but are unstable and therefore, only very less found in proteins (203). More common and stable are perpendicular interactions, where the ring planes are tilted. This interaction can also be found in **sC18F10F15F16** (Figure 33 d). Hereby, hydrophobic interactions between the positively charged hydrogens of phenylalanine 15 and the cloud of  $\pi$ -electrons of the phenylalanine ring at position 16 stabilize the peptide (203). This stabilization maybe helps the peptide to form an  $\alpha$ -helix and to better integrate into bacterial membranes. Moreover, the hydrophobic interaction of these two phenylalanines helps the peptide to insert into the lipid bilayer from the C-terminal end, which interacts with the hydrophobic tails of the lipid bilayer (204).

**Table 12: Calculated MIC<sub>50</sub> values of all isoleucine and phenylalanine variants.** Half minimal inhibitory concentration (MIC<sub>50</sub>) was calculated using the GraphPad Prism 6.0 Software. First, all graphs were depicted in a logarithmic representation and then a nonlinear regression curve fit was performed (Settings: (log) inhibitor vs. normalized response – variable slope).

MIC <sub>50</sub> in $\mu$ M	sC18	sC18I10	sC18I15	sC18I16	sC18I10I15	sC18I10I16	sC18I15I16	sC18I10I15I16
<i>B. subtilis</i>	> 25	6.9	> 25	5.9	3.8	2.5	3.6	2.2
<i>C. glutamicum</i>	>25	8.2	8.6	5.5	4.9	5.2	7.6	5.3
<i>M. luteus</i>	> 25	14.2	> 25	18.9	6	1.3	5.3	10.9
<i>M. phlei</i>	> 25	> 25	> 25	> 25	> 25	> 25	> 25	> 25
<i>P. fluorescens</i>	>25	7.6	12.6	12.6	7.2	2.3	4.5	8.2
<i>S. typhimurium</i>	> 25	4.5	6.5	16.4	1.7	2.8	9.2	2.1
<i>E. coli</i>	> 25	> 25	> 25	> 25	> 25	> 25	> 25	> 25
	sC18	sC18F10	sC18F15	sC18F16	sC18F10F15	sC18F10F16	sC18F15F16	sC18F10F15F16
<i>B. subtilis</i>	> 25	18	23.1	18.3	11.1	2	> 25	1.5
<i>C. glutamicum</i>	>25	9.7	14.3	10.5	2.1	4.3	8.6	1.5
<i>M. luteus</i>	> 25	15	23.3	21.4	6.3	13.2	13.7	3.8
<i>M. phlei</i>	> 25	> 25	> 25	> 25	> 25	> 25	> 25	> 25
<i>P. fluorescens</i>	>25	10.1	19.2	12.1	4.3	6	3.4	2.2
<i>S. typhimurium</i>	> 25	12.1	21.3	18.9	> 25	12.4	23.6	10.7



**Figure 33: 3D-structure of sC18 (above) and sC18F10F15F16 (below).** Structure was generated using PyMOL. Full peptide is shown in an  $\alpha$ -helical formation with additionally highlighted side chains of amino acid position 10, 15 and 16. On the left side, the 3D-structure is shown in side view (a: sC18 / c: sC18F10F15F16), while the right side depicted the 3D-structure in top view (b: sC18 / d: sC18F10F15F16).

To further investigate the structural relationships between activity and amino acid exchange, CD-spectrometry was performed. In particular, the connection between secondary structure and activity of position 10 should be considered with this experiment.

### 3.3.4. Characterization of peptides via CD-spectrometry

To get a first impression of the secondary structure of the peptides, CD spectroscopy was performed in 10 mM phosphate buffer (Figure 34). All isoleucine and phenylalanine variants displayed a minimum at 198 nm, which is characteristic for a random coil secondary structure. These results were expected since the sC18 peptide is relatively short with 16 amino acids, and therefore, does not build an  $\alpha$ -helix in a buffer solution. The small maxima at 195 nm of **sC18F10F16** and **sC18F10F15F16** can be a first hint for the building of an  $\alpha$ -helix, but probably it was a concentration error.

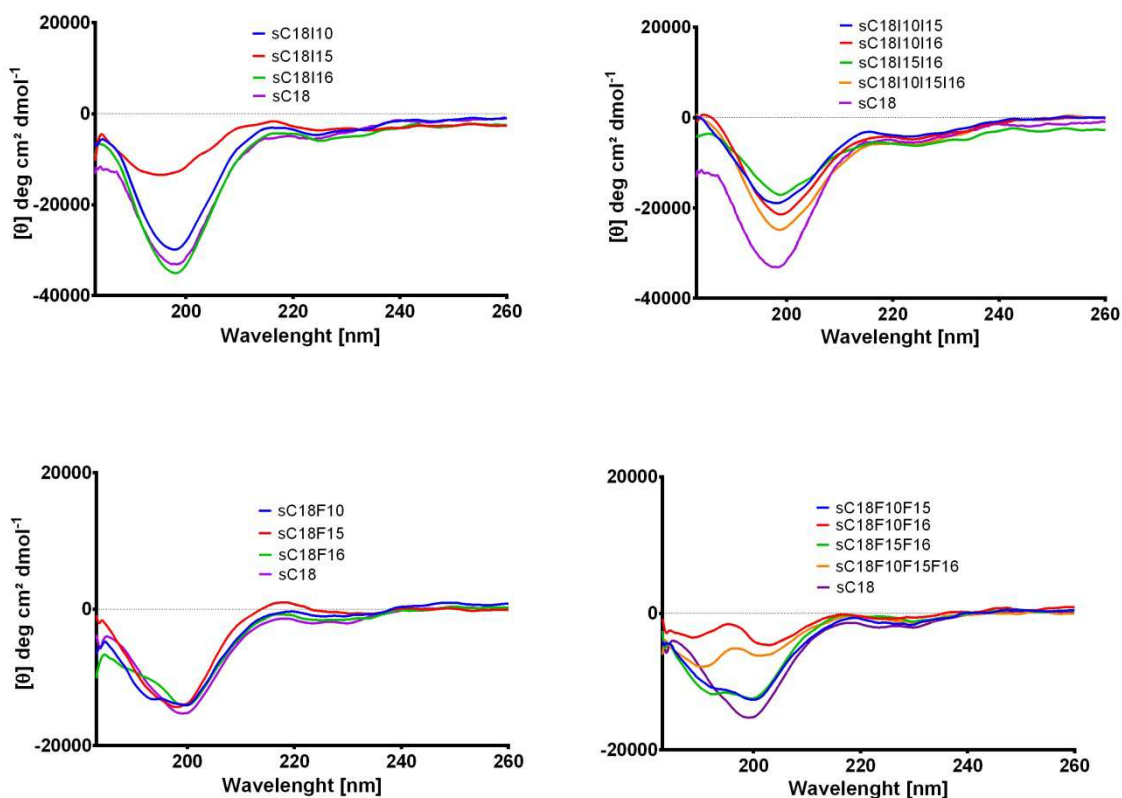


**Figure 34: Circular dichroism spectra of isoleucine and phenylalanine variants in phosphate buffer.** The spectra were measured at a peptide concentration of 20  $\mu\text{M}$  in 10 mM phosphate buffer.

To study the secondary structure in more detail, 50% 2,2,2-Trifluoroethanol (TFE) was added to the phosphate buffer solution (Figure 35). TFE is a secondary structure inducing agent, which stabilizes peptides secondary structure (205). Two minima at 208 nm and 222 nm and one maximum at 190 nm could be found for all isoleucine and phenylalanine variants as well as for **sC18** and are characteristic for an  $\alpha$ -helical secondary structure. To rigorously interpret the  $\alpha$ -helical structure the R-value, representing the ratio between the molar ellipticity values at position 222 nm and 208 nm, was calculated. An R-value of 1 represents a perfectly built  $\alpha$ -helix (206). The unmodified **sC18** peptide exhibited an R-value of 0.83. Comparing this R-value with the isoleucine single mutants, no significant changes could be detected (R-values: 0.8 – 0.82) (Figure 34). Furthermore, no changes could be detected for **sC18F10F15** and **sC10F10F16**. In contrast, slightly lower R-values of 0.78 were detected for **sC18F15F16** and the triple mutant **sC18F10F15F16** concluding that two isoleucines at the C-terminal part maybe destabilize the secondary structure or somehow hinder the formation of an  $\alpha$ -helix. Contrarily to the

results of the isoleucine mono variants, the phenylalanine mono variant **sC18F10** displayed a higher R-value of 0.9 compared to **sC18**. This observation can be connected to the high antimicrobial activity, which was detected for **sC18F10**. No significant changes were detected for **sC18F15** and **sC18F16**, which amplifies the assumption that these two amino acid positions 15 and 16 are not as important for the secondary structure as position 10. Having a closer look at the phenylalanine double and triple mutants no further changes in the R-value could be detected. All variants containing an isoleucine at position 10 (**sC18F10F15**, **sC18F10F16** and **sC18F10F15F16**) showed a calculated R-value of 0.91 or 0.92. Only the double mutant **sC18F15F16** exhibited the same R-value than **sC18** strengthening the argument that only position 10 is important for the secondary structure. An explanation why phenylalanine showed an increased R-value compared to isoleucine can be given with the  $\alpha$ -helix propensity theory of Chou and Fasman, published in 1974 (207). Hereby, the value of  $\alpha$ -helix propensity for phenylalanine is 1.12 while for isoleucine it is 1.00 showing that the introduction of phenylalanine within the peptide sequence is more suitable for an  $\alpha$ -helical secondary structure. Moreover, glutamic acid and lysine have an  $\alpha$ -helix propensity of 1.53 and 1.07, respectively. These two amino acids are the original amino acids of the sC18 at position 15 and 16. An exchange led to a decrease in the  $\alpha$ -helix propensity for glutamic acid, while there is no essential difference for lysine. Differently, the amino acid exchange of arginine at position 10 with phenylalanine increased the  $\alpha$ -helix propensity from 0.79 to 1.12, which can be also a way to explain the increased R-value of all sC18 variants containing a phenylalanine at position 10.

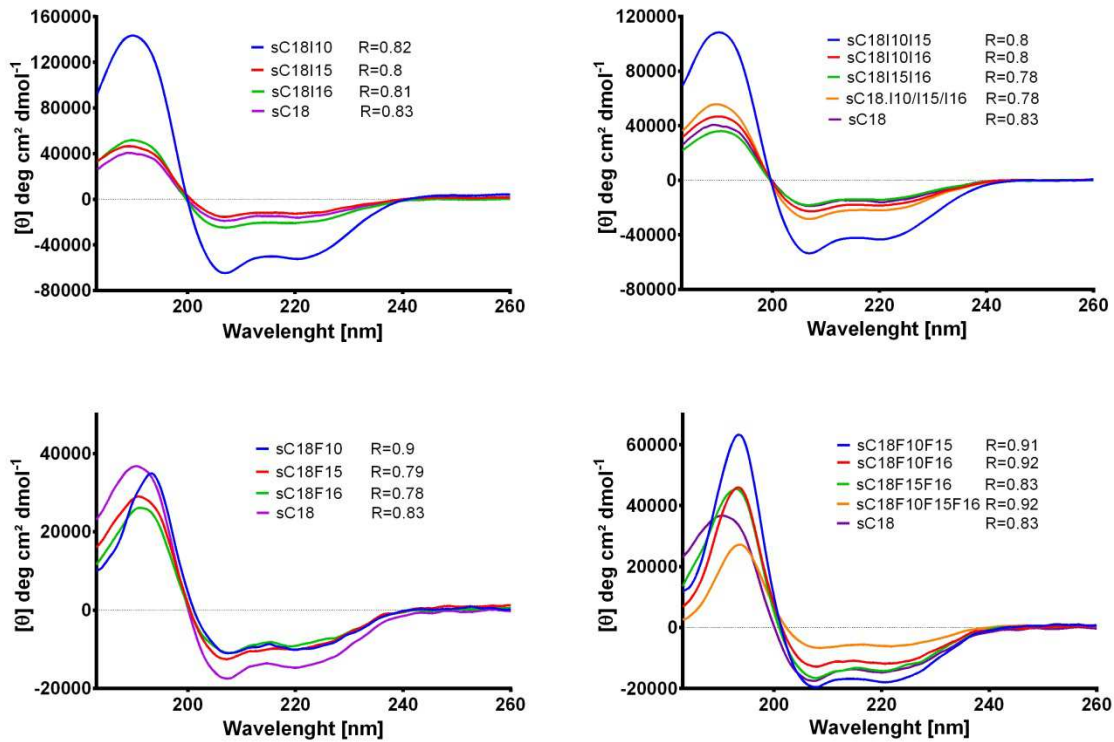


**Figure 35: Circular dichroism spectra of isoleucine and phenylalanine variants in phosphate buffer + TFE.** The spectra were measured at a peptide concentration of 20  $\mu\text{M}$  in 10 mM phosphate buffer with 50% TFE. R-values (R) represent the ratio between the molar ellipticity values at 222 nm and 208 nm.

### 3.3.5. Peptide interaction with artificial membrane vesicles

The results of CD-measurement showed that position 10 is important for the formation of the  $\alpha$ -helix. However, the function of position 15 and 16, especially in the very active triple mutant **sC18F10F15F16**, remains unclear. To answer this question, and to verify why the tested peptides in general exhibited activity against *B. subtilis*, but not against *E. coli*, two artificial membrane systems were produced using large unilamellar vesicles (LUVs). Therefore, two different LUV compositions mimicking the membranes of *B. subtilis* (DOPE:DOPG:CL 15:80:5) and *E. coli* (DOPE:DOPG 80:20) were prepared. Vesicles that should mimic the outer membrane of the gram-positive bacterium *B. subtilis* contained higher amounts of the negatively charged DOPG. In contrast, the composition, combining the inner and outer membrane of the gram-negative bacterium *E. coli* consisted of more neutral DOPE. Figure 36 shows the results of the CD experiments, which were conducted with the most active isoleucine and phenylalanine variants. Obviously, the peptides incubated with DOPE:DOPG:CL vesicles displayed a more defined

secondary structure when compared to vesicles mimicking the membrane of *E. coli*. The two isoleucine variants **sC18I10I15** and **sC18I10I16** showed two minima at 208 nm and 220 nm and a maximum at 195 nm indicating an  $\alpha$ -helical secondary structure. Furthermore, also **sC18F10F16** and **sC18F10F15F16** exhibited structural elements revealing an  $\alpha$ -helix, although the structure was not as distinct as for the isoleucine variants. This can be explained by the use of two different LUV stock solutions that were used. In comparison, the structure of the four peptides incubated with DOPE:DOPG vesicles seemed to be unstructured. While for the isoleucine variants only a minimum at 222 nm was detected, phenylalanine variants show a maximum at 200 nm. These structural differences in the presence of different vesicles can be a hint why the peptides are more active against *B. subtilis* than *E. coli*. Nevertheless, the structural elements do not seem to be the only important factor for antimicrobial activity. Especially for **sC18F10F15F16**, there could exist a combination of secondary structure, peptide stabilization and interaction with the hydrophobic tails of the lipid bilayer leading to the highest antimicrobial activity of all sC18 variants.

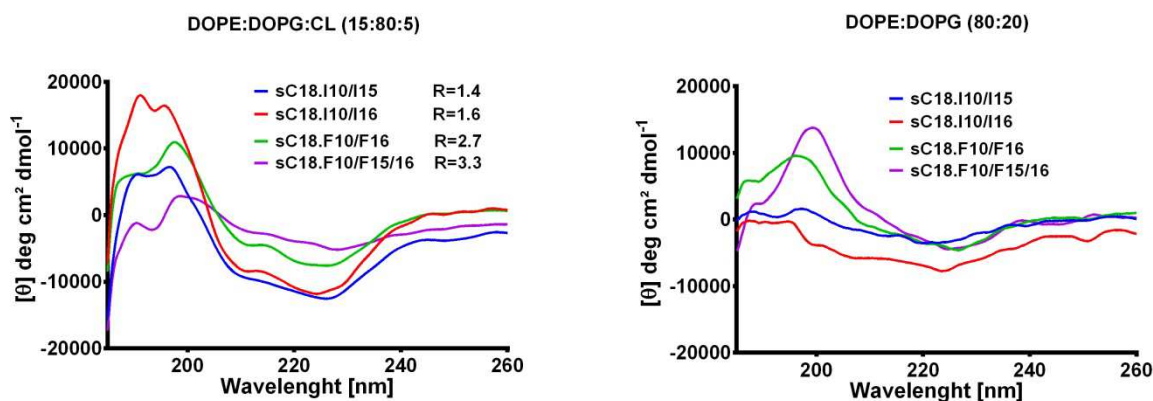


**Figure 36: Circular dichroism spectra with artificial membrane vesicles.** LUVs containing DOPE:DOPG:CL (15:80:5) and DOPE:DOPG (80:20) was prepared to imitate the membrane of *B. subtilis* and *E. coli*, respectively. The spectra were measured at a peptide concentration of 20  $\mu$ M in 10 mM phosphate buffer with 1 mM LUVs. R-values (R) represent the ratio between the molar ellipticity values at 222 nm and 208 nm.

Stella *et al.* already showed that the main difference between CPP and AMP activity could be their affinities towards bacterial membranes (200). Especially a positive charge is needed to bind more strongly to the anionic bilayer. Since the increased

activity in this work could not be explained with a higher positive charge, there seem to be other characteristics. Concluding all results, two further characteristics can be emphasized. On the one hand, position 10 stabilizes the  $\alpha$ -helical structure and maybe increases the hydrophobic interaction between the hydrophobic parts of two AMPs during pore formation. On the other hand, position 15 and 16 interact with each other, especially when exchanged with phenylalanine, and further interact as first amino acids with the hydrophobic tails of the lipid molecules, resulting in a higher affinity to the bacterial membrane. This model was already published in literature for cytolytic peptides, describing that hydrophobic interaction also increases the cytolytic activity (204). LUV experiments, imitating *B. subtilis* or *E. coli* membranes, gave a further hint that the bacterial membrane composition is related to peptide activity. This would explain why the sC18 variants exhibited different activities against different bacteria. Nevertheless, this result cannot be generalized for all gram-positive and gram-negative bacteria because every group has their exceptions. For the gram-negative bacterium *C. crescentus*, the absence of phosphatidylethanolamine (208) is as unusual as the high amount of phosphatidylethanolamine in the gram-positive bacterium *B. polymyxa* (209). This observation shows that also in the bacterial subgroups every bacterium differs in their lipid composition making it very hard to treat all bacteria of one subgroup equally.

To give an overview about the interaction of the **sC18F10F15F16** peptide with the membrane bilayer a mechanism of action model was proposed in Figure 37. In a first step, the positive charged amino acids of **sC18F10F15F16** get attached to the negatively charged phospholipids (for example DOPG). Hereby, the positive peptide net charge of +8 (Table 11) is very helpful for this interaction. In a second step, the phenylalanine at position 15 and 16 start an interaction with the hydrophobic lipid tails leading to an insertion of the peptide into the membrane. Furthermore, an interaction between the phenylalanines at position 10 of different peptides can be hypothesized resulting in an  $\alpha$ -helix stabilization (stripped black line in Figure 37). This hypothesis can be reinforced, because all sC18 variants with a phenylalanine at position 10 exhibited a better distinct  $\alpha$ -helix (Figure 35). The last step is the complete integration of more peptides building a pore, which then leads to a destabilization of the membrane and an antimicrobial effect. The inside of the pore is built by the hydrophilic sides of the peptides.

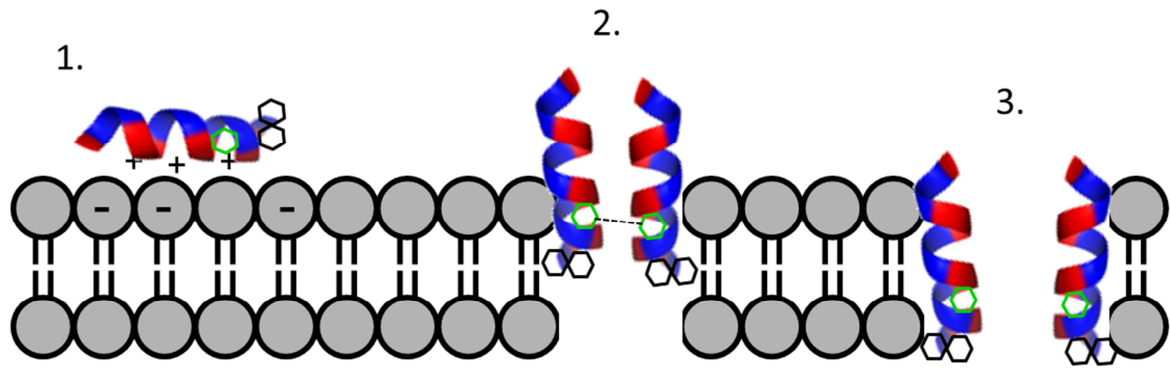


**Figure 37: Mechanism of action model for sC18F10F15F16.** (1) Positive arginine and lysine residue interact with negatively charged phospholipids (red: hydrophilic side, blue: hydrophobic side). Hereby, the peptide gets attached to the membrane. (2) Phenylalanine's at position 15 and 16 (black hexamers) are the first amino acids, which interact with the hydrophobic tails of the lipid molecules starting the incorporation of the peptides in the membrane bilayer. The phenylalanine's at position 10 (green hexamers) interact among themselves (striped black line) stabilizing the  $\alpha$ -helical structure. (3) Peptides are integrated into the membrane bilayer building a pore.

## 4. Conclusion and Outlook

Within this work, different strategies are described to increase the antimicrobial activity of AMPs, e.g. conjugation to imidazolium salts, immobilization on membranes, or amino acid exchanges.

In a first step, a branched imidazolium-salt compound was designed and successfully conjugated to sC18 and LL-37. The combination of the antimicrobial characteristics of AMPs and imidazolium-salts led to a highly increased antimicrobial activity, especially against hard to medicate multi-drug resistant strains like MRSA and VRE. The secondary structure of compound **3c** was characterized under very basic and acidic conditions. No changes in the secondary structure were detected, showing that the peptide is stable under these extreme conditions. To use the compound as future antibiotic, its stability against proteases and human blood plasma should be investigated. Another important attribute of antibiotics is their selectivity. **3b** and **3c** exhibited very strong antimicrobial activity, but were only less selective against human red blood cells, while on the other hand **3a** showed better selectivity. Furthermore, the influence of cholesterol as a membrane compound was investigated, since only eukaryotic cells contain cholesterol. Compounds **3b** and **3c** were less active against vesicles containing cholesterol, concluding that the compounds also show selectivity towards eukaryotic cells. In conclusion, this work demonstrated for the first time that imidazolium salts conjugated to antimicrobial peptides led to highly active compounds, especially against resistant bacterial strains. Since compound **3a** exhibits highest selectivity, this compound could be a future lead structure for new antibiotic agents.

In a second step, the novel designed compound **3a** was immobilized on a polyether sulfone membrane using different linkers (compounds **3a**, **3d**, **3e** and **3f**) to achieve a surface with high antimicrobial activity. The immobilization with electron beam radiation and chemical coupling was very successful for all compounds. To increase the activity range, further polyethylene glycol (PEG) chains could be coupled to the C-terminus, which also should lead to a better flexibility. In general, an introduction of a hydrophobic linker seemed to be more effective for a successful electron beam radiation. Anyway, the electron radiation is a technique without the use of catalyst or toxic reagents, but has the problem that the integration position of the compound is not completely understood yet (210). Consequently, the chemical coupling method

seems to be more attractive for the immobilization of peptide compounds since the peptide is arranged at the surface of the membrane via a peptide bond and not integrated into the membrane. Conclusively, both immobilization methods are easy and powerful to coat antimicrobial compounds on polyether sulfone membranes retaining their antimicrobial effect.

Finally, the thin line between cell-penetrating peptides and antimicrobial peptides was investigated modulating the CPP sC18 to an antimicrobial peptide via amino acid exchanges. The **sC18** peptide already consists of a lot of positively charged amino acids, whereas the focus had been on increasing the hydrophobic face of **sC18** including phenylalanine and isoleucine. The antimicrobial activity already was increased with one amino acid substitution and showed the highest effect for **sC18F10F15F16**. The hydrophobic face seemed to be as important for antimicrobial activity as the cationic charge. Position 15 showed the weakest effects since the hydrophobic amino acid was incorporated in the hydrophilic face of the  $\alpha$ -helix. Therefore, a substitution of glutamic acid at position 15 with arginine or lysine should enhance the antimicrobial activity further. Therefore, in a next step of experiments, the selectivity of the novel sC18 variants should be determined to verify if the lytic activity against human cell lines or human red blood cells also increases through the different amino acid exchanges. Moreover, bacteria with high phosphatidylethanolamine content seem to be more resistant against the treatment with antimicrobial peptides since the role of phosphatidylethanolamine is to spread out the negatively charged phospholipids and reduce the negatively overall membrane charge (177).

Recently, the appearance of more and more multi-resistant strains has forced the development of novel antimicrobial compounds. However, the use of AMPs as clinical application is still far away because of their low specificity and their toxic side effects. In this work, it could be shown that small modifications of the peptide sequence can lead to characteristic changes, but predicting these changes remains challenging. To use AMPs as antibiotics, the mechanism of action should be better understood. However, especially their unique membrane targeting mechanism makes AMPs to a benefit in public health in the near future.

## 5. Literature

- (1) **Morar, M., and Wright, G. D. (2010)** The Genomic Enzymology of Antibiotic Resistance. *Annu Rev Genet* 44, 25-51.
- (2) **Marr, A. K., Gooderham, W. J., and Hancock, R. E. W. (2006)** Antibacterial peptides for therapeutic use: obstacles and realistic outlook. *Curr Opin Pharmacol* 6, 468-472.
- (3) **Mygind, P. H., Fischer, R. L., Schnorr, K. M., Hansen, M. T., Sonksen, C. P., Ludvigsen, S., Raventos, D., Buskov, S., Christensen, B., De Maria, L., Taboureau, O., Yaver, D., Elvig-Jorgensen, S. G., Sorensen, M. V., Christensen, B. E., Kjaerulff, S., Frimodt-Moller, N., Lehrer, R. I., Zasloff, M., and Kristensen, H. H. (2005)** Plectasin is a peptide antibiotic with therapeutic potential from a saprophytic fungus. *Nature* 437, 975-980.
- (4) **van 't Hof, W., Veerman, E. C. I., Helmerhorst, E. J., and Amerongen, A. V. N. (2001)** Antimicrobial peptides: Properties and applicability. *Biol Chem* 382, 597-619.
- (5) **Davies, S. C., Fowler, T., Watson, J., Livermore, D. M., and Walker, D. (2013)** Annual Report of the Chief Medical Officer: infection and the rise of antimicrobial resistance. *Lancet* 381, 1606-1609.
- (6) **Davies, J., and Davies, D. (2010)** Origins and Evolution of Antibiotic Resistance. *Microbiol Mol Biol R* 74, 417-+.
- (7) **Enright, M. C., Robinson, D. A., Randle, G., Feil, E. J., Grundmann, H., and Spratt, B. G. (2002)** The evolutionary history of methicillin-resistant *Staphylococcus aureus* (MRSA). *P Natl Acad Sci USA* 99, 7687-7692.
- (8) **Martinez, J. L., and Baquero, F. (2002)** Interactions among strategies associated with bacterial infection: Pathogenicity, epidemicity, and antibiotic resistance. *Clin Microbiol Rev* 15, 647-+.
- (9) **Dzidic, S., Suskovic, J., and Kos, B. (2008)** Antibiotic resistance mechanisms in bacteria: Biochemical and genetic aspects. *Food Technol Biotech* 46, 11-21.
- (10) **Russell, A. D. (1986)** Mechanisms of Bacterial-Resistance to Antibacterial Agents. *Pharm Int* 7, 300-305.
- (11) **Raghunath, D. (2008)** Emerging antibiotic resistance in bacteria with special reference to India. *Journal of biosciences* 33, 593-603.
- (12) **Hickey, S. M., and Nelson, J. D. (1997)** Mechanisms of antibacterial resistance. *Advances in pediatrics* 44, 1-41.
- (13) **Wright, G. D. (2005)** Bacterial resistance to antibiotics: enzymatic degradation and modification. *Advanced drug delivery reviews* 57, 1451-70.
- (14) **Thomson, J. M., and Bonomo, R. A. (2005)** The threat of antibiotic resistance in Gram-negative pathogenic bacteria: beta-lactams in peril! *Curr Opin Microbiol* 8, 518-524.
- (15) **Strateva, T., and Yordanov, D. (2009)** *Pseudomonas aeruginosa* - a phenomenon of bacterial resistance. *J Med Microbiol* 58, 1133-1148.
- (16) **Maurice, F., Broutin, I., Podglajen, I., Benas, P., Collatz, E., and Dardel, F. (2008)** Enzyme structural plasticity and the emergence of broad-spectrum antibiotic resistance. *Embo Rep* 9, 344-349.
- (17) **Depardieu, F., Podglajen, I., Leclercq, R., Collatz, E., and Courvalin, P. (2007)** Modes and modulations of antibiotic resistance gene expression. *Clin Microbiol Rev* 20, 79-114.
- (18) **Livermore, D. M. (1991)** Mechanisms of Resistance to Beta-Lactam Antibiotics. *Scand J Infect Dis*, 7-16.
- (19) **Mingeot-Leclercq, M. P., Glupczynski, Y., and Tulkens, P. M. (1999)** Aminoglycosides: Activity and resistance. *Antimicrob Agents Ch* 43, 727-737.
- (20) **Gutmann, L., Alobeid, S., Billotklein, D., Guerrier, M. L., and Collatz, E. (1994)** Synergy and Resistance to Synergy between Beta-Lactam Antibiotics and Glycopeptides against Glycopeptide-Resistant Strains of *Enterococcus-Faecium*. *Antimicrob Agents Ch* 38, 824-829.

- (21) **Speer, B. S., Shoemaker, N. B., and Salyers, A. A. (1992)** Bacterial-Resistance to Tetracycline - Mechanisms, Transfer, and Clinical-Significance. *Clin Microbiol Rev* 5, 387-399.
- (22) **Fernandez, M., Conde, S., de la Torre, J., Molina-Santiago, C., Ramos, J. L., and Duque, E. (2012)** Mechanisms of Resistance to Chloramphenicol in *Pseudomonas putida* KT2440. *Antimicrob Agents Ch* 56, 1001-1009.
- (23) **Hancock, R. E. W., and Lehrer, R. (1998)** Cationic peptides: a new source of antibiotics. *Trends Biotechnol* 16, 82-88.
- (24) **Brogden, K. A., Ackermann, M., McCray, P. B., and Tack, B. F. (2003)** Antimicrobial peptides in animals and their role in host defences. *Int J Antimicrob Ag* 22, 465-478.
- (25) **Aoki, W., Kuroda, K., and Ueda, M. (2012)** Next generation of antimicrobial peptides as molecular targeted medicines. *J Biosci Bioeng* 114, 365-370.
- (26) **Hancock, R. E. W., and Sahl, H. G. (2006)** Antimicrobial and host-defense peptides as new anti-infective therapeutic strategies. *Nat Biotechnol* 24, 1551-1557.
- (27) **Nguyen, L. T., Haney, E. F., and Vogel, H. J. (2011)** The expanding scope of antimicrobial peptide structures and their modes of action. *Trends Biotechnol* 29, 464-472.
- (28) **Yang, D., Biragyn, A., Hoover, D. M., Lubkowski, J., and Oppenheim, J. J. (2004)** Multiple roles of antimicrobial defensins, cathelicidins, and eosinophil-derived neurotoxin in host defense. *Annu Rev Immunol* 22, 181-215.
- (29) **Melo, M. N., Ferre, R., and Castanho, M. A. R. B. (2009)** OPINION Antimicrobial peptides: linking partition, activity and high membrane-bound concentrations. *Nat Rev Microbiol* 7, 245-250.
- (30) **Zasloff, M. (2002)** Antimicrobial peptides of multicellular organisms. *Nature* 415, 389-395.
- (31) **Powers, J. P. S., and Hancock, R. E. W. (2003)** The relationship between peptide structure and antibacterial activity. *Peptides* 24, 1681-1691.
- (32) **Andersson, M., Boman, A., and Boman, H. G. (2003)** *Ascaris* nematodes from pig and human make three antibacterial peptides: isolation of cecropin P1 and two ASABF peptides. *Cell Mol Life Sci* 60, 599-606.
- (33) **Agerberth, B., Gunne, H., Odeberg, J., Kogner, P., Boman, H. G., and Gudmundsson, G. H. (1995)** Fall-39, a Putative Novel Human Peptide Antibiotic, Cystein-Free and Expressed in Bone-Marrow and Testis. *J Cell Biochem*, 265-265.
- (34) **Falla, T. J., Karunaratne, D. N., and Hancock, R. E. W. (1996)** Mode of action of the antimicrobial peptide indolicidin. *J Biol Chem* 271, 19298-19303.
- (35) **Frank, R. W., Gennaro, R., Schneider, K., Przybylski, M., and Romeo, D. (1990)** Amino-Acid-Sequences of 2 Proline-Rich Bactenecins - Antimicrobial Peptides of Bovine Neutrophils. *J Biol Chem* 265, 18871-18874.
- (36) **Wu, M. H., and Hancock, R. E. W. (1999)** Interaction of the cyclic antimicrobial cationic peptide bactenecin with the outer and cytoplasmic membrane. *J Biol Chem* 274, 29-35.
- (37) **Misiewicz, J., Berditsch, M., Afonin, S., and Ulrich, A. S. (2014)** The Antimicrobial Peptide Gramicidin S Forms Intracellular Nano-Globules with High Energy Phosphates in *Aneurinibacillus Migulanus*. *J Pept Sci* 20, S204-S204.
- (38) **Dings, R. P. M., Haseman, J. R., Leslie, D. B., Luong, M., Dunn, D. L., and Mayo, K. H. (2013)** Bacterial membrane disrupting dodecapeptide SC4 improves survival of mice challenged with *Pseudomonas aeruginosa*. *Bba-Gen Subjects* 1830, 3454-3457.
- (39) **Rozek, A., Friedrich, C. L., and Hancock, R. E. W. (2000)** Structure of the bovine antimicrobial peptide indolicidin bound to dodecylphosphocholine and sodium dodecyl sulfate micelles. *Biochemistry-Us* 39, 15765-15774.
- (40) **Peters, B. M., Shirliff, M. E., and Jabra-Rizk, M. A. (2010)** Antimicrobial Peptides: Primeval Molecules or Future Drugs? *Plos Pathog* 6.
- (41) **Fjell, C. D., Hiss, J. A., Hancock, R. E. W., and Schneider, G. (2012)** Designing antimicrobial peptides: form follows function. *Nat Rev Drug Discov* 11, 37-51.

- (42) **Findlay, B., Zhanel, G. G., and Schweizer, F. (2010)** Cationic Amphiphiles, a New Generation of Antimicrobials Inspired by the Natural Antimicrobial Peptide Scaffold. *Antimicrob Agents Ch* 54, 4049-4058.
- (43) **Strom, M. B., Haug, B. E., Skar, M. L., Stensen, W., Stiberg, T., and Svendsen, J. S. (2003)** The pharmacophore of short cationic antibacterial peptides. *J Med Chem* 46, 1567-1570.
- (44) **Thaker, H. D., Sgolastra, F., Clements, D., Scott, R. W., and Tew, G. N. (2011)** Synthetic Mimics of Antimicrobial Peptides from Triaryl Scaffolds. *J Med Chem* 54, 2241-2254.
- (45) **Reinhardt, A., and Neundorff, I. (2016)** Design and Application of Antimicrobial Peptide Conjugates. *Int J Mol Sci* 17.
- (46) **Gordon, Y. J., Romanowski, E. G., and McDermott, A. M. (2005)** A review of antimicrobial peptides and their therapeutic potential as anti-infective drugs. *Curr Eye Res* 30, 505-515.
- (47) **Li, W. F., Ma, G. X., and Zhou, X. X. (2006)** Apidaecin-type peptides: Biodiversity, structure-function relationships and mode of action. *Peptides* 27, 2350-2359.
- (48) **Lee, E., Shin, A., and Kim, Y. (2015)** Anti-Inflammatory Activities of Cecropin a and Its Mechanism of Action. *Arch Insect Biochem* 88, 31-44.
- (49) **Han, J., Jyoti, M. A., Song, H. Y., and Jang, W. S. (2016)** Antifungal Activity and Action Mechanism of Histatin 5-Halocidin Hybrid Peptides against *Candida* ssp. *Plos One* 11.
- (50) **Subbalakshmi, C., and Sitaram, N. (1998)** Mechanism of antimicrobial action of indolicidin. *Fems Microbiol Lett* 160, 91-96.
- (51) **McGrath, D. M., Barbu, E. M., Driessen, W. H. P., Lasco, T. M., Tarrand, J. J., Okhuysen, P. C., Kontoyiannis, D. P., Sidman, R. L., Pasqualini, R., and Arap, W. (2013)** Mechanism of action and initial evaluation of a membrane active all-D-enantiomer antimicrobial peptidomimetic. *P Natl Acad Sci USA* 110, 3477-3482.
- (52) **Bjorstad, A., Askarieh, G., Brown, K. L., Christenson, K., Forsman, H., Onnheim, K., Li, H. N., Teneberg, S., Maier, O., Hoekstra, D., Dahlgren, C., Davidson, D. J., and Bylund, J. (2009)** The Host Defense Peptide LL-37 Selectively Permeabilizes Apoptotic Leukocytes. *Antimicrob Agents Ch* 53, 1027-1038.
- (53) **Matsuzaki, K. (1998)** Magainins as paradigm for the mode of action of pore forming polypeptides. *Bba-Rev Biomembranes* 1376, 391-400.
- (54) **Yang, L., Harroun, T. A., Weiss, T. M., Ding, L., and Huang, H. W. (2001)** Barrel-stave model or toroidal model? A case study on melittin pores. *Biophys J* 81, 1475-1485.
- (55) **Splith, K., and Neundorff, I. (2011)** Antimicrobial peptides with cell-penetrating peptide properties and vice versa. *Eur Biophys J Biophys* 40, 387-397.
- (56) **Li, A., Lee, P. Y., Ho, B., Ding, J. L., and Lim, C. T. (2007)** Atomic force microscopy study of the antimicrobial action of Sushi peptides on Gram negative bacteria. *Biochim Biophys Acta* 1768, 411-8.
- (57) **Belaid, A., Aouni, M., Khelifa, R., Trabelsi, A., Jemmali, M., and Hani, K. (2002)** In vitro antiviral activity of dermaseptins against herpes simplex virus type-1. *J Med Virol* 66, 229-234.
- (58) **Robinson, W. E., McDougall, B., Tran, D., and Selsted, M. E. (1998)** Anti-HIV-1 activity of indolicidin, an antimicrobial peptide from neutrophils. *J Leukocyte Biol* 63, 94-100.
- (59) **Sitaram, N., and Nagaraj, R. (1999)** Interaction of antimicrobial peptides with biological and model membranes: structural and charge requirements for activity. *Bba-Biomembranes* 1462, 29-54.
- (60) **Yasin, B., Wang, W., Pang, M., Cheshenko, N., Hong, T., Waring, A. J., Herold, B. C., Wagar, E. A., and Lehrer, R. I. (2004)** theta defensins protect cells from infection by herpes simplex virus by inhibiting viral adhesion and entry. *J Virol* 78, 5147-5156.
- (61) **Sinha, S., Cheshenko, N., Lehrer, R. I., and Herold, B. C. (2003)** NP-1, a rabbit alpha-defensin, prevents the entry and intercellular spread of herpes simplex virus type 2. *Antimicrob Agents Ch* 47, 494-500.
- (62) **de Lucca, A. J., and Walsh, T. J. (1999)** Antifungal peptides: Novel therapeutic compounds against emerging pathogens. *Antimicrob Agents Ch* 43, 1-11.

- (63) **Lee, Y. T., Kim, D. H., Suh, J. Y., Chung, J. H., Lee, B. L., Lee, Y., and Choi, S. (1999)** Structural characteristics of tenecin 3, an insect antifungal protein. *Biochem Mol Biol Int* 47, 369-376.
- (64) **Lustig, F., Hoebeke, J., OstergrenLunden, G., VelgeRoussel, F., Bondjers, G., Olsson, U., Ruetschi, U., and Fager, G. (1996)** Alternative splicing determines the binding of platelet-derived growth factor (PDGF-AA) to glycosaminoglycans. *Biochemistry-Us* 35, 12077-12085.
- (65) **Pushpanathan, M., Rajendhran, J., Jayashree, S., Sundarakrishnan, B., Jayachandran, S., and Gunasekaran, P. (2012)** Identification of a Novel Antifungal Peptide with Chitin-Binding Property from Marine Metagenome. *Protein Peptide Lett* 19, 1289-1296.
- (66) **van der Weerden, N. L., Hancock, R. E. W., and Anderson, M. A. (2010)** Permeabilization of Fungal Hyphae by the Plant Defensin NaD1 Occurs through a Cell Wall-dependent Process. *J Biol Chem* 285, 37513-37520.
- (67) **Moerman, L., Bosteels, S., Noppe, W., Willems, J., Clynen, E., Schoofs, L., Thevissen, K., Tytgat, J., Van Eldere, J., van der Walt, J., and Verdonck, F. (2002)** Antibacterial and antifungal properties of alpha-helical, cationic peptides in the venom of scorpions from southern Africa. *Eur J Biochem* 269, 4799-4810.
- (68) **Zasloff, M. (1987)** Magainins, a Class of Antimicrobial Peptides from *Xenopus* Skin - Isolation, Characterization of 2 Active Forms, and Partial Cdna Sequence of a Precursor. *P Natl Acad Sci USA* 84, 5449-5453.
- (69) **Park, Y., Jang, S. H., Lee, D. G., and Hahm, K. S. (2004)** Antinematodal effect of antimicrobial peptide, PMAP-23, isolated from porcine myeloid against *Caenorhabditis elegans*. *J Pept Sci* 10, 304-311.
- (70) **Shai, Y. (2002)** Mode of action of membrane active antimicrobial peptides. *Biopolymers* 66, 236-248.
- (71) **Jenssen, H., Hamill, P., and Hancock, R. E. W. (2006)** Peptide antimicrobial agents. *Clin Microbiol Rev* 19, 491-+.
- (72) **Brogden, K. A. (2005)** Antimicrobial peptides: Pore formers or metabolic inhibitors in bacteria? *Nat Rev Microbiol* 3, 238-250.
- (73) **Brumfitt, W., Salton, M. R. J., and Hamilton-Miller, J. M. T. (2002)** Nisin, alone and combined with peptidoglycan-modulating antibiotics: activity against methicillin-resistant *Staphylococcus aureus* and vancomycin-resistant enterococci. *J Antimicrob Chemoth* 50, 731-734.
- (74) **Selsted, M. E., Novotny, M. J., Morris, W. L., Tang, Y. Q., Smith, W., and Cullor, J. S. (1992)** Indolicidin, a Novel Bactericidal Tridecapeptide Amide from Neutrophils. *J Biol Chem* 267, 4292-4295.
- (75) **Larrick, J. W., Morgan, J. G., Palings, I., Hirata, M., and Yen, M. H. (1991)** Complementary-DNA Sequence of Rabbit Cap18 - a Unique Lipopolysaccharide Binding-Protein. *Biochemical and biophysical research communications* 179, 170-175.
- (76) **Tossi, A., Scocchi, M., Skerlavaj, B., and Gennaro, R. (1994)** Identification and Characterization of a Primary Antibacterial Domain in Cap18, a Lipopolysaccharide-Binding Protein from Rabbit Leukocytes. *Febs Lett* 339, 108-112.
- (77) **Kichler, A., Mason, A. J., and Bechinger, B. (2006)** Cationic amphipathic histidine-rich peptides for gene delivery. *Bba-Biomembranes* 1758, 301-307.
- (78) **Neundorf, I., Rennert, R., Hoyer, J., Schramm, F., Lobner, K., Kitanovic, I., and Wolf, S. (2009)** Fusion of a Short HA2-Derived Peptide Sequence to Cell-Penetrating Peptides Improves Cytosolic Uptake, but Enhances Cytotoxic Activity. *Pharmaceuticals (Basel)* 2, 49-65.
- (79) **Hu, W., Splith, K., Neundorf, I., Merz, K., and Schatzschneider, U. (2012)** Influence of the metal center and linker on the intracellular distribution and biological activity of organometal-peptide conjugates. *Journal of biological inorganic chemistry : JBIC : a publication of the Society of Biological Inorganic Chemistry* 17, 175-85.

- (80) **Splith, K., Hu, W., Schatzschneider, U., Gust, R., Ott, I., Onambele, L. A., Prokop, A., and Neundorf, I. (2010)** Protease-activatable organometal-Peptide bioconjugates with enhanced cytotoxicity on cancer cells. *Bioconjugate chemistry* 21, 1288-96.
- (81) **Reichart, F., Horn, M., and Neundorf, I. (2016)** Cyclization of a cell-penetrating peptide via click-chemistry increases proteolytic resistance and improves drug delivery. *J Pept Sci* 22, 421-426.
- (82) **Horn, M., Reichart, F., Natividad-Tietz, S., Diaz, D., and Neundorf, I. (2016)** Tuning the properties of a novel short cell-penetrating peptide by intramolecular cyclization with a triazole bridge. *Chem Commun* 52, 2261-2264.
- (83) **Scott, M. G., Yan, H., and Hancock, R. E. W. (1999)** Biological properties of structurally related alpha-helical cationic antimicrobial peptides. *Infect Immun* 67, 2005-2009.
- (84) **Scott, M. G., Gold, M. R., and Hancock, R. E. W. (1999)** Interaction of cationic peptides with lipoteichoic acid and gram-positive bacteria. *Infect Immun* 67, 6445-6453.
- (85) **Malanovic, N., and Lohner, K. (2016)** Gram-positive bacterial cell envelopes: The impact on the activity of antimicrobial peptides. *Bba-Biomembranes* 1858, 936-946.
- (86) **Madani, F., Lindberg, S., Langel, U., Futaki, S., and Graslund, A. (2011)** Mechanisms of cellular uptake of cell-penetrating peptides. *J Biophys* 2011, 414729.
- (87) **Song, Y. M., Park, Y., Lim, S. S., Yang, S. T., Woo, E. R., Park, I. S., Lee, J. S., Kim, J. I., Hahm, K. S., Kim, Y., and Shin, S. Y. (2005)** Cell selectivity and mechanism of action of antimicrobial model peptides containing peptoid residues. *Biochemistry-Us* 44, 12094-12106.
- (88) **Matsuzaki, K., Murase, O., Fujii, N., and Miyajima, K. (1996)** An antimicrobial peptide, magainin 2, induced rapid flip-flop of phospholipids coupled with pore formation and peptide translocation. *Biochemistry-Us* 35, 11361-11368.
- (89) **Shai, Y. (1999)** Mechanism of the binding, insertion and destabilization of phospholipid bilayer membranes by alpha-helical antimicrobial and cell non-selective membrane-lytic peptides. *Bba-Biomembranes* 1462, 55-70.
- (90) **Ladokhin, A. S., and White, S. H. (2001)** 'Detergent-like' permeabilization of anionic lipid vesicles by melittin. *Bba-Biomembranes* 1514, 253-260.
- (91) **Ebenhan, T., Gheysens, O., Kruger, H. G., Zeevaert, J. R., and Sathekge, M. M. (2014)** Antimicrobial Peptides: Their Role as Infection-Selective Tracers for Molecular Imaging. *Biomed Res Int*.
- (92) **Bahar, A., and Ren, D. (2013)** Antimicrobial Peptides. *Pharmaceuticals* 6, 1543.
- (93) **Otvos, L., Jr. (2005)** Antibacterial peptides and proteins with multiple cellular targets. *J Pept Sci* 11, 697-706.
- (94) **Mookherjee, N., Lippert, D. N., Hamill, P., Falsafi, R., Nijnik, A., Kindrachuk, J., Pistolic, J., Gardy, J., Miri, P., Naseer, M., Foster, L. J., and Hancock, R. E. (2009)** Intracellular receptor for human host defense peptide LL-37 in monocytes. *J Immunol* 183, 2688-96.
- (95) **McGillivray, G., and Bakaletz, L. O. (2010)** The multifunctional host defense peptide SPLUNC1 is critical for homeostasis of the mammalian upper airway. *Plos One* 5, e13224.
- (96) **Hilpert, K., McLeod, B., Yu, J., Elliott, M. R., Rautenbach, M., Ruden, S., Burck, J., Muhle-Goll, C., Ulrich, A. S., Keller, S., and Hancock, R. E. (2010)** Short cationic antimicrobial peptides interact with ATP. *Antimicrob Agents Chemother* 54, 4480-3.
- (97) **Park, C. B., Kim, H. S., and Kim, S. C. (1998)** Mechanism of action of the antimicrobial peptide buforin II: buforin II kills microorganisms by penetrating the cell membrane and inhibiting cellular functions. *Biochemical and biophysical research communications* 244, 253-7.
- (98) **Castle, M., Nazarian, A., Yi, S. S., and Tempst, P. (1999)** Lethal effects of apidaecin on Escherichia coli involve sequential molecular interactions with diverse targets. *J Biol Chem* 274, 32555-64.

- (99) **Nishikata, M., Kanehira, T., Oh, H., Tani, H., Tazaki, M., and Kuboki, Y. (1991)** Salivary Histatin as an Inhibitor of a Protease Produced by the Oral Bacterium *Bacteroides-Gingivalis*. *Biochemical and biophysical research communications* 174, 625-630.
- (100) **Kragol, G., Lovas, S., Varadi, G., Condie, B. A., Hoffmann, R., and Otvos, L. (2001)** The antibacterial peptide pyrrocoricin inhibits the ATPase actions of DnaK and prevents chaperone-assisted protein folding. *Biochemistry-Us* 40, 3016-3026.
- (101) **Ishikawa, M., Kubo, T., and Natori, S. (1992)** Purification and Characterization of a Dipterin Homolog from *Sarcophaga-Peregrina* (Flesh Fly). *Biochem J* 287, 573-578.
- (102) **Westerhoff, H. V., Juretic, D., Hendler, R. W., and Zasloff, M. (1989)** Magainins and the disruption of membrane-linked free-energy transduction. *Proc Natl Acad Sci U S A* 86, 6597-601.
- (103) **Oren, Z., and Shai, Y. (1996)** A class of highly potent antibacterial peptides derived from pardaxin, a pore-forming peptide isolated from Moses sole fish *Pardachirus marmoratus*. *Eur J Biochem* 237, 303-10.
- (104) **Pace, C. N., and Scholtz, J. M. (1998)** A helix propensity scale based on experimental studies of peptides and proteins. *Biophys J* 75, 422-7.
- (105) **Boman, H. G., Agerberth, B., and Boman, A. (1993)** Mechanisms of action on *Escherichia coli* of cecropin P1 and PR-39, two antibacterial peptides from pig intestine. *Infect Immun* 61, 2978-84.
- (106) **Cabiaux, V., Agerberth, B., Johansson, J., Homble, F., Goormaghtigh, E., and Ruyschaert, J. M. (1994)** Secondary structure and membrane interaction of PR-39, a Pro+Arg-rich antibacterial peptide. *Eur J Biochem* 224, 1019-27.
- (107) **Nicolas, P., and Mor, A. (1995)** Peptides as Weapons against Microorganisms in the Chemical Defense System of Vertebrates. *Annu Rev Microbiol* 49, 277-304.
- (108) **Vaara, M. (1992)** Agents That Increase the Permeability of the Outer-Membrane. *Microbiol Rev* 56, 395-411.
- (109) **Yeaman, M. R., and Yount, N. Y. (2003)** Mechanisms of antimicrobial peptide action and resistance. *Pharmacol Rev* 55, 27-55.
- (110) **Jiang, Z. Q., Vasil, A. I., Hale, J., Hancock, R. E. W., Vasil, M. L., and Hodges, R. S. (2009)** Effects of net charge and the number of positively charged residues on the biological activity of amphipathic alpha-helical cationic antimicrobial peptides. *Adv Exp Med Biol* 611, 561-562.
- (111) **Tossi, A., Sandri, L., and Giangaspero, A. (2000)** Amphipathic, alpha-helical antimicrobial peptides. *Biopolymers* 55, 4-30.
- (112) **Dathe, M., Wieprecht, T., Nikolenko, H., Handel, L., Maloy, W. L., MacDonald, D. L., Beyermann, M., and Bienert, M. (1997)** Hydrophobicity, hydrophobic moment and angle subtended by charged residues modulate antibacterial and haemolytic activity of amphipathic helical peptides. *Febs Lett* 403, 208-212.
- (113) **Parachin, N. S., and Franco, O. L. (2014)** New edge of antibiotic development: antimicrobial peptides and corresponding resistance. *Front Microbiol* 5.
- (114) **Zhang, T. H., Muraih, J. K., Tishbi, N., Herskowitz, J., Victor, R. L., Silverman, J., Uwumarenogie, S., Taylor, S. D., Palmer, M., and Mintzer, E. (2014)** Cardiolipin Prevents Membrane Translocation and Permeabilization by Daptomycin. *J Biol Chem* 289, 11584-11591.
- (115) **Biot, F. V., Lopez, M. M., Poyot, T., Neulat-Ripoll, F., Lignon, S., Caclard, A., Thibault, F. M., Peinnequin, A., Pages, J. M., and Valade, E. (2013)** Interplay between Three RND Efflux Pumps in Doxycycline-Selected Strains of *Burkholderia thailandensis*. *Plos One* 8.
- (116) **Peschel, A., Otto, M., Jack, R. W., Kalbacher, H., Jung, G., and Gotz, F. (1999)** Inactivation of the *dlt* operon in *Staphylococcus aureus* confers sensitivity to defensins, protegrins, and other antimicrobial peptides. *J Biol Chem* 274, 8405-8410.
- (117) **Gunn, J. S., Ryan, S. S., Van Velkinburgh, J. C., Ernst, R. K., and Miller, S. I. (2000)** Genetic and functional analysis of a PmrA-PmrB-regulated locus necessary for lipopolysaccharide

- modification, antimicrobial peptide resistance, and oral virulence of *Salmonella enterica* serovar typhimurium. *Infect Immun* 68, 6139-6146.
- (118) **Costerton, J. W., Stewart, P. S., and Greenberg, E. P. (1999)** Bacterial biofilms: A common cause of persistent infections. *Science* 284, 1318-1322.
- (119) **Harro, J. M., Peters, B. M., O'May, G. A., Archer, N., Kerns, P., Prabhakara, R., and Shirliff, M. E. (2010)** Vaccine development in *Staphylococcus aureus*: taking the biofilm phenotype into consideration. *Fems Immunol Med Mic* 59, 306-323.
- (120) **Donlan, R. M., and Costerton, J. W. (2002)** Biofilms: Survival mechanisms of clinically relevant microorganisms. *Clin Microbiol Rev* 15, 167-+.
- (121) **Fey, P. D. (2010)** Modality of bacterial growth presents unique targets: how do we treat biofilm-mediated infections? *Curr Opin Microbiol* 13, 610-615.
- (122) **Hoiby, N., Bjarnsholt, T., Givskov, M., Molin, S., and Ciofu, O. (2010)** Antibiotic resistance of bacterial biofilms. *Int J Antimicrob Ag* 35, 322-332.
- (123) **Yang, L. A., Liu, Y., Wu, H., Hoiby, N., Molin, S., and Song, Z. J. (2011)** Current understanding of multi-species biofilms. *Int J Oral Sci* 3, 74-81.
- (124) **Wolcott, R., Costerton, J. W., Raoult, D., and Cutler, S. J. (2013)** The polymicrobial nature of biofilm infection. *Clin Microbiol Infect* 19, 107-112.
- (125) **Chang, Y. W., Fragkopoulos, A. A., Marquez, S. M., Kim, H. D., Angelini, T. E., and Fernandez-Nieves, A. (2015)** Biofilm formation in geometries with different surface curvature and oxygen availability. *New J Phys* 17.
- (126) **Flemming, H. C., and Wingender, J. (2010)** The biofilm matrix. *Nat Rev Microbiol* 8, 623-633.
- (127) **Kragh, K. N., Hutchison, J. B., Melaugh, G., Rodesney, C., Roberts, A. E. L., Irie, Y., Jensen, P. O., Diggle, S. P., Allen, R. J., Gordon, V., and Bjarnsholt, T. (2016)** Role of Multicellular Aggregates in Biofilm Formation. *Mbio* 7.
- (128) **Koch, H., Lucker, S., Albertsen, M., Kitzinger, K., Herbold, C., Spieck, E., Nielsen, P. H., Wagner, M., and Daims, H. (2015)** Expanded metabolic versatility of ubiquitous nitrite-oxidizing bacteria from the genus *Nitrospira*. *P Natl Acad Sci USA* 112, 11371-11376.
- (129) **de Carvalho, C. C. (2007)** Biofilms: recent developments on an old battle. *Recent patents on biotechnology* 1, 49-57.
- (130) **Monteiro, D. R., Gorup, L. F., Takamiya, A. S., Ruvollo, A. C., Camargo, E. R., and Barbosa, D. B. (2009)** The growing importance of materials that prevent microbial adhesion: antimicrobial effect of medical devices containing silver. *Int J Antimicrob Ag* 34, 103-110.
- (131) **Rendueles, O., and Ghigo, J. M. (2015)** Mechanisms of Competition in Biofilm Communities. *Microbiol Spectr* 3.
- (132) **Harbers, G. M., Emoto, K., Greef, C., Metzger, S. W., Woodward, H. N., Mascali, J. J., Grainger, D. W., and Lochhead, M. J. (2007)** Functionalized poly(ethylene glycol)-based bioassay surface chemistry that facilitates bio-immobilization and inhibits nonspecific protein, bacterial, and mammalian cell adhesion. *Chem Mater* 19, 4405-4414.
- (133) **Chapman, R. G., Ostuni, E., Liang, M. N., Meluleni, G., Kim, E., Yan, L., Pier, G., Warren, H. S., and Whitesides, G. M. (2001)** Polymeric thin films that resist the adsorption of proteins and the adhesion of bacteria. *Langmuir* 17, 1225-1233.
- (134) **Goncalves, I. C., Martins, M. C. L., Barbosa, M. A., Naeemi, E., and Ratner, B. D. (2009)** Selective protein adsorption modulates platelet adhesion and activation to oligo(ethylene glycol)-terminated self-assembled monolayers with C18 ligands. *J Biomed Mater Res A* 89A, 642-653.
- (135) **Chung, D. W., Papadakis, S. E., and Yam, K. L. (2003)** Evaluation of a polymer coating containing triclosan as the antimicrobial layer for packaging materials. *Int J Food Sci Tech* 38, 165-169.
- (136) **Ravikumar, T., Murata, H., Koepsel, R. R., and Russell, A. J. (2006)** Surface-active antifungal polyquaternary amine. *Biomacromolecules* 7, 2762-2769.

- (137) **Aumsuwan, N., Danyus, R., Heinhorst, S., and Urban, M. W. (2008)** PMSE 450-Attachment of ampicilin to expanded poly(tetrafluoroethylene) (ePTFE): Surface reactions leading to inhibition of microbial growth. *Abstr Pap Am Chem S* 236.
- (138) **Cevher, E., Orhan, Z., Mulazimoglu, L., Sensoy, D., Alper, M., Yildiz, A., and Ozsoy, Y. (2006)** Characterization of biodegradable chitosan microspheres containing vancomycin and treatment of experimental osteomyelitis caused by methicillin-resistant *Staphylococcus aureus* with prepared microspheres. *Int J Pharm* 317, 127-135.
- (139) **Aumsuwan, N., Heinhorst, S., and Urban, M. W. (2007)** Antibacterial surfaces on expanded polytetrafluoroethylene; penicillin attachment. *Biomacromolecules* 8, 713-718.
- (140) **Smit, J., Kamio, Y., and Nikaido, H. (1975)** Outer Membrane of *Salmonella-Typhimurium* - Chemical-Analysis and Freeze-Fracture Studies with Lipopolysaccharide Mutants. *J Bacteriol* 124, 942-958.
- (141) **Kamio, Y., and Nikaido, H. (1976)** Outer Membrane of *Salmonella-Typhimurium* - Accessibility of Phospholipid Head Groups to Phospholipase-C and Cyanogen-Bromide Activated Dextran in External Medium. *Biochemistry-Us* 15, 2561-2570.
- (142) **Lugtenberg, E. J. J., and Peters, R. (1976)** Distribution of Lipids in Cytoplasmic and Outer Membranes of *Escherichia-Coli-K12*. *Biochim Biophys Acta* 441, 38-47.
- (143) **Ishinaga, M., Kanamoto, R., and Kito, M. (1979)** Distribution of Phospholipid Molecular-Species in Outer and Cytoplasmic Membranes of *Escherichia-Coli*. *J Biochem-Tokyo* 86, 161-165.
- (144) **Nikaido, H. (2003)** Molecular basis of bacterial outer membrane permeability revisited. *Microbiol Mol Biol R* 67, 593-+.
- (145) **Raetz, C. R. H., and Whitfield, C. (2002)** Lipopolysaccharide endotoxins. *Annu Rev Biochem* 71, 635-700.
- (146) **Tokuda, H. (2007)** Sorting of lipoproteins to the outer membrane of gram-negative bacteria. *Faseb J* 21, A41-A41.
- (147) **Miyadai, H., Tanaka-Masuda, K., Matsuayama, S., and Tokuda, H. (2004)** Effects of lipoprotein overproduction on the induction of DegP (HtrA) involved in quality control in the *Escherichia coli* periplasm. *J Biol Chem* 279, 39807-39813.
- (148) **Vollmer, W., Blanot, D., and de Pedro, M. A. (2008)** Peptidoglycan structure and architecture. *FEMS microbiology reviews* 32, 149-167.
- (149) **Mullineaux, C. W., Nenninger, A., Ray, N., and Robinson, C. (2006)** Diffusion of green fluorescent protein in three cell environments in *Escherichia coli*. *J Bacteriol* 188, 3442-3448.
- (150) **Raetz, C. R. H., and Dowhan, W. (1990)** Biosynthesis and Function of Phospholipids in *Escherichia-Coli*. *J Biol Chem* 265, 1235-1238.
- (151) **Vollmer, W., Blanot, D., and de Pedro, M. A. (2008)** Peptidoglycan structure and architecture. *Fems Microbiol Rev* 32, 149-67.
- (152) **Neuhaus, F. C., and Baddiley, J. (2003)** A continuum of anionic charge: Structures and functions of D-Alanyl-Teichoic acids in gram-positive bacteria. *Microbiol Mol Biol R* 67, 686-+.
- (153) **Dramsi, S., Magnet, S., Davison, S., and Arthur, M. (2008)** Covalent attachment of proteins to peptidoglycan. *FEMS microbiology reviews* 32, 307-320.
- (154) **Bansal-Mutalik, R., and Nikaido, H. (2014)** Mycobacterial outer membrane is a lipid bilayer and the inner membrane is unusually rich in diacyl phosphatidylinositol dimannosides. *P Natl Acad Sci USA* 111, 4958-4963.
- (155) **Lavollay, M., Arthur, M., Fourgeaud, M., Dubost, L., Marie, A., Veziris, N., Blanot, D., Gutmann, L., and Mainardi, J. L. (2008)** The peptidoglycan of stationary-phase *Mycobacterium tuberculosis* predominantly contains cross-links generated by L,D-transpeptidation. *J Bacteriol* 190, 4360-4366.
- (156) **Sani, M., Houben, E. N., Geurtsen, J., Pierson, J., de Punder, K., van Zon, M., Wever, B., Piersma, S. R., Jimenez, C. R., Daffe, M., Appelmelk, B. J., Bitter, W., van der Wel, N., and**

- Peters, P. J. (2010)** Direct visualization by cryo-EM of the mycobacterial capsular layer: a labile structure containing ESX-1-secreted proteins. *Plos Pathog* 6, e1000794.
- (157) **Takayama, K., Wang, C., and Besra, G. S. (2005)** Pathway to synthesis and processing of mycolic acids in *Mycobacterium tuberculosis*. *Clin Microbiol Rev* 18, 81-101.
- (158) **Hett, E. C., and Rubin, E. J. (2008)** Bacterial growth and cell division: a mycobacterial perspective. *Microbiology and molecular biology reviews : MMBR* 72, 126-56, table of contents.
- (159) **Brown, L., Wolf, J. M., Prados-Rosales, R., and Casadevall, A. (2015)** Through the wall: extracellular vesicles in Gram-positive bacteria, mycobacteria and fungi. *Nat Rev Microbiol* 13, 620-630.
- (160) **Carson, L., Chau, P. K. W., Earle, M. J., Gilea, M. A., Gilmore, B. F., Gorman, S. P., McCann, M. T., and Seddon, K. R. (2009)** Antibiofilm activities of 1-alkyl-3-methylimidazolium chloride ionic liquids. *Green Chem* 11, 492-497.
- (161) **Martins, M. A. P., Frizzo, C. P., Tier, A. Z., Moreira, D. N., Zanatta, N., and Bonaccorso, H. G. (2014)** Update 1 of: Ionic Liquids in Heterocyclic Synthesis. The root paper of this title was published in *Chem. Rev.* 2008, 108 (6), 2015-2050. *Chem Rev* 114, Pr1-+.
- (162) **Dreyer, S., and Kragl, U. (2008)** Ionic liquids for aqueous two-phase extraction and stabilization of enzymes. *Biotechnol Bioeng* 99, 1416-1424.
- (163) **Frizzo, C. P., Villetti, M. A., Tier, A. Z., Gindri, I. M., Buriol, L., Rosa, F. A., Claramunt, R. M., Sanz, D., and Martins, M. A. P. (2013)** Structural and thermodynamic properties of new pyrazolo[3,4-d]pyridazinones. *Thermochim Acta* 574, 63-72.
- (164) **Wasserscheid, P., and Keim, W. (2000)** Ionic liquids - New "solutions" for transition metal catalysis. *Angew Chem Int Edit* 39, 3772-3789.
- (165) **Welton, T. (1999)** Room-temperature ionic liquids. Solvents for synthesis and catalysis. *Chem Rev* 99, 2071-2083.
- (166) **Meine, N., Benedito, F., and Rinaldi, R. (2010)** Thermal stability of ionic liquids assessed by potentiometric titration. *Green Chem* 12, 1711-1714.
- (167) **Sheldrake, G. N., and Schleck, D. (2007)** Dicationic molten salts (ionic liquids) as re-usable media for the controlled pyrolysis of cellulose to anhydrosugars. *Green Chem* 9, 1044-1046.
- (168) **Weingarh, D., Czekaj, I., Fei, Z. F., Foelske-Schmitz, A., Dyson, P. J., Wokaun, A., and Kotz, R. (2012)** Electrochemical Stability of Imidazolium Based Ionic Liquids Containing Cyano Groups in the Anion: A Cyclic Voltammetry, XPS and DFT Study. *J Electrochem Soc* 159, H611-H615.
- (169) **Wang, C. M., Luo, H. M., Luo, X. Y., Li, H. R., and Dai, S. (2010)** Equimolar CO<sub>2</sub> capture by imidazolium-based ionic liquids and superbases systems. *Green Chem* 12, 2019-2023.
- (170) **Zhao, H. (2005)** Effect of ions and other compatible solutes on enzyme activity, and its implication for biocatalysis using ionic liquids. *J Mol Catal B-Enzym* 37, 16-25.
- (171) **Jungnickel, C., Luczak, J., Ranke, J., Fernandez, J. F., Muller, A., and Thoming, J. (2008)** Micelle formation of imidazolium ionic liquids in aqueous solution. *Colloid Surface A* 316, 278-284.
- (172) **Radosevic, K., Cvjetko, M., Kopjar, N., Novak, R., Dumic, J., and Srcek, V. G. (2013)** In vitro cytotoxicity assessment of imidazolium ionic liquids: Biological effects in fish Channel Catfish Ovary (CCO) cell line. *Ecotox Environ Safe* 92, 112-118.
- (173) **Egorova, K. S., and Ananikov, V. P. (2014)** Toxicity of Ionic Liquids: Eco(cyto)activity as Complicated, but Unavoidable Parameter for Task-Specific Optimization. *Chemsuschem* 7, 336-360.
- (174) **Agerberth, B., Gunne, H., Odeberg, J., Kogner, P., Boman, H. G., and Gudmundsson, G. H. (1995)** FALL-39, a putative human peptide antibiotic, is cysteine-free and expressed in bone marrow and testis. *Proc Natl Acad Sci U S A* 92, 195-9.
- (175) **Oren, Z., Lerman, J. C., Gudmundsson, G. H., Agerberth, B., and Shai, Y. (1999)** Structure and organization of the human antimicrobial peptide LL-37 in phospholipid membranes:

- relevance to the molecular basis for its non-cell-selective activity. *Biochem J* 341 ( Pt 3), 501-13.
- (176) **Reinhardt, A., Horn, M., Schmauck, J. P. G., Brohl, A., Giernoth, R., Oelkrug, C., Schubert, A., and Neundorf, I. (2014)** Novel Imidazolium Salt-Peptide Conjugates and Their Antimicrobial Activity. *Bioconjugate chemistry* 25, 2166-2174.
- (177) **Epand, R. F., Savage, P. B., and Epand, R. M. (2007)** Bacterial lipid composition and the antimicrobial efficacy of cationic steroid compounds (Ceragenins). *Bba-Biomembranes* 1768, 2500-2509.
- (178) **Ahmed, M. H., Ibrahim, M. A., Zhang, J., Melek, F. R., El-Hawary, S. S., Jacob, M. R., and Muhammad, I. (2014)** Methicillin-resistant *Staphylococcus aureus*, Vancomycin-resistant *Enterococcus faecalis* and *Enterococcus faecium* active Dimeric Isobutyrylphloroglucinol from *Ivesia gordonii*. *Nat Prod Commun* 9, 221-224.
- (179) **Reis, A. O., Cordeiro, J. C., Machado, A. M., and Sader, H. S. (2001)** In vitro antimicrobial activity of linezolid tested against vancomycin-resistant enterococci isolated in Brazilian hospitals. *The Brazilian journal of infectious diseases : an official publication of the Brazilian Society of Infectious Diseases* 5, 243-51.
- (180) **Brender, J. R., McHenry, A. J., and Ramamoorthy, A. (2012)** Does cholesterol play a role in the bacterial selectivity of antimicrobial peptides? *Front Immunol* 3.
- (181) **McHenry, A. J., Sciacca, M. F. M., Brender, J. R., and Ramamoorthy, A. (2012)** Does cholesterol suppress the antimicrobial peptide induced disruption of lipid raft containing membranes? *Bba-Biomembranes* 1818, 3019-3024.
- (182) **Oren, Z., Lerman, J. C., Gudmundsson, G. H., Agerberth, B., and Shai, Y. (1999)** Structure and organization of the human antimicrobial peptide LL-37 in phospholipid membranes: relevance to the molecular basis for its non-cell-selective activity. *Biochem J* 341, 501-513.
- (183) **Marcotte, I., Wegener, K. L., Lam, Y. H., Chia, B. C. S., de Planque, M. R. R., Bowie, J. H., Auger, M., and Separovic, F. (2003)** Interaction of antimicrobial peptides from Australian amphibians with lipid membranes. *Chem Phys Lipids* 122, 107-120.
- (184) **Feigin, A. M., Teeter, J. H., and Brand, J. G. (1995)** The Influence of Sterols on the Sensitivity of Lipid Bilayers to Melittin. *Biochemical and biophysical research communications* 211, 312-317.
- (185) **Zheng, Z. Q., Xu, Q. M., Guo, J. N., Qin, J., Mao, H. L., Wang, B., and Yan, F. (2016)** Structure-Antibacterial Activity Relationships of Imidazolium-Type Ionic Liquid Monomers, Poly(ionic liquids) and Poly(ionic liquid) Membranes: Effect of Alkyl Chain Length and Cations. *Acs Appl Mater Inter* 8, 12684-12692.
- (186) **Luczak, J., Jungnickel, C., Lacka, I., Stolle, S., and Hupka, J. (2010)** Antimicrobial and surface activity of 1-alkyl-3-methylimidazolium derivatives. *Green Chem* 12, 593-601.
- (187) **Stolte, S., Matzke, M., Arning, J., Boschen, A., Pitner, W. R., Welz-Biermann, U., Jastorff, B., and Ranke, J. (2007)** Effects of different head groups and functionalised side chains on the aquatic toxicity of ionic liquids. *Green Chem* 9, 1170-1179.
- (188) **Birnie, C. R., Malamud, D., and Schnaare, R. L. (2000)** Antimicrobial evaluation of N-alkyl betaines and N-alkyl-N,N-dimethylamine oxides with variations in chain length. *Antimicrob Agents Ch* 44, 2514-2517.
- (189) **Ho, J. Y., Matsuura, T., and Santerre, J. P. (2000)** The effect of fluorinated surface modifying macromolecules on the surface morphology of polyethersulfone membranes. *J Biomat Sci-Polym E* 11, 1085-1104.
- (190) **Van der Bruggen, B. (2009)** Chemical Modification of Polyethersulfone Nanofiltration Membranes: A Review. *J Appl Polym Sci* 114, 630-642.
- (191) **Zhao, C. S., Xue, J. M., Ran, F., and Sun, S. D. (2013)** Modification of polyethersulfone membranes - A review of methods. *Prog Mater Sci* 58, 76-150.
- (192) **Schulze, A., Stoelzer, A., Striegler, K., Starke, S., and Prager, A. (2015)** Biocatalytic Self-Cleaning Polymer Membranes. *Polymers-Basel* 7, 1837-1849.

- (193) **Starke, S., Went, M., Prager, A., and Schulze, A. (2013)** A novel electron beam-based method for the immobilization of trypsin on poly(ethersulfone) and poly(vinylidene fluoride) membranes. *React Funct Polym* 73, 698-702.
- (194) **Kim, S. M., Fan, H., Cho, Y. J., Eo, M. Y., Park, J. H., Kim, B. N., Lee, B. C., and Lee, S. K. (2015)** Electron beam effect on biomaterials I: focusing on bone graft materials. *Biomaterials research* 19, 10.
- (195) **Rapsch, K., Bier, F. F., Tadros, M., and von Nickisch-Roseneck, M. (2014)** Identification of antimicrobial peptides and immobilization strategy suitable for a covalent surface coating with biocompatible properties. *Bioconjugate chemistry* 25, 308-19.
- (196) **Richter, S., Bouvet, V., Wuest, M., Bergmann, R., Steinbach, J., Pietzsch, J., Neundorff, I., and Wuest, F. (2012)** (18)F-Labeled phosphopeptide-cell-penetrating peptide dimers with enhanced cell uptake properties in human cancer cells. *Nuclear medicine and biology* 39, 1202-12.
- (197) **Zhu, W. L., and Shin, S. Y. (2009)** Effects of dimerization of the cell-penetrating peptide Tat analog on antimicrobial activity and mechanism of bactericidal action. *J Pept Sci* 15, 345-352.
- (198) **Zhu, W. L., and Shin, S. Y. (2009)** Antimicrobial and Cytolytic Activities and Plausible Mode of Bactericidal Action of the Cell Penetrating Peptide Penetratin and Its Lys-linked Two-Stranded Peptide. *Chem Biol Drug Des* 73, 209-215.
- (199) **Zhu, W. L., Lan, H. L., Park, I. S., Kim, J. I., Jin, H. Z., Hahm, K. S., and Shin, S. Y. (2006)** Design and mechanism of action of a novel bacteria-selective antimicrobial peptide from the cell-penetrating peptide Pep-1. *Biochemical and biophysical research communications* 349, 769-774.
- (200) **Bobone, S., Piazzon, A., Orioni, B., Pedersen, J. Z., Nan, Y. H., Hahm, K. S., Shin, S. Y., and Stella, L. (2011)** The thin line between cell-penetrating and antimicrobial peptides: the case of Pep-1 and Pep-1-K. *J Pept Sci* 17, 335-341.
- (201) **Kim, H., Jang, J. H., Kim, S. C., and Cho, J. H. (2014)** De novo generation of short antimicrobial peptides with enhanced stability and cell specificity. *J Antimicrob Chemoth* 69, 121-132.
- (202) **Monera, O. D., Sereda, T. J., Zhou, N. E., Kay, C. M., and Hodges, R. S. (1995)** Relationship of sidechain hydrophobicity and alpha-helical propensity on the stability of the single-stranded amphipathic alpha-helix. *J Pept Sci* 1, 319-29.
- (203) **Singh, J., and Thornton, J. M. (1985)** The Interaction between Phenylalanine Rings in Proteins. *Febs Lett* 191, 1-6.
- (204) **Fan, R., Yuan, Y., Zhang, Q., Zhou, X. R., Jia, L., Liu, Z., Yu, C., Luo, S. Z., and Chen, L. (2017)** Isoleucine/leucine residues at "a" and "d" positions of a heptad repeat sequence are crucial for the cytolytic activity of a short anticancer lytic peptide. *Amino acids* 49, 193-202.
- (205) **Dev, S., Khan, R. H., and Surolia, A. (2006)** 2,2,2-Trifluoroethanol-Induced structural change of peanut agglutinin at different pH: A comparative account. *IUBMB life* 58, 473-9.
- (206) **Lakshminarayanan, R., Fan, D., Du, C., and Moradian-Oldak, J. (2007)** The role of secondary structure in the entropically driven amelogenin self-assembly. *Biophys J* 93, 3664-74.
- (207) **Chou, P. Y., and Fasman, G. D. (1974)** Conformational parameters for amino acids in helical, beta-sheet, and random coil regions calculated from proteins. *Biochemistry-U S* 13, 211-22.
- (208) **Desiervo, A. J., and Homola, A. D. (1980)** Analysis of Caulobacter-Crescentus Lipids. *J Bacteriol* 143, 1215-1222.
- (209) **Daron, H. H. (1970)** Fatty Acid Composition of Lipid Extracts of a Thermophilic Bacillus Species. *J Bacteriol* 101, 145-&.
- (210) **Schulze, A., Marquardt, B., Kaczmarek, S., Schubert, R., Prager, A., and Buchmeiser, M. R. (2010)** Electron Beam-Based Functionalization of Poly(ethersulfone) Membranes. *Macromol Rapid Comm* 31, 467-472.

## 6. Attachment

### 6.1. List of abbreviations

AEMA	2-aminoethyl methacrylate hydrochloride
Ahx	6-hexanoic acid
AMP	Antimicrobial peptide
BD	Bacto brain heart infusion
CD	Circular dichroism
CF	5(6)-carboxyfluorescein
CL	Cardiolipin
CLSM	Confocal laser scanning microscopy
CPP	Cell-penetrating peptide
DCM	Dichlormethan
Dde	2-acetyldimedone
DIC	N,N'-diisopropylcarbodiimide
DIPEA	N,N-diisopropylethylamine
DMF	N,N-dimethylformamide
DOPC	1,2-dioleoyl- <i>sn</i> -glycero-3-phosphocholine
DOPE	1,2-dioleoyl- <i>sn</i> -glycero-3-phosphoethanolamine
DOPG	1,2-di-(9Z-octadecenoyl)- <i>sn</i> -glycero-3-phospho-(1'-rac-glycerol)
EDC	1-ethyl-3-(3-dimethylaminopropyl)carbodiimide
ESI-MS	Electrospray ionization mass-spectrometry
FA	Formic acid
GUV	Giant unilamellar vesicle
HATU	N-methylmethanaminium hexafluorophosphate N-oxide
HC <sub>20</sub>	Minimal hemolytic concentration of 20% living red blood cells

h-RBCs	Human red blood cells
HSV	Herpes-simplex-virus
IL	Ionic liquid
INT	Iodnitrotetrazolium
kGy	Kilogray
Leu	Leucine
LPS	Lipopolysaccharides
LUV	Large unilamellar vesicle
Lys	Lysine
MHB	Mueller-Hinton broth
MIC <sub>50</sub>	Minimal inhibitory concentration of 50% living bacteria
MRSA	Methicillin-resistant <i>Staphylococcus aureus</i>
NHS	N-hydroxysuccinimide
OD	Optical density
OM	Outer membrane
PBS	Phosphate buffered saline
PES	Polyether sulfone
RP-HPLC	Reversed-phase high-performance liquid chromatography
SEM	Standard error of mean
SI	Selectivity index
TFA	Trifluoroacetic acid
TFE	2,2,2-trifluoroethanol
TIS	Triisopropylsilane
Trp	Tryptophan

VRE	Vancomycin-resistant <i>Enterococci</i>
XPS	X-ray photoelectron spectroscopy

## 6.2. List of Figures

<i>Figure 1: The four classes of antimicrobial peptides represented by protein models..</i>	3
<i>Figure 2: Membrane disrupting mechanism of AMPs.</i>	8
<i>Figure 3: Schematic overview of AMP resistance mechanism.</i>	11
<i>Figure 4: Cell-wall structure of gram-negative, gram-positive and mycobacteria. ..</i>	14
<i>Figure 5: The imidazolium cation with different anions.</i>	15
<i>Figure 6: Final structure of 3a, 3b and 3c.</i>	16
<i>Figure 7: Antimicrobial activity of 3a, 3b and 3c.</i>	17
<i>Figure 8: Structure of the imidazolium salt used for peptide 3a, 3b and 3c</i>	36
<i>Figure 9: Final structure of 3a, 3b and 3c.</i>	36
<i>Figure 10: HPLC-MS analysis of 3a before and after purification via preparative HPLC.</i>	37
<i>Figure 11: HPLC-MS analysis of 3c before and after purification via preparative HPLC.</i>	38
<i>Figure 12: Circular dichroism spectra of 3c at different pH values.</i>	39
<i>Figure 13: Antimicrobial activity against resistant bacterial strains.</i>	40
<i>Figure 14: Hemolytic activity of all novel conjugates against human red blood cells.</i>	43
<i>Figure 15: Interaction of peptide 3b* with GUVs and different DOPC/cholesterol compositions.</i>	44
<i>Figure 16: Interaction of peptide 3c* with GUVs and different DOPC/cholesterol compositions.</i>	47
<i>Figure 17: SEM images of immobilized PES membranes.</i>	53
<i>Figure 18: INT-assay of immobilized membranes.</i>	54
<i>Figure 19: Time-experiments of immobilized membranes.</i>	55
<i>Figure 20: Grown bacteria after incubation with immobilized membranes.</i>	56
<i>Figure 21: Agar plate assay of immobilized membranes.</i>	56
<i>Figure 22: HPLC-MS analysis of sC18I15 before purification via preparative HPLC.</i>	62
<i>Figure 23 HPLC-MS analysis of sC18I15 after purification via preparative HPLC..</i>	63
<i>Figure 24: Antimicrobial activity of sC18 isoleucine variants.</i>	65
<i>Figure 25: Helical wheel projection of sC18, sC18I10, sC18I15 and sC18I16.</i>	66

<i>Figure 26: Antimicrobial activity of sC18 isoleucine variants against B. subtilis. ....</i>	67
<i>Figure 27: Antimicrobial activity of sC18 isoleucine variants against C. glutamicum and M. luteus.....</i>	68
<i>Figure 28: Antimicrobial activity of sC18 isoleucine variants against P. fluorescens and S. typhimurium.....</i>	69
<i>Figure 29: Helical wheel projection.....</i>	70
<i>Figure 30: Antimicrobial activity of sC18 phenylalanine variants against B. subtilis..</i> <i>.....</i>	71
<i>Figure 31: Antimicrobial activity of sC18 phenylalanine variants against C. glutamicum and M. luteus.....</i>	72
<i>Figure 32: Antimicrobial activity of sC18 phenylalanine variants against P. fluorescens and S. typhimurium..</i> .....	73
<i>Figure 33: 3D-structure of sC18 (above) and sC18F10F15F16 (below).....</i>	76
<i>Figure 34: Circular dichroism spectra of isoleucine and phenylalanine variants in phosphate buffer.....</i>	77
<i>Figure 35: Circular dichroism spectra of isoleucine and phenylalanine variants in phosphate buffer + TFE.....</i>	79
<i>Figure 36: Circular dichroism spectra with artificial membrane vesicles.....</i>	80
<i>Figure 37: Mechanism of action model for sC18F10F15F16.....</i>	82

### 6.3. List of tables

<i>Table 1: Common antibiotics and their bacterial resistance mechanisms. ....</i>	<i>2</i>
<i>Table 2: Some examples of antimicrobial peptides, their sequences, structures and mechanisms of action.....</i>	<i>4</i>
<i>Table 3: Equipment used during this work.....</i>	<i>20</i>
<i>Table 4: Buffers used during this work. ....</i>	<i>21</i>
<i>Table 5: Peptides synthesized during this work.....</i>	<i>22</i>
<i>Table 6: Analytical and synthetic data of all imidazolium salt compounds.....</i>	<i>35</i>
<i>Table 7: Minimal inhibitory concentration (MIC<sub>50</sub>) of all tested compounds.....</i>	<i>41</i>
<i>Table 8: Selectivity index (SI) of all conjugates calculated with HC<sub>20</sub>/MIC<sub>50</sub>.....</i>	<i>43</i>
<i>Table 9: Analytical und synthetic data of all peptide derivates.. ....</i>	<i>50</i>
<i>Table 10: Atomic composition of the membranes (as determined by XPS analysis). .....</i>	<i>52</i>
<i>Table 11: Analytic data of all synthesized sC18 variants.....</i>	<i>59</i>
<i>Table 12: Calculated MIC<sub>50</sub> values of all isoleucine and phenylalanine variants. ...</i>	<i>75</i>

## 6.4. Acknowledgment

An dieser Stelle möchte ich allen Leuten danken, die mich während meiner Arbeit sehr unterstütz und geholfen haben.

An erster Stelle Prof. Dr. Ines Neundorf als meine Betreuerin und Doktormutter für das interessante Thema, welches ich nach meiner Masterarbeit fortsetzen konnte. Sie hat mich super betreut und viele Inspirationen und Ideen für meine Arbeit geliefert. Außerdem dafür, dass sie mir viele Freiheiten während meiner Arbeit gelassen hat, aber bei Problemen jeglicher Art immer ein offenes Ohr hatte.

Zudem möchte ich Prof. Dr. Karin Schnetz für die Übernahme des Zweitgutachtens und 3-jährige Betreuung in der Graduate School of Biological Sciences danken. Auch Sie hat mir einige neue Ideen für meine Arbeit geliefert. Prof. Dr. Tobias Bollenbach danke ich für die Übernahme des Prüfungsvorsitzenden. Auch Prof. Dr. Ralf Giernoth möchte ich danken für die gute Kooperation beim Thema der ionischen Flüssigkeiten, sowie für die gute Betreuung in der GfSBS. Zudem danke ich Julie Pieper gen. Schmauck für die Herstellung der ionischen Flüssigkeiten und weiterer Experimente. Bei Christian Oelkrug und Dr. Andreas Schubert vom Fraunhofer Institute bedanke ich mich für die durchgeführten Test an den S2-Bakterienstämmen VRE und MRSA. Für die Immobilisierung meiner Peptide möchte ich Isabell Thomas und Dr. Agnes Schulze vom IOM Leipzig danken.

Ein riesiger Dank geht an meine Arbeitsgruppe und alle ehemaligen Arbeitsmitglieder, welche das Arbeiten im Labor jeden Tag verbessert haben: Bei Florian Reichart für die Kooperation in Business Angelegenheiten, bei Stephanie Natividad-Tietz für die lange Sitznachbarschaft, bei Anja Gronewold und Mareike Horn (alias die Twins) für viele tolle Abende auch außerhalb des Labors und die Herstellung der Lipidvesikel, bei Annika Klimpel für die besten Tanzmoves, bei Lucia Feni für den Ausflug nach Italien sowie das verlorene Elfmeterschießen der Italiener im EM-Viertelfinale und bei Tamara Lützenburg für die Einführung in die Welt der Frauenkosmetik. Außerdem geht ein Dank an meine männliche Unterstützung Alex Trimborn und meinen Kinocheck-Buddy Florian Küster. Zudem geht ein Dank an meine Studenten Julian Koch, Volker Kinast, Kübra Solak, Markus Schütz und Petra Sprengart für viele Ergebnisse. Anja Hochheiser danke ich für die Messung vieler ESI-MS Proben und Constance Chollet für die Hilfe vieler

wissenschaftlicher Fragen sowie Claudia Drogd für jegliche Art der Organisation und Gabi Sitek für die Autoklavierung unzähliger Medien und Kulturen.

Außerdem möchte ich meinen Eltern danken, die mich das ganze Studium unterstützt haben und mich ertragen mussten, wenn es mit dem Studium mal nicht so gut geklappt hat. Zu guter Letzt, möchte ich meiner Freundin Lena danken, welche mich ebenfalls immer unterstützt, motiviert und wieder aufgebaut hat, auch wenn es mal nicht so gut lief.

Ein großer Dank an euch alle, ohne die ich diese Arbeit nie hätte schreiben können.

## 6.5. Erklärung

Ich versichere, dass ich die von mir vorgelegte Dissertation selbständig angefertigt, die benutzten Quellen und Hilfsmittel vollständig angegeben und die Stellen der Arbeit –einschließlich Tabellen, Karten und Abbildungen –, die anderen Werken im Wortlaut oder dem Sinn nach entnommen sind, in jedem Einzelfall als Entlehnung kenntlich gemacht habe; dass diese Dissertation noch keiner anderen Fakultät oder Universität zur Prüfung vorgelegen hat; dass sie – abgesehen von unten angegebenen Teilpublikationen – noch nicht veröffentlicht worden ist, sowie, dass ich eine solche Veröffentlichung vor Abschluss des Promotionsverfahrens nicht vornehmen werde. Die Bestimmungen der Promotionsordnung sind mir bekannt. Die von mir vorgelegte Dissertation ist von Prof. Dr. Ines Neundorf betreut worden.

Teilpublikationen:

- **Reinhardt, A., and Neundorf, I. (2016)** Design and Application of Antimicrobial Peptide Conjugates. *Int J Mol Sci* 17.
- **Reinhardt, A., Horn, M., Schmauck, J. P. G., Brohl, A., Giernoth, R., Oelkrug, C., Schubert, A., and Neundorf, I. (2014)** Novel Imidazolium Salt-Peptide Conjugates and Their Antimicrobial Activity. *Bioconjugate chemistry* 25, 2166-2174.
- **Reinhardt, A., Schmauck, J., Giernoth, R., and Neundorf, I. (2014)** Antimicrobial activity of mixtures out of antimicrobial peptides and ionic liquids. *Proceedings of the 33<sup>rd</sup> Eur. Pept. Symp.* p.282.

Posterpräsentationen:

- **Reinhardt, A., and Neundorf, I. (2017)** Reversing the activity of the cell-penetrating peptide sC18: How to improve antimicrobial activity by expansion of the hydrophobic face. *34<sup>th</sup> European Peptide Symposium, Leipzig*
- **Reinhardt, A., Horn, M., Schmauck, J., Giernoth, R., and Neundorf, I. (2015)** Novel Imidazolium Salt–Peptide Conjugates and Their Antimicrobial Activity. *12<sup>th</sup> German Peptide Symposium, Darmstadt*
- **Reinhardt, A., Schmauck, J., Giernoth, R., Neundorf, I. (2014)** Synthesis of imidazolium salt-peptide conjugates and their antimicrobial activity. *33<sup>rd</sup> European Peptide Symposium, Sofia, Bulgarien*

---

Ort, Datum

---

Andre Reinhardt

## 6.6. Lebenslauf

### **Persönliche Daten:**

Name: André Reinhardt

Geburtsdatum: 06.10.1988

Geburtsort: Reutlingen

Staatsangehörigkeit: deutsch

### **Ausbildung:**

Seit 10/2013 Promotion am Institut für Biochemie, Universität zu Köln bei Frau Prof. Dr. Ines Neundorff

10/2011 – 10/2013 Masterstudium Biological Sciences, Universität zu Köln, Abschluss: Master of Science

10/2008 – 10/2011 Bachelorstudium Biologie, Universität zu Köln  
Abschluss: Bachelor of Science

08/1999 – 06/2008 Friedrich-Wilhelm-Gymnasium, Köln,  
Abschluss: Abitur

08/1995 – 06/1999 St. Nikolaus Grundschule, Köln